Supporting Information for

Ion-hydrocarbon and/or Ion-Ion Interactions: The Direct and Reverse Hofmeister Effects in a Synthetic Host

Jacobs H. Jordan, Corinne L. D. Gibb, Anthony Wishard, Thu Pham, and Bruce C. Gibb*

Department of Chemistry
Tulane University
New Orleans, LA 70118, USA
*bgibb@tulane.edu

1. Table of Contents

2. Materials, instrumentation and sample preparation procedures

A. Materials and Instrumentation

Reagents were purchased from commercial suppliers Sigma-Aldrich Corp. or TCI America and were used without further purification. All sodium salts, with the exception of sodium cyanoborohydride ($NaBH_3CN$ > 95 %), were of purity ≥ 98 %, and were used as received. All solvents were purchased from Fisher Scientific and were used as received. Positand **1** (Figure S1) was synthesized by the procedures reported previously.[1-2] ^1H NMR spectra were collected on a Bruker 500 MHz or Varian 400 MHz spectrometer at 25 ˚C, and utilized deuterium oxide (Cambridge Isotopes, 99.9%+). Changes in chemical shift ($\Delta\delta$) were referenced to the residual solvent signal (δ = 4.70 ppm). Spectral processing was performed using Mnova software (Mestrelab Research, S.L.), with results fitted using either the online software BINDFIT[3] or EXCEL. Dynamic light scattering (DLS) measurements were performed on a Nicomp ZLS Z3000 particle size analyzer (Particle Sizing Systems – Port Richey, FL) with a 50 mW laser diode (660 nm wavelength) and an avalanche photodiode (APD) detector. Measurements of scattered light were made at 90˚, with data collected at 23 ˚C and processed using a non-negative least squares Nicomp analysis. Precipitation assays involved monitoring samples at a 500 nm wavelength and a temperature of 23 °C, using an Enspire Multimode plate reader (PerkinElmer, Inc – Waltham, MA) equipped with a Xenon flash lamp, quad monochromator, dual temperature controller, and dispenser. In all cases, Fisherbrand (Fisher Scientific) high-binding clear polystyrene 96-well plates were used. Kinetic data was acquired using Corning™ clear polystyrene 96-well non-treated ½-area micro-plates (Fisher Scientific) sealed with a clear polyethylene film (Fisher Scientific) at 23 °C with a +2.0 °C differential heating applied to the upper surface of the plate to prevent condensation. Isothermal Titration Calorimetric (ITC) experiments were performed using a VP-ITC MicroCalorimeter from Microcal, USA.

B. NMR solution sample preparation procedure.

All solutions were prepared in 10 mM phosphate buffered D_2O, pD 7.3 ± 0.1. All titrations of positand **2** were performed on a 0.5 mM host solution prepared from a concentrated stock of ~2 mM host. The concentration of this stock solution was itself determined by titration in triplicate with 25 mM sodium ethanesulfonate (SES) solutions. Integration of the methyl peak of SES and the H_n methylene of positand **2** (Figure S1) gave the concentration of the host and hence the numbers of waters of crystallization.

Stock solutions of the guest adamantane carboxylate (~2 mM) were prepared and titrated as per the procedure for positand **2**. All titrations for the 1:1 complex of positand **2** and guest were prepared as 1:1.05 solutions from concentrated stock solutions for a final concentration of 0.5 mM **2** and 0.525 mM adamantane carboxylate (Figure S2).

A concentrated salt solution was prepared for use in each titration with the pD of the salt solution equal to 7.3 ± 0.1. The pD of each solution was adjusted as needed during dilution from concentrated stocks. In each experiment 0.5 mL of **2** or its 1:1 complex with adamantane carboxylate were titrated in an NMR tube with careful additions of small aliquots of the sodium salt of the requisite anion. Typically, this salt solution was of a concentration of 25 mM, prepared in 10 mM phosphate buffered D_2O, pD 7.3 ± 0.1. The pD was adjusted with small amounts of NaOH solution if needed.

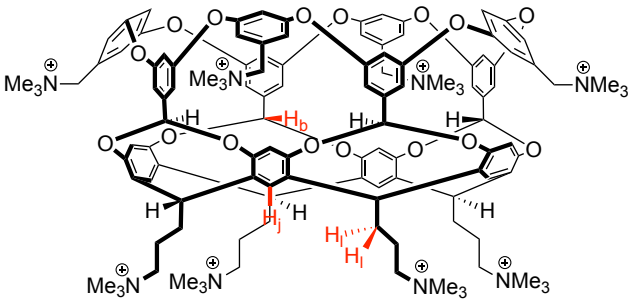

2

Figure S1. Chemical structures of positand **2** (proton assignments highlighted).

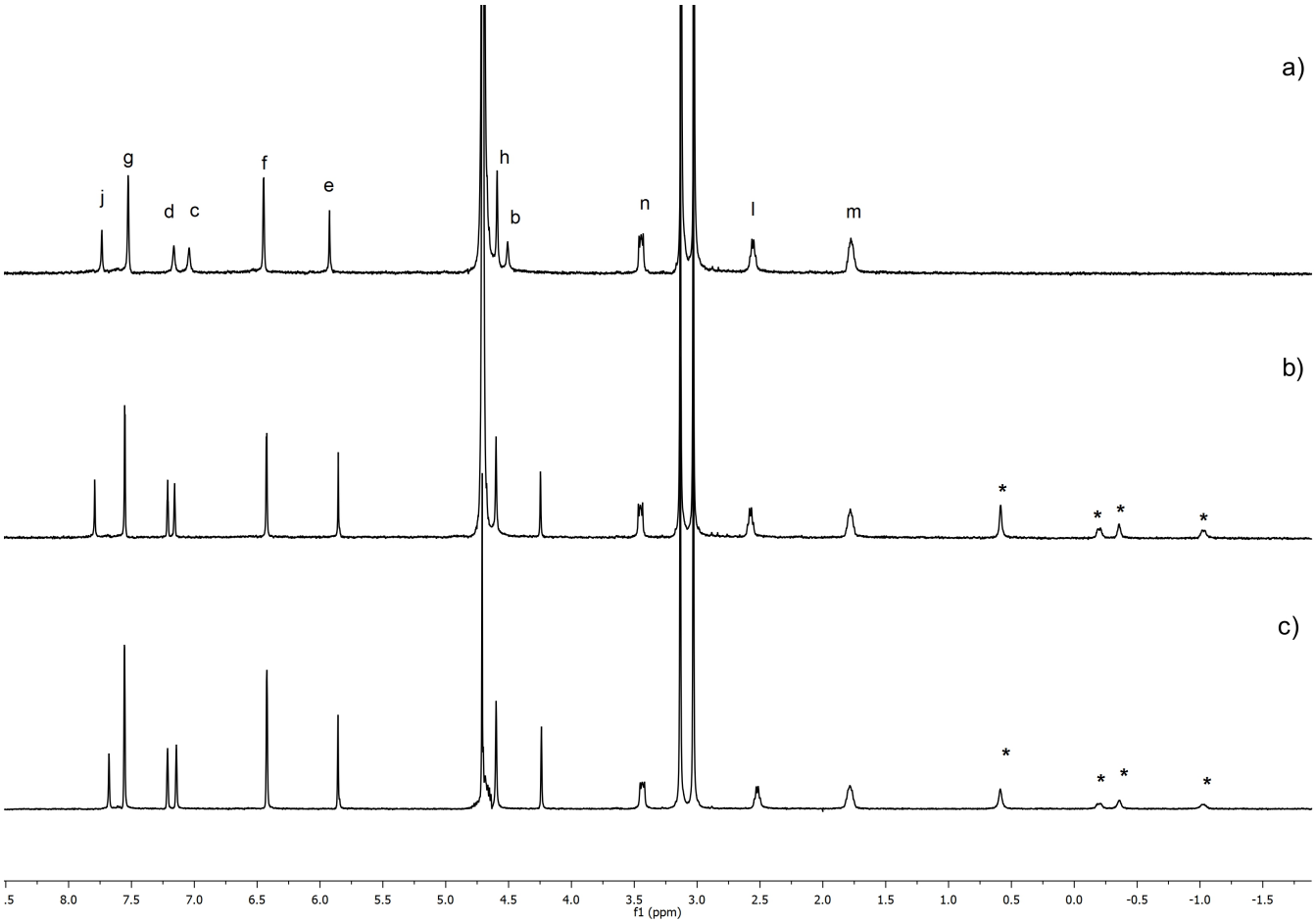

Figure S2: ^{1}H NMR (500 MHz, D_2O) of: a) positand **1**; b) **2**.adamantane carboxylate, and; c) ^{1}H PGSE NMR (500 MHz, H_2O) **2**.adamantane carboxylate. Proton signal assignments as per Figure S1. The signal for H_a is coincident with the HOD signal. *Indicates signals from bound adamantane carboxylate.

C. DLS solution preparation procedure

All solutions were prepared using a 40 mM phosphate buffer in 18.2 MΩ H_2O, pH 7.30 ± 0.01. For free-host titrations, all solutions of positand **2** were prepared by diluting a concentrated stock of positand **2** to 2.00 mM. For titrations with the complex between **2** and adamantane carboxylate, solutions were 2.00 mM in host and a 2.1 mM in adamantane carboxylate. Full complexation was confirmed by Pulsed Gradient Spin Echo (PGSE) NMR (see Figure S2) in H_2O locked with D_2O in a 5 mm coaxial capillary insert (Wilmad-Labglass – Vineland, NJ). A concentrated salt solution was prepared for use in each titration.

Samples were centrifuged for 10 minutes at 10,000 rpm prior to each titration but not centrifuged thereafter. Solutions of host were titrated with salt, then shaken and vortexed to ensure mixing before acquiring DLS measurements. All analyses were performed at a channel width of 5 microseconds (μs), with volume-weighted size distribution data collected.

D. Precipitation assay sample preparation procedure

Precipitation assays involved: 1) Initial screening of salts; 2) critical precipitation concentration (CPC) determinations for each salt; 3) precipitation kinetics determinations.

For the initial screening all solutions were prepared using a 10 mM phosphate buffer in distilled H_2O, pH 7.30 ± 0.02. Separate stock solutions of salts were prepared as 0.5 M solutions and diluted as necessary. Positand **2** was prepared as 2.0 mM stock solutions. Titrations of the host-guest complex (**2.3**) used a solution of 2.00 mM **2** and 2.1 mM guest adamantane carboxylate, with complexation confirmed by PGSE NMR. The precipitation assays were conducted at a final host and host-guest complex concentration of 0.5 mM. Initial screening assays were conducted from 250 mM to 1.95 mM salt concentrations by successive serial ½ dilutions of the stock 0.5 M solution of the salt. Final solutions were made using 50 μL of stock salt solutions added to 25 μL of assay buffer followed by the addition of 25 μL stock host solutions.

For determination of the CPC value for each salt, measurements were performed in at least triplicate from separate stock solutions of hosts and salts typically prepared between 20 – 150 mM. Two exceptions, trichloroacetate ($Cl_3C_2O_2^-$) and iodide (I^-), were prepared at 0.4 M due to the large excess of salt needed to induce precipitation. The pH of the stock solutions was 7.3 ± 0.2 and adjusted as necessary during dilution. For each CPC determination 25 μL of host or host-guest complex (2.0 mM host, 2.1 mM guest) were added to wells containing 25 – 75 μL assay buffer, and 0 – 50 μL of salts of variable concentration, for a final volume of 100 μL and a final host concentration of 0.5 mM. Assessments of precipitation were made within $t < 15$ min to minimize kinetic effects.

For precipitation kinetic determinations, the extent of precipitation of **2**, or its complex with adamantane carboxylate, as a function of time were obtained at fixed salt concentrations. The salt concentrations used were increments of 5 % of the final CPC value (50-95 %). For data collection, a two-stage protocol was employed featuring a signal acquisition every 240 s for sixteen hours, followed by signal acquisition every 3600 s for 152 hours, for a total acquisition time of 168 h (1 week). For each, salt solutions were prepared at twice the final CPC value and added by fixed aliquot of 25.0 – 47.5 μL of salt solution (2.5 μL increments) to wells containing 27.5 – 50 μL buffer. To these prepared salt solutions were then added 25 μL of host or host-guest complex (2.0 mM) for a final volume of 100 μL and final host concentration of 0.5 mM.

E. ITC sample preparation procedure.

Solutions of host and guest were prepared in 10 mM phosphate buffer (pH = 11.3) in 18.2 MΩ H_2O. Solutions of host and guest were prepared from a concentrated stock solution to achieve a final host **2** concentration of 0.075 mM or 0.150 mM **2** and 0.750 mM or 1.50 mM guest adamantane carboxylate or $Cl_3C_2O_2^-$. The pH was adjusted if necessary during dilution.

F. Errors

Results are expressed as the average when possible with the coefficient of variation (CV) expressed as a percentage of the mean when applicable, where *s* is the sample standard deviation and μ is the sample mean:

$$CV\% = \frac{s}{\mu} \times 100 \qquad \text{Eq. (1)}$$

3. Analytical data

A. NMR Titration data

a. Overview

We initially screened 31 monovalent sodium salts and selected 14 anions for determining the strength of association. Of those, at higher concentrations nine induced aggregation of the host and ultimately resulted in formation of a precipitate (e.g. thiocyanate (SCN^-), Figure S3). For NMR binding constant determinations to the cavity and crown (K_a^{cav} and K_a^{cown}) we used H_b to monitor binding to the cavity, and H_j to monitor binding to the crown (see **2** in Figure S1). The latter was chosen because the maximal shift in its signal (δ_{maxH_j}) in titrating with an anion was generally much larger than the corresponding shifts in signals of other protons in the pendent chains. Optimally, we would have preferred to titrate anions to the free host and fit the data globally, simultaneously using protons H_b and H_j. For such a 1:2 global binding model there are six unknown variables: the two binding constants (K_a^{cav}, K_a^{crown}), and the maximal contributions to the shifts in the signals from H_b and H_j arising from cavity binding ($\delta_{maxH_b}^{cav}$, $\delta_{maxH_j}^{cav}$) and crown binding ($\delta_{maxH_b}^{crown}$, $\delta_{maxH_j}^{crown}$). However, we did not obtain stable solutions from such an analysis. Consequently, we reverted to a two-step strategy in which K_a^{cown} (and $\delta_{maxH_j}^{crown}$) were first determined by blocking the cavity of **2** using strongly binding adamantane carboxylate (Ada-CO_2^-, $K_a \approx 7.21 \times 10^6$ M^{-1} as determined by ITC, Section 3B) and monitoring the shift in H_j. This led to the K_a^{crown} values shown in Table S3. In the case of trichloroacetate ($Cl_3CCO_2^-$) this strategy was however unsuccessful. This anion was found to bind so strongly to the cavity (5.45×10^4 M^{-1} by ITC) that it competed for the pocket of the host and lowered the apparent affinity of the adamantane carboxylate (the salting-in Hofmeister effect).

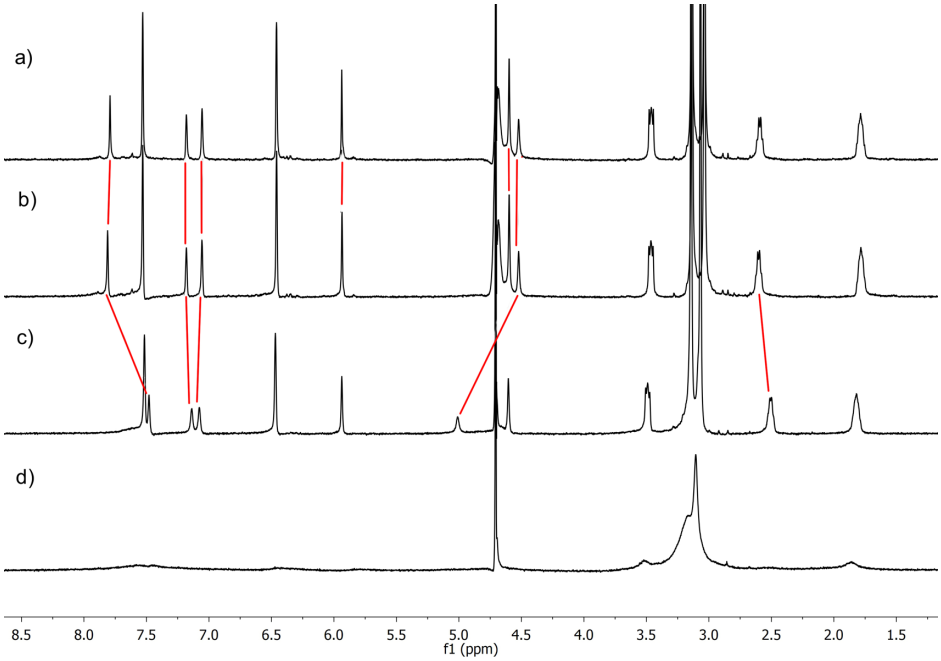

Figure S3: ^1H NMR spectra of positand **2** (0.5 mM, D_2O, 500 MHz). a) Positand **2** after the addn. of 10 equiv. NaF; b) free host **2**; c) positand **2** after the addn. of 10 equiv. NaSCN, and; d) positand **2** after the addn. of 100 equiv. NaSCN.

With the K_a^{crown} values determined, we then used this data to fit a 1:2 model for anion binding to the free host. The location of the two reporter atoms facilitated this considerably. Thus, although anion binding to the cavity of the free host was found to affect the signal shift of H_j ($\delta_{maxH_j}^{cav} \neq 0$), binding to the crown did not influence the signal of H_b ($\delta_{maxH_b}^{crown} = 0$). We interpret these facts as arising because binding of an anion to the crown does not change the shape of the cavity, but binding to the cavity does, and this influences the signals from both H_b and H_j. Thus, using the K_a^{crown} values, fitting the

shift in H_b of the free host using a 1:2 model involved only two unknowns K_a^{cav} and δ_{maxH_b} (= $\delta_{maxH_b}^{cav}$ + $\delta_{maxH_b}^{crown}$). The resulting K_a^{cav} values are also listed in Table S4. The NMR data from hexafluorophosphate (PF_6^-) did not fit this model well, indicating that pseudo-specific binding to the outer trimethylammonium groups was significant. Additionally, only limited data for the binding of triflate ($CF_3SO_3^-$) could be collected because of peak coincidence of the H_b signal and the benzylic signal. In base cases a minimum K_a value is quoted.

b. ^{1}H NMR Screening of anions

All solutions were prepared as described in the solution preparation procedures (Section 2B). An initial ^{1}H NMR screening assay using 1, 10 and 100 equivalents of 31 sodium salts (Table S1) indicated which anion was binding in the non-polar pocket of **2** (monitoring of proton H_b, Figure S1), and which salt induced host aggregation or precipitation (line, broadening, attenuation or visual appearance of a precipitate). An example is shown in Figure S4 for F^- (a non-binding and non-aggregating anion) and Figure S5 for SCN^- (a binder and precipitator).

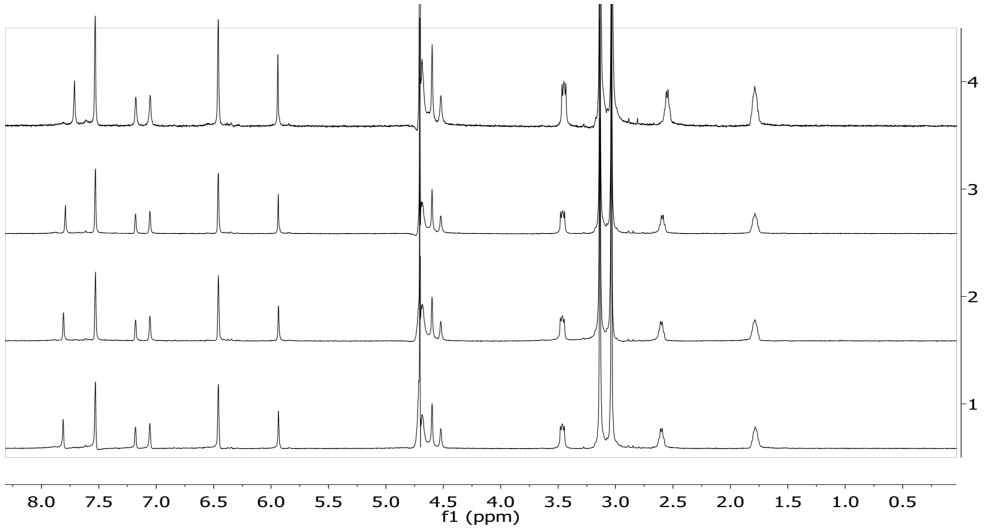

Figure S4: Example of the three-point titration of 0.5 mM positand **2** in D_2O with NaF: 1) free host; 2) 1 equiv. of salt; 3) 10 equiv.; 4) 100 equiv.

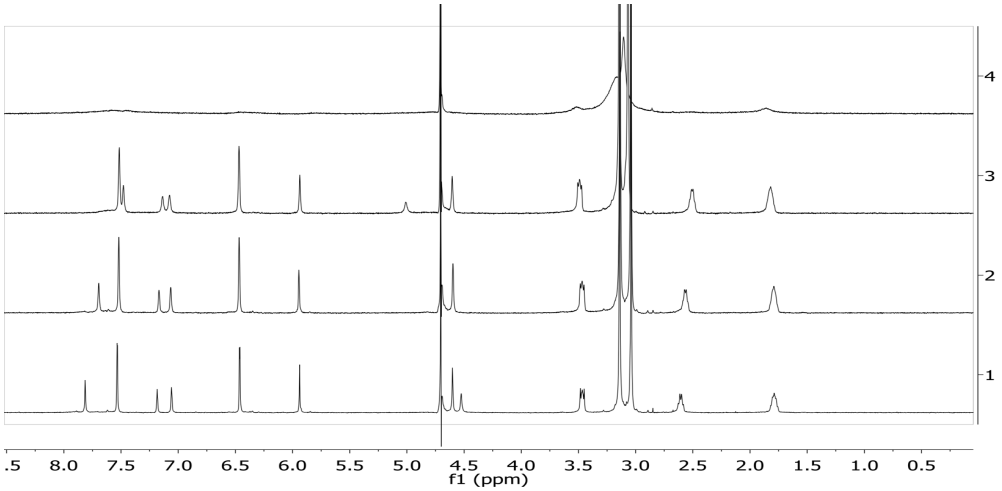

Figure S5: Example of the three-point titration of 0.5 mM positand **2** in D_2O with NaSCN: 1) free host; 2) 1 equiv. of salt; 3) 10 equiv.; 4) 100 equiv.

Num.	Molecular Formula	Anion Name	Equiv. salt for detectable shift in host H_b signal	Equiv. salt for detectable aggregate (in NMR expt)
1	F^-	fluoride	—	—
2	Cl^-	chloride	—	—
3	$CH_3CH_2SO_3^-$	ethane sulfonate	—	—
4	$CH_3CO_2^-$	acetate	—	—
5	HCO_2^-	formate	—	—
6	$CF_3CO_2^-$	trifluoroacetate	—	—
7	CNO^-	cyanate	—	—
8	N_3^-	azide	100	—
9	BH_4^-	borohydride	10	—
10	BrO_3^-	Bromate	10	—
11	NO_3^-	Nitrate	10	—
12	Br^-	Bromide	100	—
13	$CH_3SO_3^-$	methane sulfonate	1	—
14	$CH_3SO_2S^-$	methane thiosulfate	1	—
15	$Cl_2CHCO_2^-$	dichloroacetate	1	—
16	ClO_3^-	Chlorate	1	—
17	$N(CN)_2^-$	dicyanamide	1	—
18	$CBr_3CO_2^-$	tribromoacetate	1	100
19	MnO_4^-	permanganate	1	10
20	$CCl_3CO_2^-$	trichloroacetate	1	—
21	I^-	Iodide	1	100
22	BF_4^-	tetrafluoroborate	1	100
23	SCN^-	thiocyanate	1	100
24	IO_4^-	Periodate	1	100
25	BH_3CN^-	cyanoborohydride	1	100
26	ClO_4^-	perchlorate	1	100
27	F_6Sb^-	hexafluoroantimonate	1	100
28	ReO_4^-	perrhenate	1	100
29	PF_6^-	hexafluorophosphate	1	10
30	$CF_3SO_3^-$	trifluoromethanesulfonate	1	100
31	$AuCl_4^-$	tetrachloroaurate	1	10

Table S1. List of sodium salts screened for association to the pocket of host **1** (using the H_b signal NMR (0.5 mM host concentration)) and for aggregation as judged by NMR signal broadening and attenuation.

c. ^{1}H NMR titrations of the positand **2**-AdaCO_2^- complex with salts

From the initial screening (Table S1) a selection of salts were chosen for further study (Table S3). Figure S6 shows the differences in the shift of the H_j signal for the free and complex of **2** with adamantane carboxylate (further details below) for the titration with $NaClO_4$. The differences between the curves suggest that binding to the crown and the non-polar cavity are cooperative, and/or that anion binding to the pocket affects the shift of H_j (as previously observed for certain guests, e.g. adamantane carboxylate Figure S2). Thus, accurate determinations of the binding of anions to the ammonium crown of the host required blocking the non-polar cavity of **2** with adamantane carboxylate (K_a = 7.2 × 10^6 M^{-1} (± 8%), see Section 3.B).

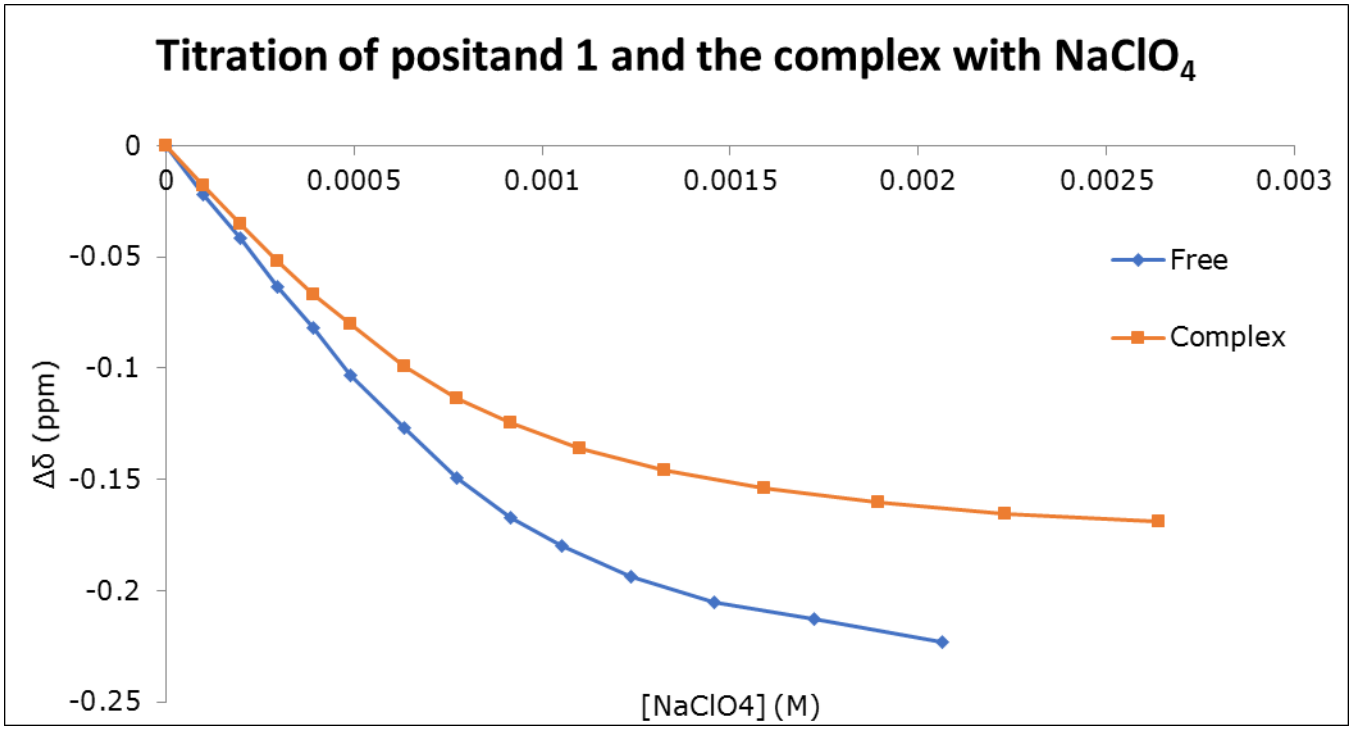

Figure S6: Shift of proton H_j during the titration of $NaClO_4$ with free **2** and its complex with adamantane carboxylate

For all salts examined, titrations monitoring either H_j or H_l (see figure S7) were performed substantially below the critical precipitation concentration (CPC) of the salts to maximize mono-dispersity and ensure homogeneity of the **2**.adamantane carboxylate complex. The results obtained by plotting the chemical shift ($\Delta\delta$) of either the H_j or the H_l signal were similar, but where possible H_j was utilized as the observed chemical shift during the titration was generally larger. The exception was I^-, where the chemical shift with H_j was < 0.02 ppm and large inherent errors made reproducibility difficult. Therefore, for I^- the value quoted is for the resonance of H_l.

With the non-polar pocket blocked, and in the absence of any aggregation or precipitation, it can be assumed that Equation 2:

$$G_t = [G] + [HG]_{crown} + n[HG_n]_{other} \qquad \text{Eq. (2)}$$

where $[G_t]$ is the total guest concentration, $[HG]_{crown}$ is the concentration of the complex with the anion binding to the cationic crown at the feet of the cavitand, and $[HG_n]_{other}$ is the concentration of the complexes arising from pseudo specific complexations.

Assuming weak pseudo specific binding, Eq. (2) can be simplified to Eq. (3):

$$G_t \approx [G] + [HG]_{crown} \text{ since } [G] + [HG]_{crown} >> n[HG_n]_{other} \qquad \text{Eq. (3)}$$

Eq. 3 was applied to all of the titrations as a simple 1:1 binding model.[4] As an example, Figure S7 shows the superimposed ^{1}H NMR spectra for the $NaClO_4$ titration involving the complex.

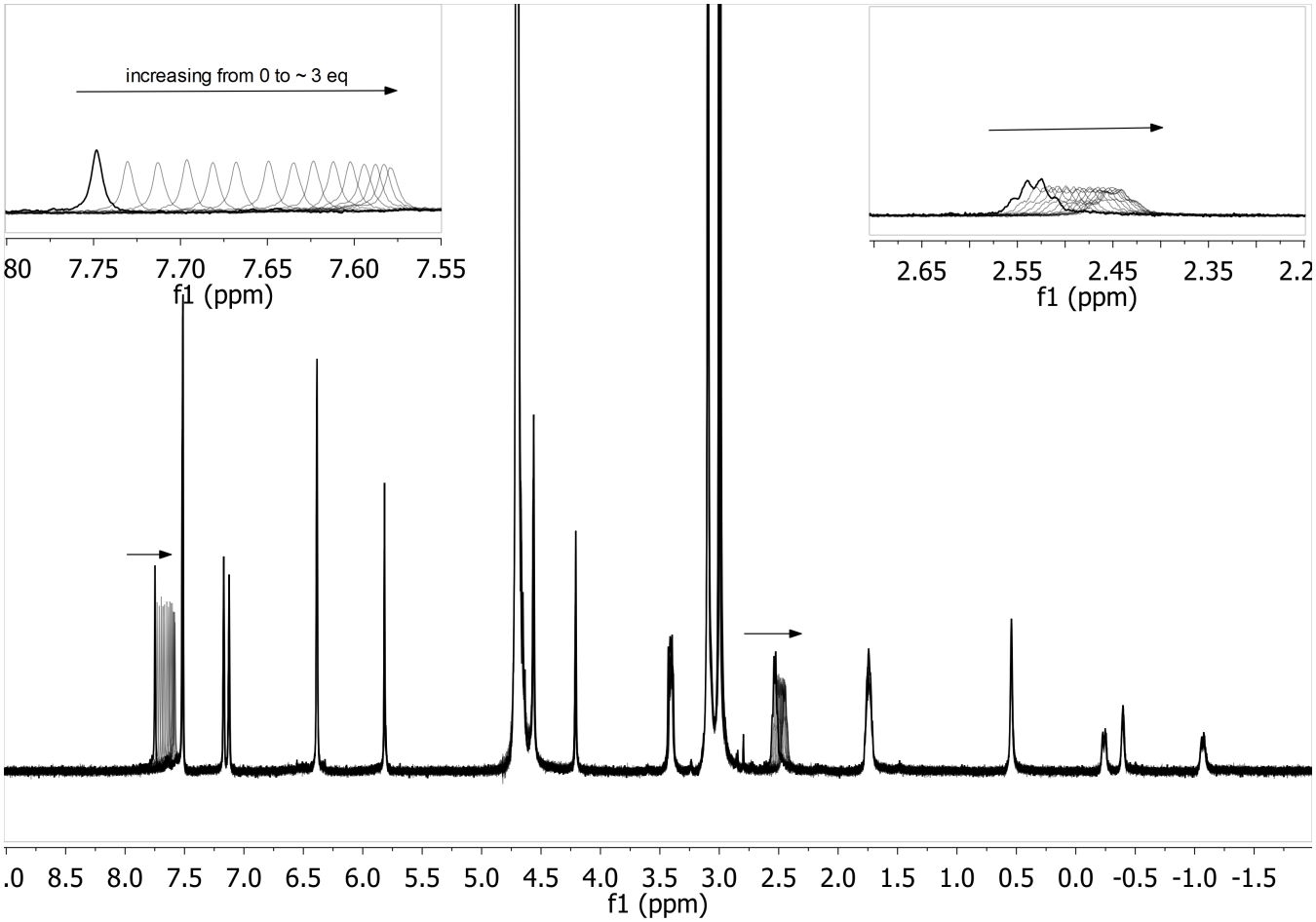

Figure S7: Superimposed NMR spectra from the titration of $NaClO_4$ to the **2**.adamantane carboxylate complex.

This strategy was successful for all anions with the exception of $CCl_3CO_2^-$, which bound sufficiently strongly to the cavity to effectively compete with the blocking guest adamantane carboxylate (Figure S8).

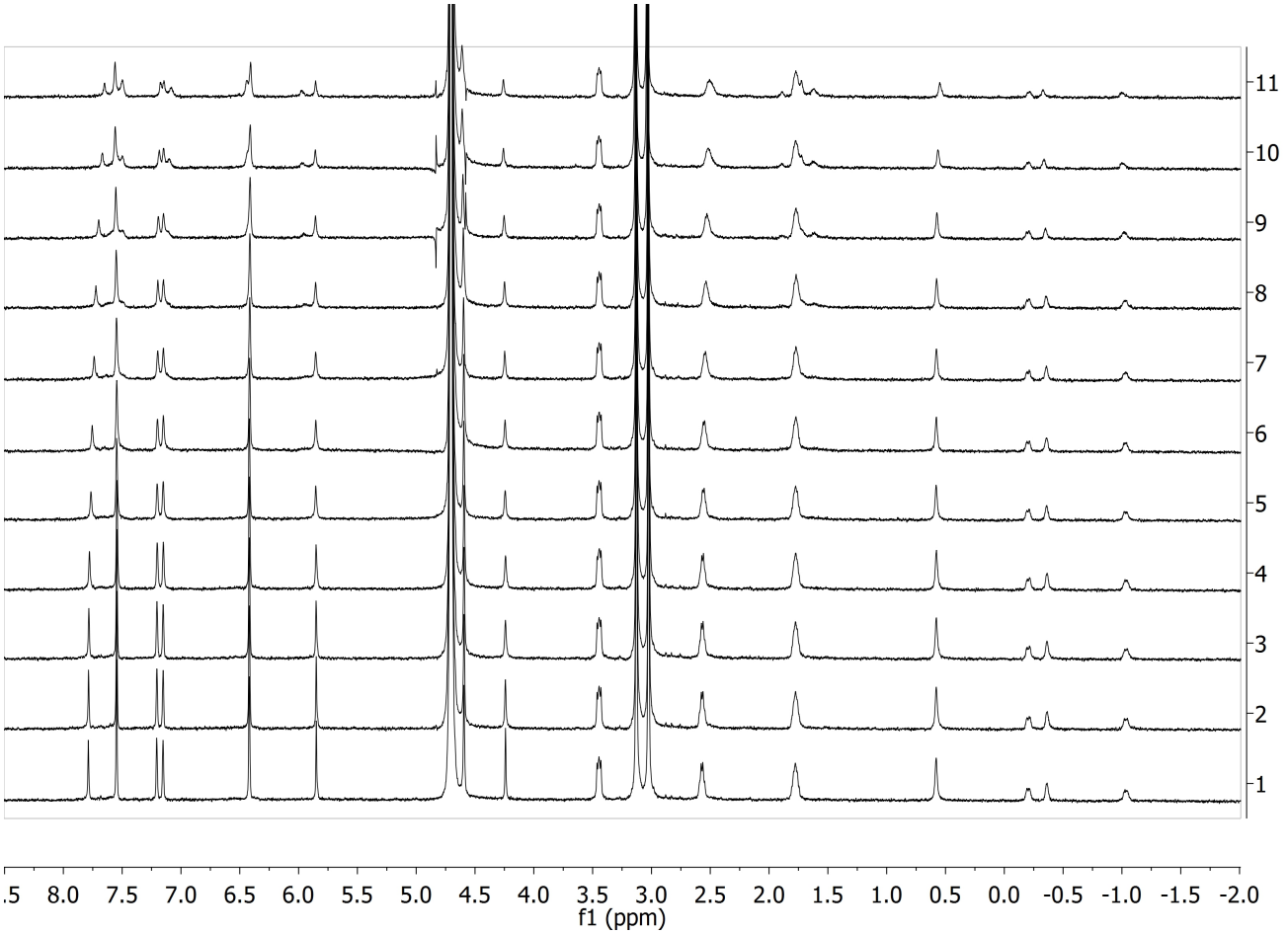

Figure S8: ^{1}H NMR titration data for the **2**.adamantane carboxylate complex with CCl_3CO_2Na (up to 7 equivalents). Data could not be fitted to a 1:1 model because of competition with adamantane carboxylate for the non-polar pocket.

In the case of F^- and $Cl_2CHCO_2^-$ there was negligible shift of H_j and no evidence of saturation even at high salt concentration (~ 100 equiv.), demonstrating that there is no binding or very weak binding to the ammonium crown. However, in the case of Cl^-, Br^- and NO_3^- it was possible to use Eq. 3 to calculate the K_a values for crown binding. For example, Figure S9–10 shows the titration data of the complex with nitrate (NO_3^-) and the fit using a 1:1 model (BINDFIT). Note that the shift of proton H_j upon addition of NO_3^- to **2** and **2**.adamantane carboxylate complex is the same (Figure S11) showing that for this weakly associating anion cavity binding does not affect the shift of H_j even in the free host (there is a low probability of having two sites filled at this low salt concentration).

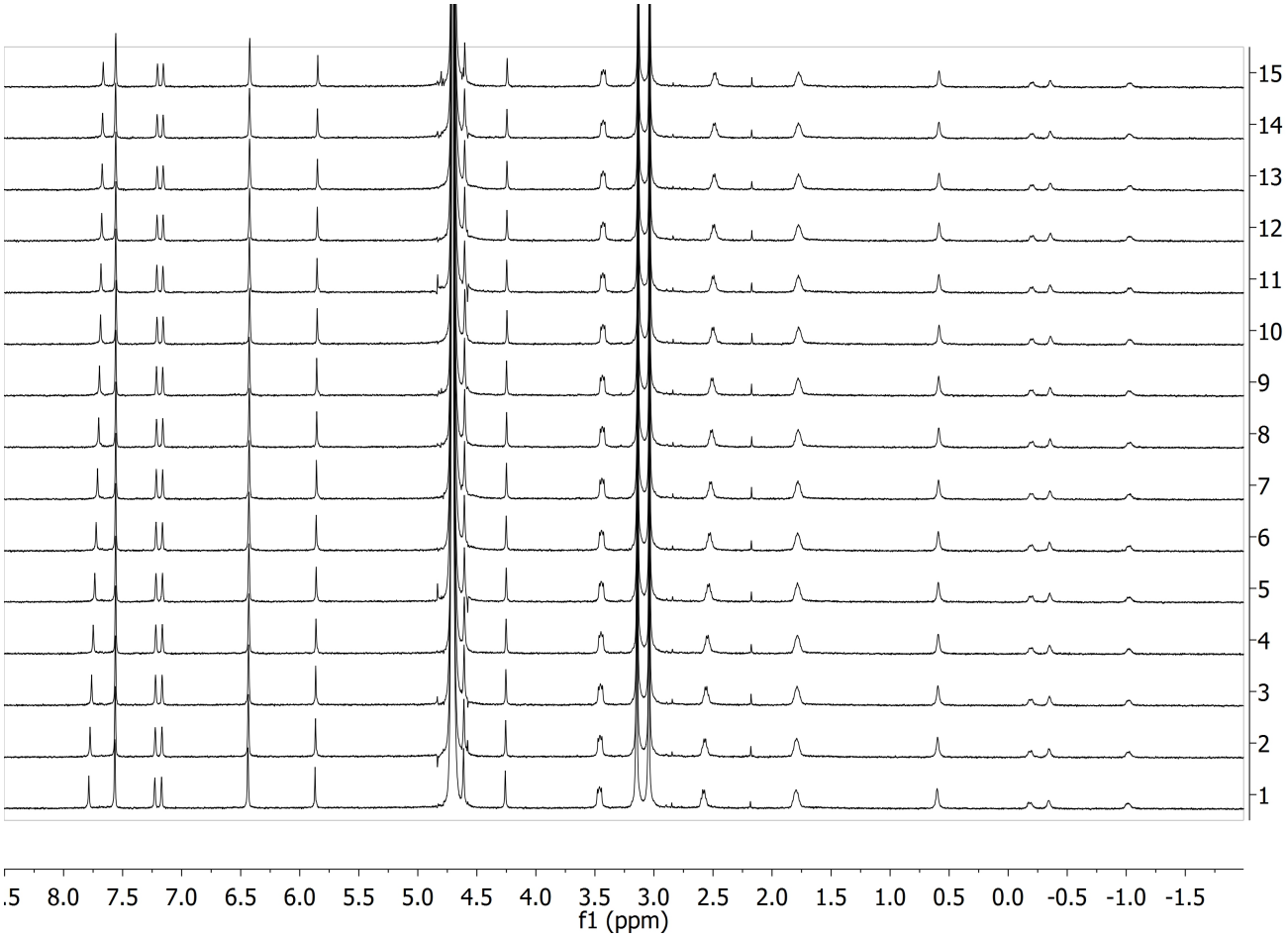

Figure S9: Representative NMR titration of the **2**.adamantane carboxylate complex with $NaNO_3$ (up to 59 equivalents).

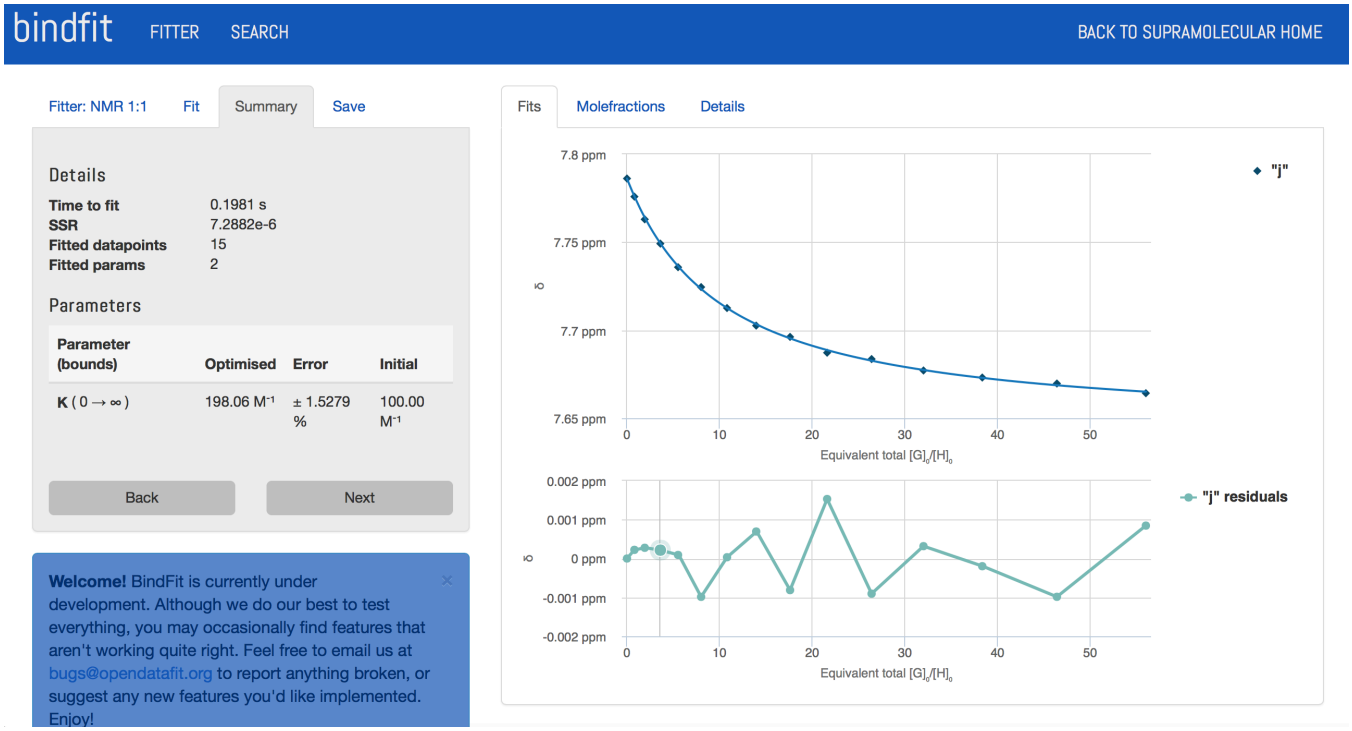

Figure S10: Fitting of H_j shift (Δδ ppm) from S9 using a 1:1 model.

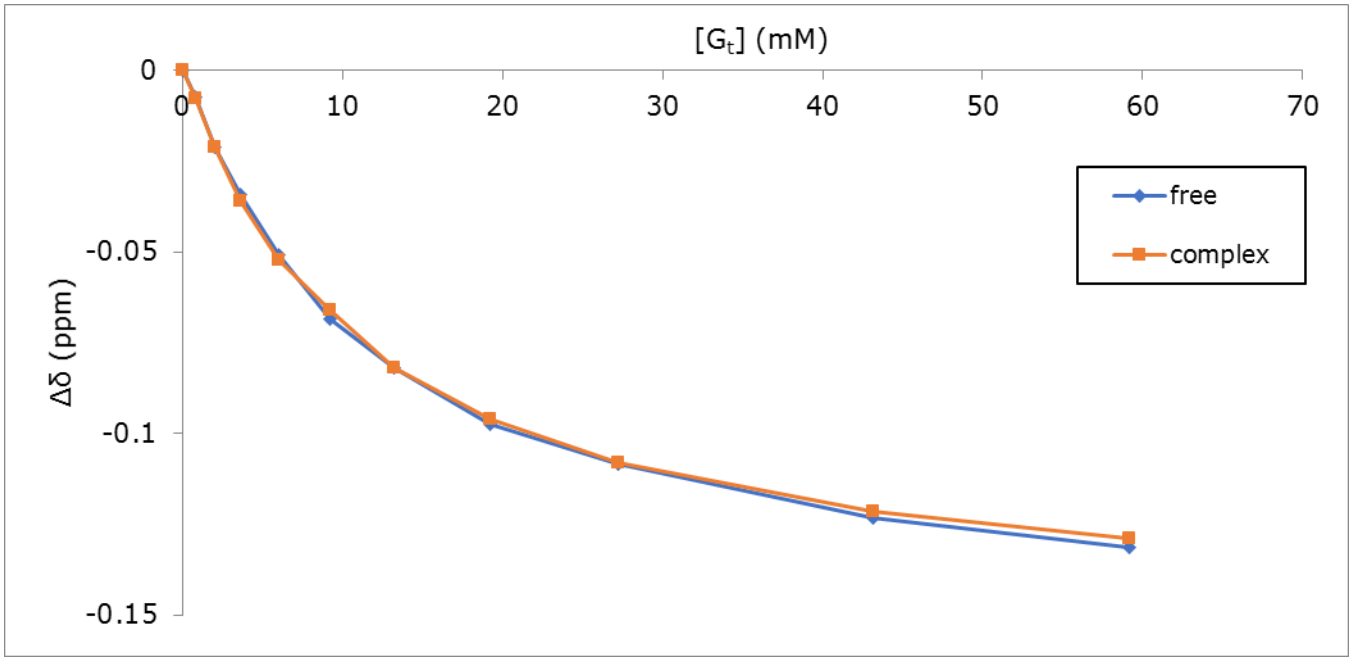

Figure S11: Shift of H_j during the titration of free **2** and the **2**.adamantane carboxylate complex with 100 mM sodium nitrate.

Table S2 shows the data obtained from three different titrations, with the % error, covariance and average K_a value for NO_3^- (180 M^{-1} ± 9%), Cl^- (116 M^{-1} ± 5%; Figures S12 and 13) and Br^- (742 M^{-1} ± 8%; Figure S14–S15).

Salt	*Titration*	K_a (M^{-1})	Error (%)	Covariance	K_a^{feet} (M^{-1})
NaBr	1	700	3.0	4.39×10^{-4}	742 ± (8%)
	2	810	3.1	6.32×10^{-4}	
	3	718	3.4	8.24×10^{-4}	
$NaNO_3$	1	166	2.0	2.81×10^{-4}	180 ± (9%)
	2	177	2.6	9.66×10^{-4}	
	3	198	1.5	3.18×10^{-4}	
NaCl	1	122	1.1	7.63×10^{-5}	116 ± (5%)
	2	112	0.7	5.19×10^{-5}	
	3	114	0.9	9.69×10^{-5}	

Table S2: Summary of 1:1 fitting of the ^{1}H NMR titration of the **2**.adamantane carboxylate complex with various salts

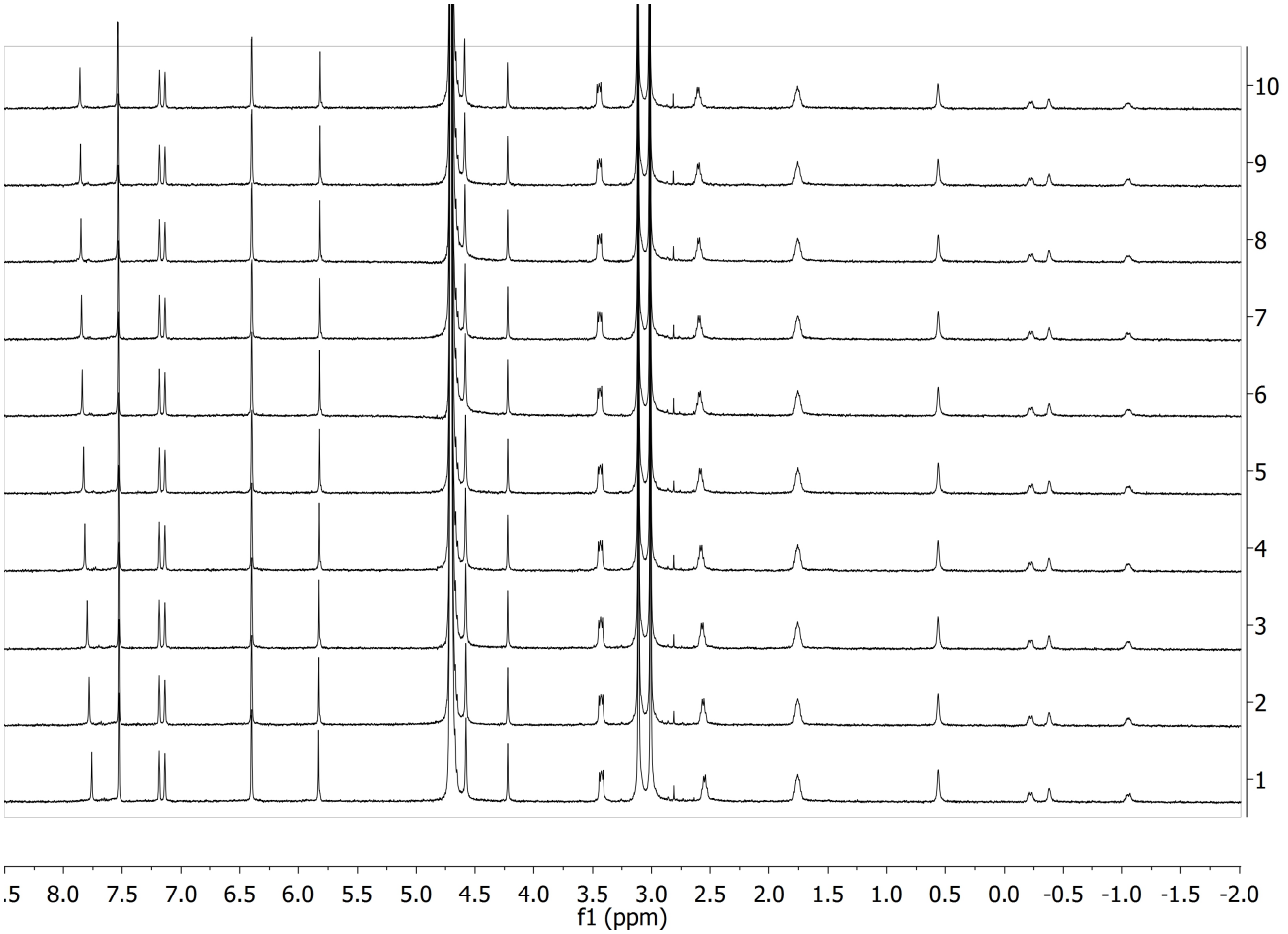

Figure S12: Representative NMR titration of the **2**.adamantane carboxylate complex with NaCl (up to 100 equivalents).

Figure S13: Fitting of H_j shift ($\Delta\delta$ ppm) from S12 using a 1:1 model.

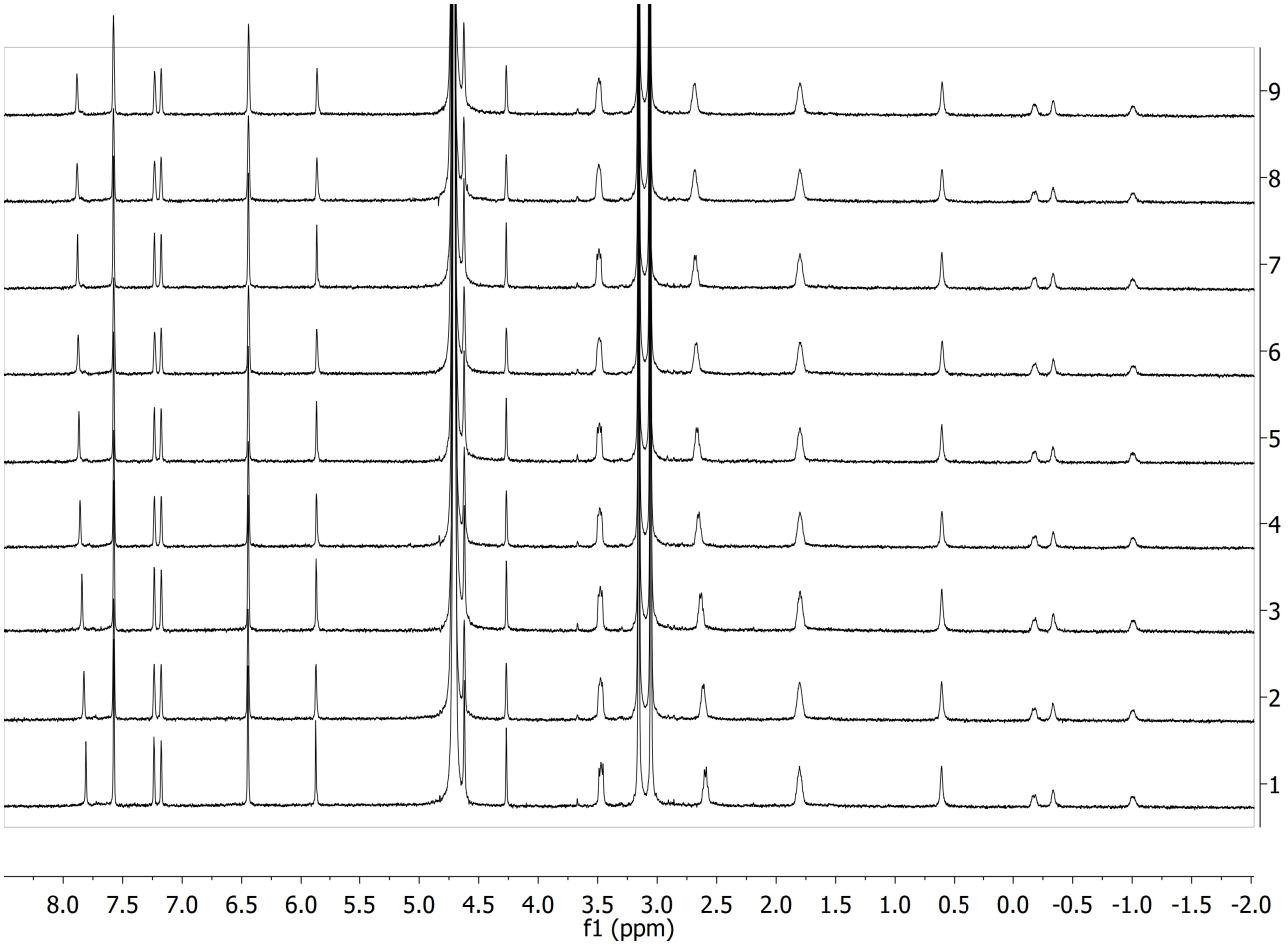

Figure S14: Representative NMR titration of the **2**.adamantane carboxylate complex with NaBr (up to 13 equivalents).

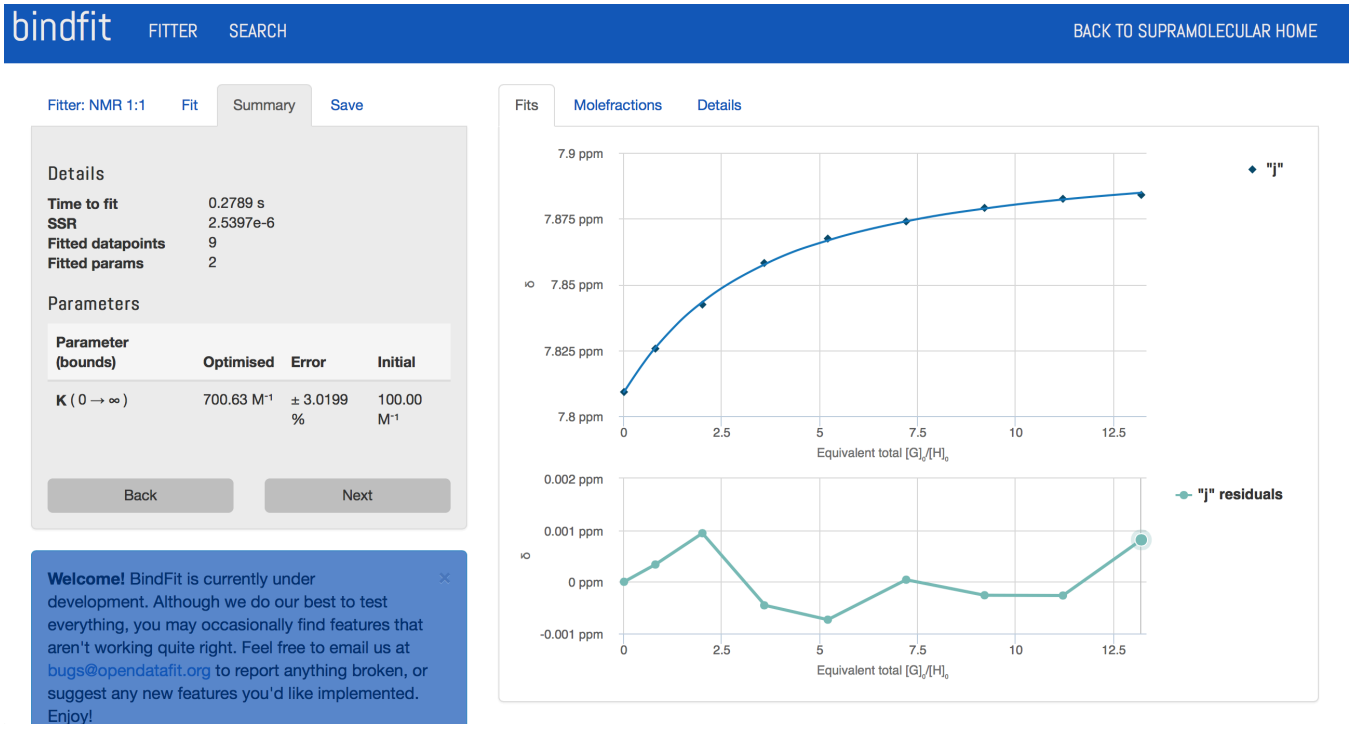

Figure S15: Fitting of H_j shift (Δδ ppm) from S14 using a 1:1 model.

The situation was different with the precipitating anions: iodide (I^-), thiocyanate (SCN^-), tetrafluoroborate (BF_4^-), cyanoborohydride (BH_3CN^-), perchlorate (ClO_4^-), perrhenate (ReO_4^-), triflate ($CF_3SO_3^-$), and hexafluorophosphate (PF_6^-), particularly for ClO_4^-, ReO_4^-, PF_6^-. Figure S16 to S31 show typical titrations and BINDFIT results for each of these precipitating anions.

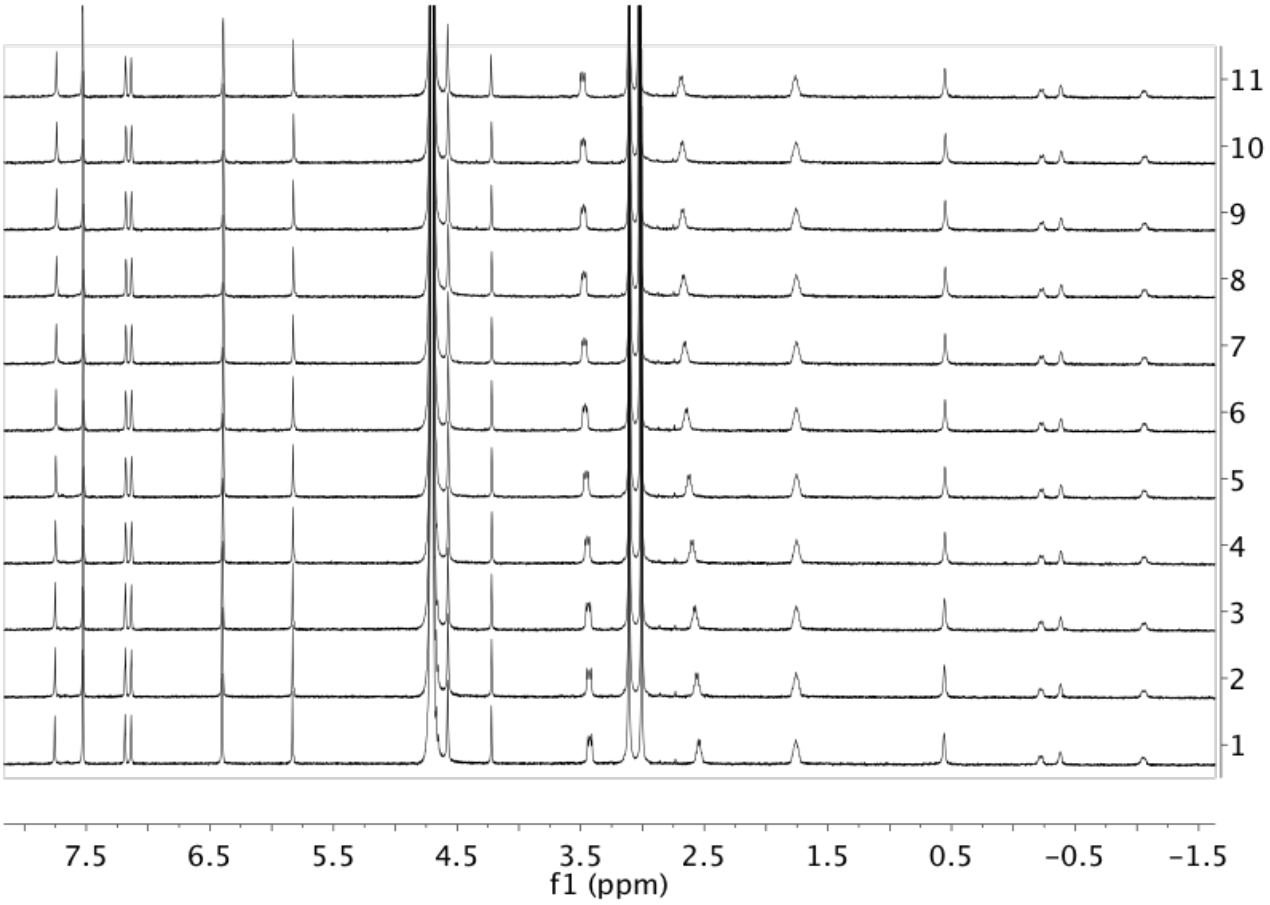

Figure S16: Representative NMR titration of the **2**.adamantane carboxylate complex with NaI (up to 5.6 equivalents).

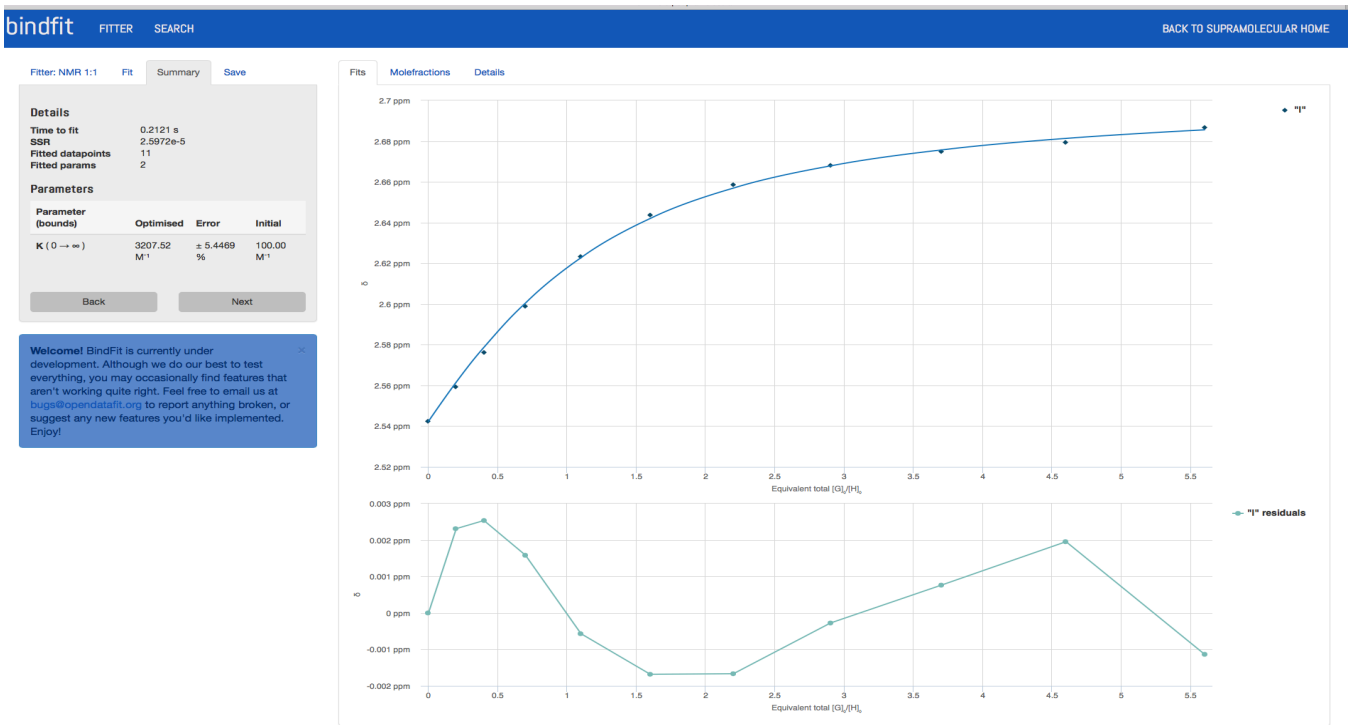

Figure S17: Fitting of H_I shift ($\Delta\delta$ ppm) from S16 using a 1:1 model.

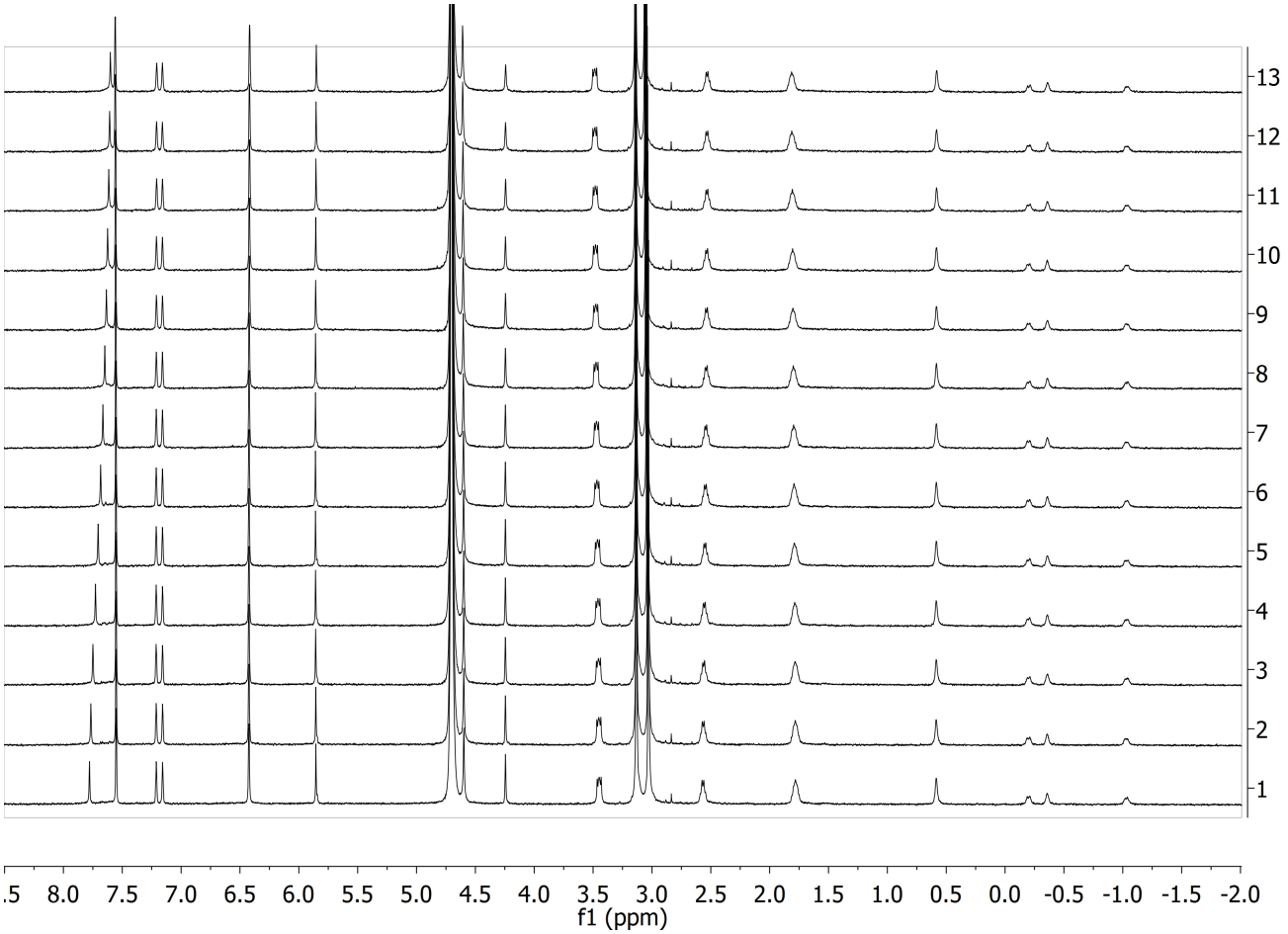

Figure S18: Representative NMR titration of the **2**.adamantane carboxylate complex with NaSCN (up to 9.3 equivalents).

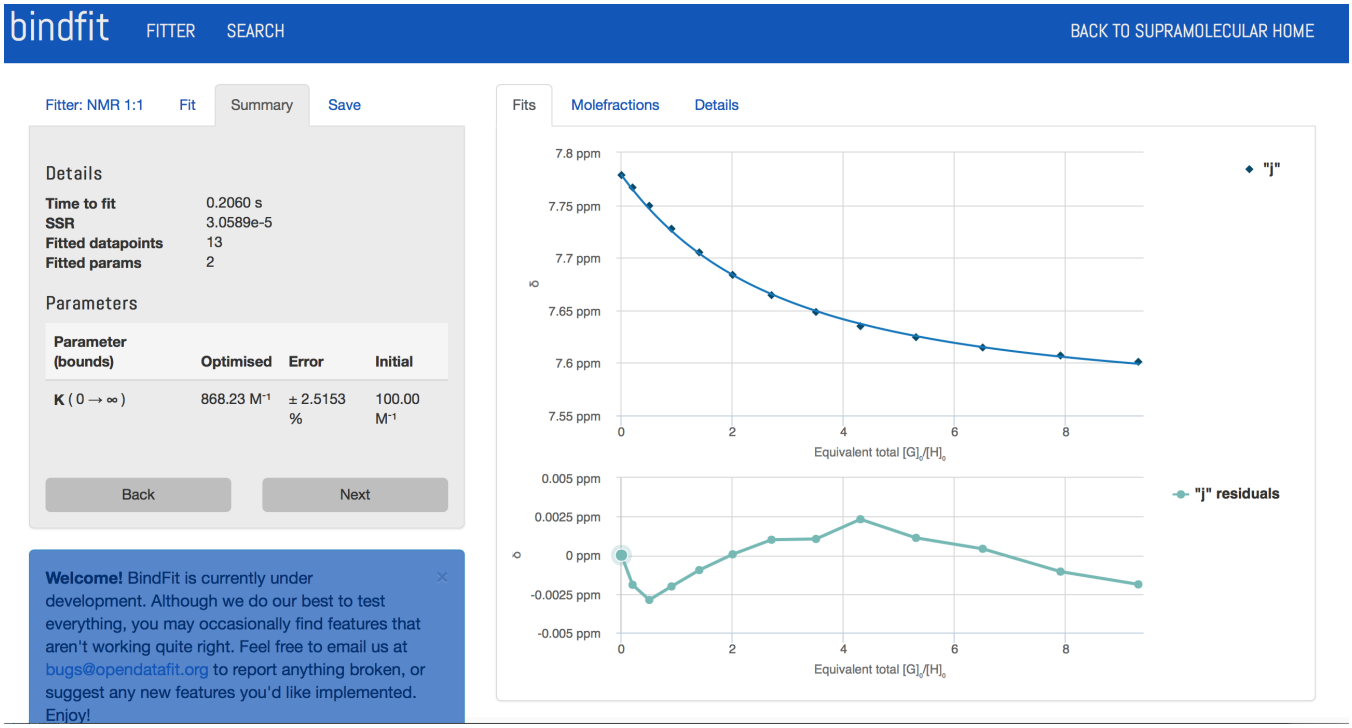

Figure S19: Fitting of H_j shift ($\Delta\delta$ ppm) from S18 using a 1:1 model.

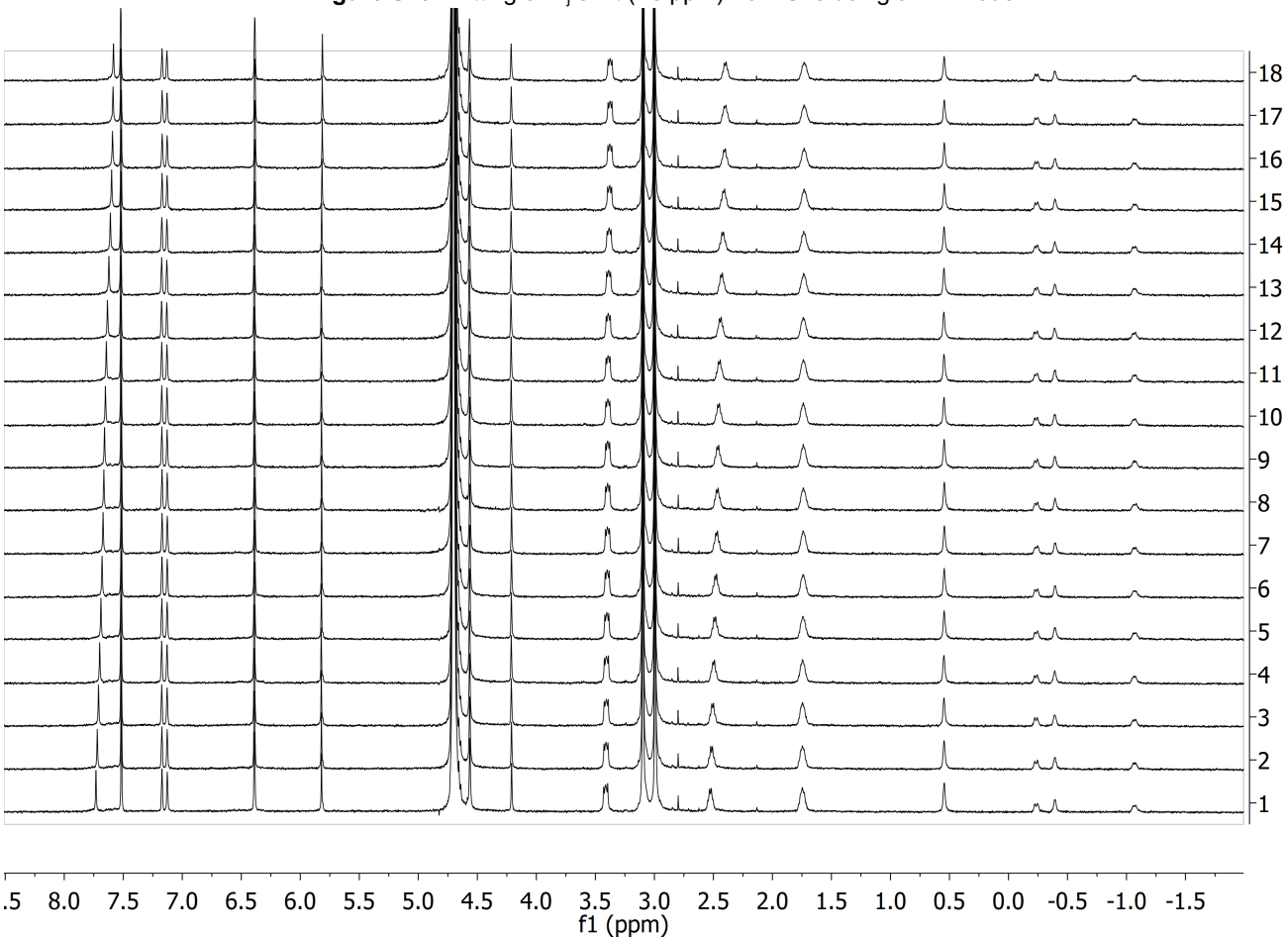

Figure S20: Representative NMR titration of the **2**.adamantane carboxylate complex with $NaBF_4$ (up to 10.5 equivalents).

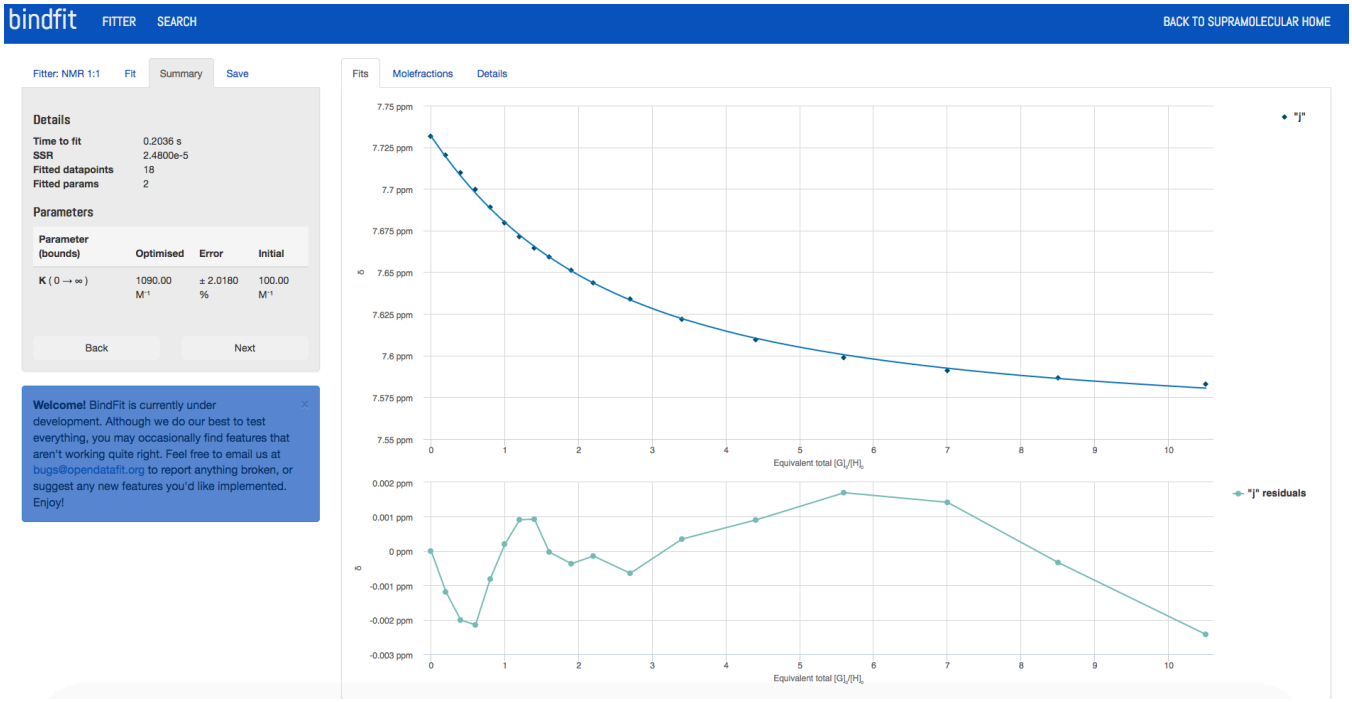

Figure S21: Fitting of H_j shift ($\Delta\delta$ ppm) from S20 using a 1:1 model.

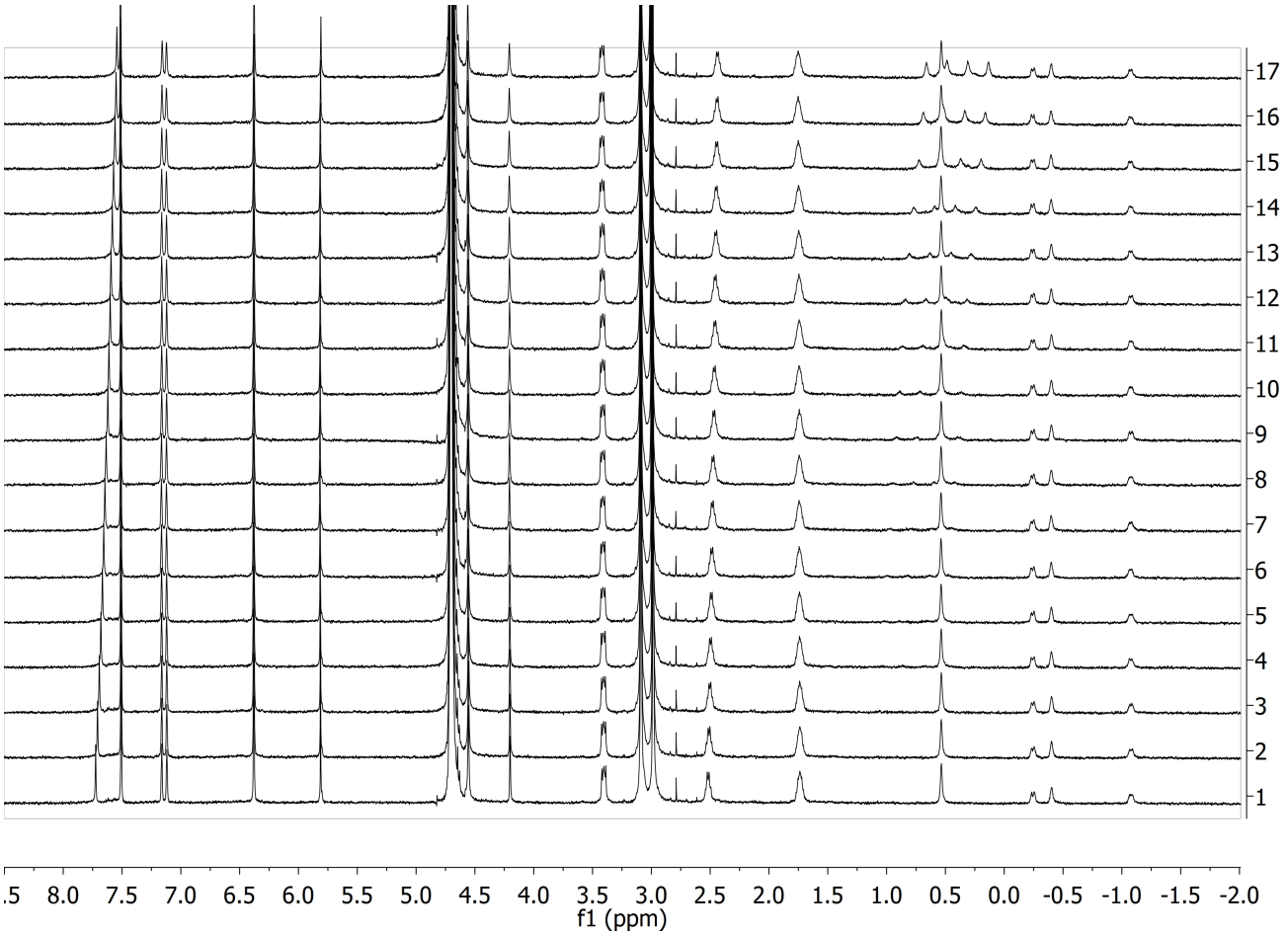

Figure S22: Representative NMR titration of the **2**.adamantane carboxylate complex with $NaCNBH_3$ (up to 7.2 equivalents).

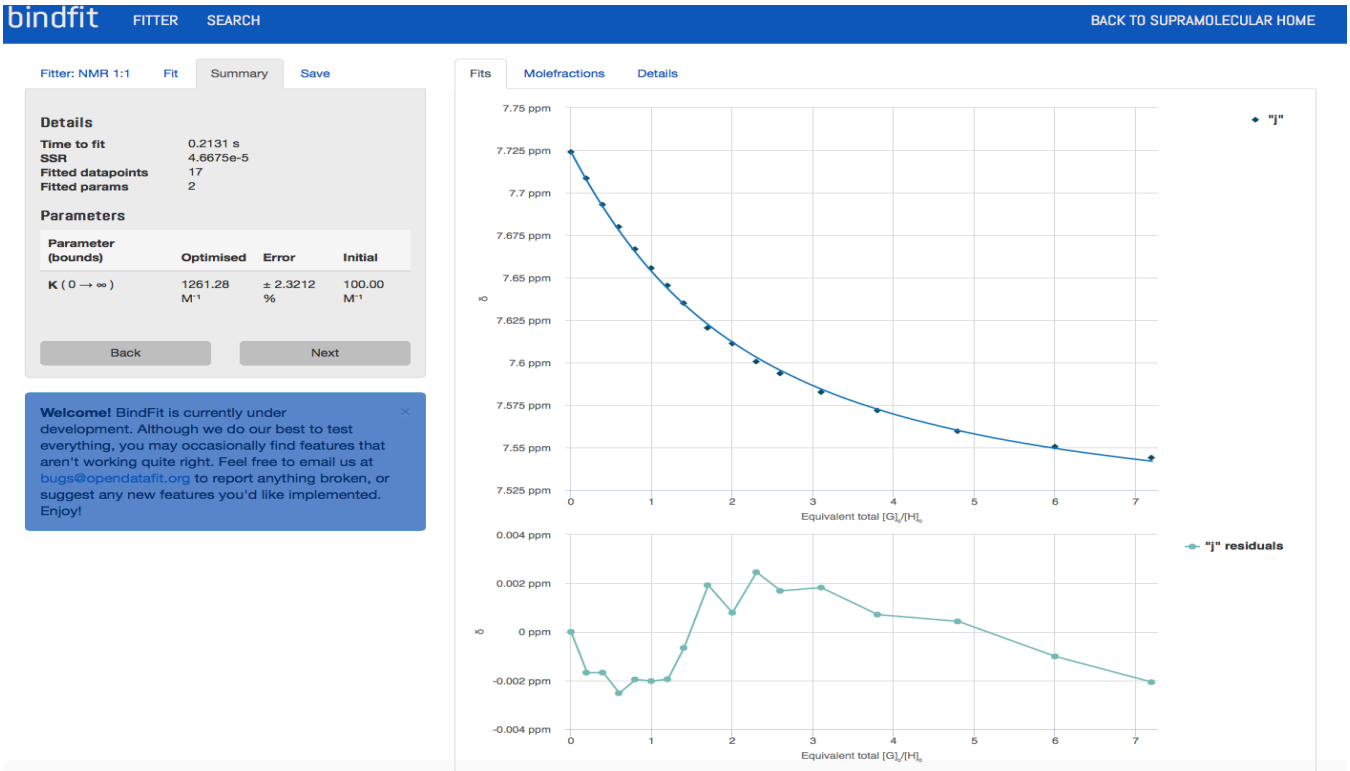

Figure S23: Fitting of H_j shift ($\Delta\delta$ ppm) from S22 using a 1:1 model.

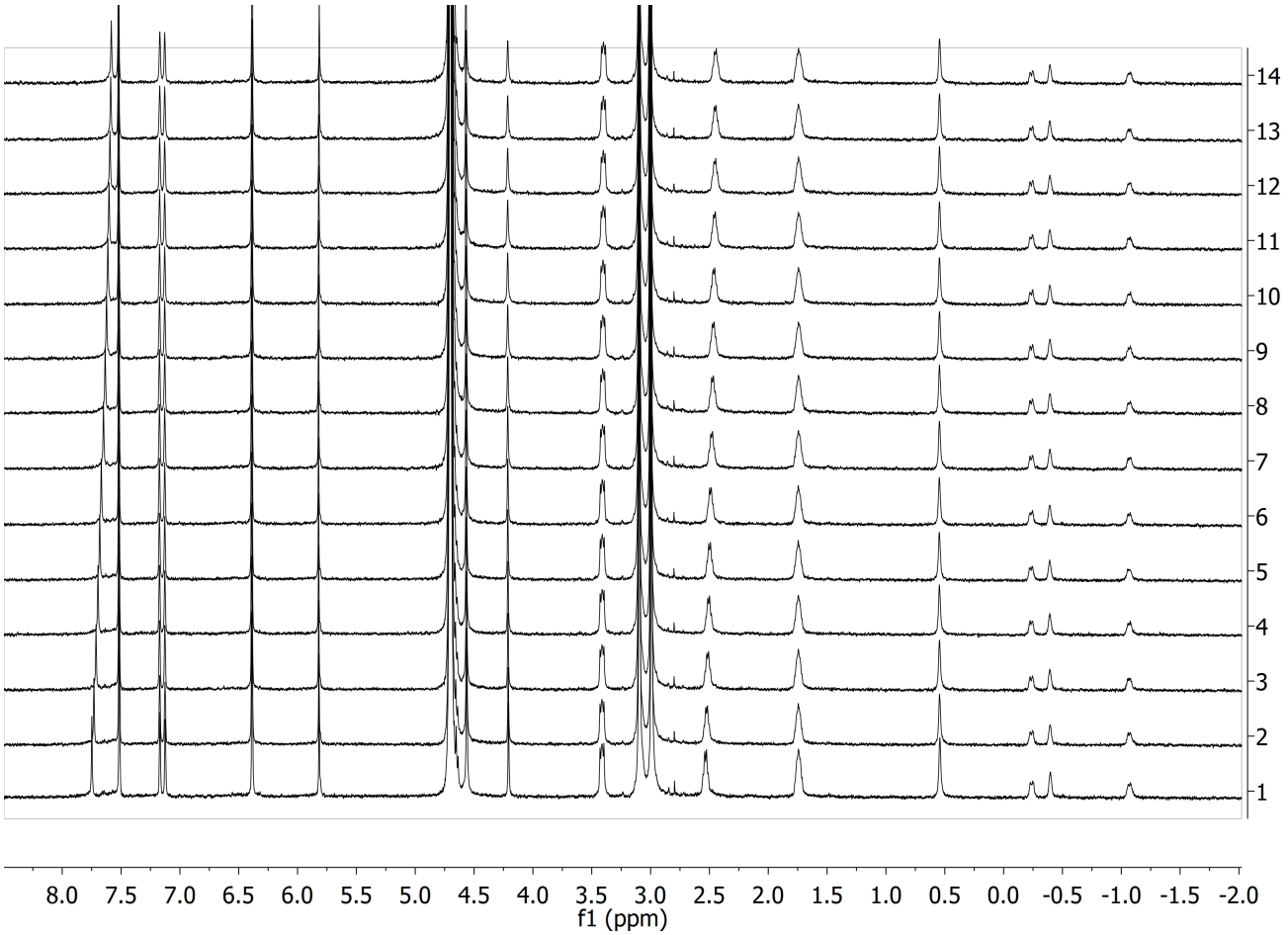

Figure S24: Representative NMR titration of the **2**.adamantane carboxylate complex with $NaClO_4$ (up to 4.9 equivalents).

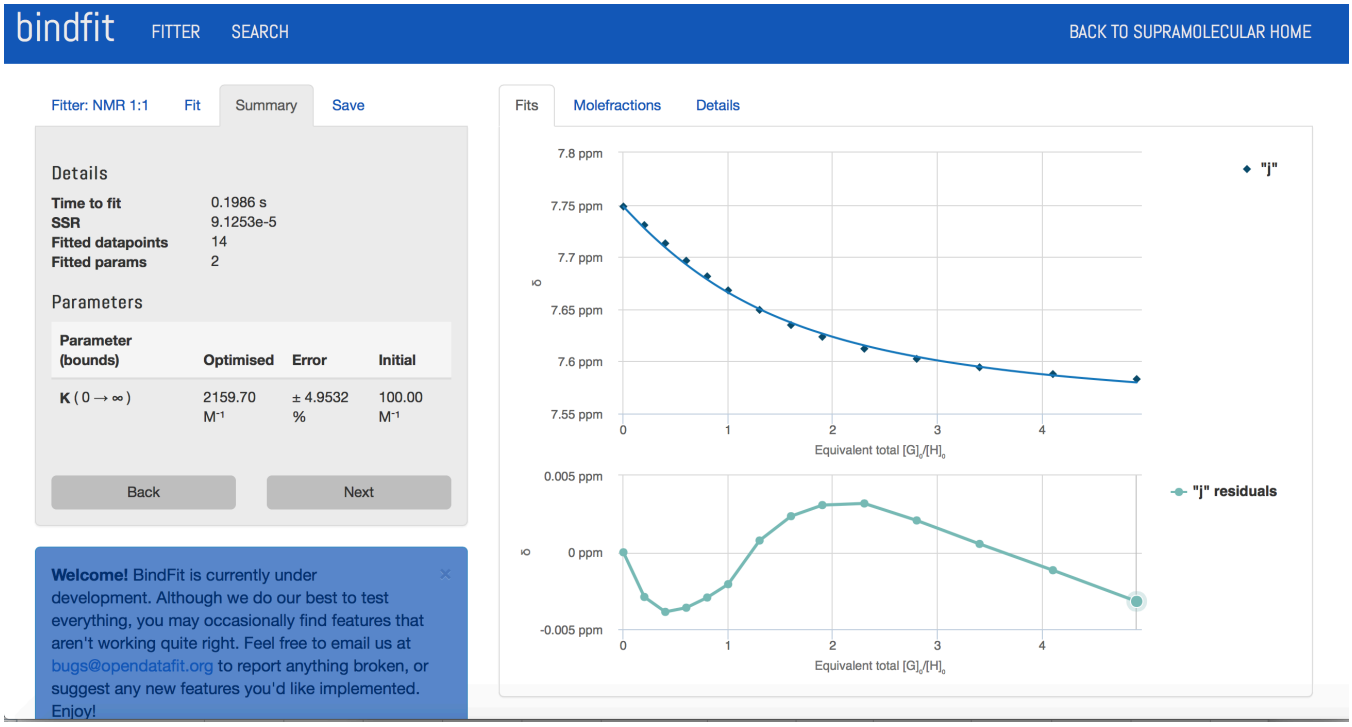

Figure S25: Fitting of H_j shift (Δδ ppm) from S24 using a 1:1 model.

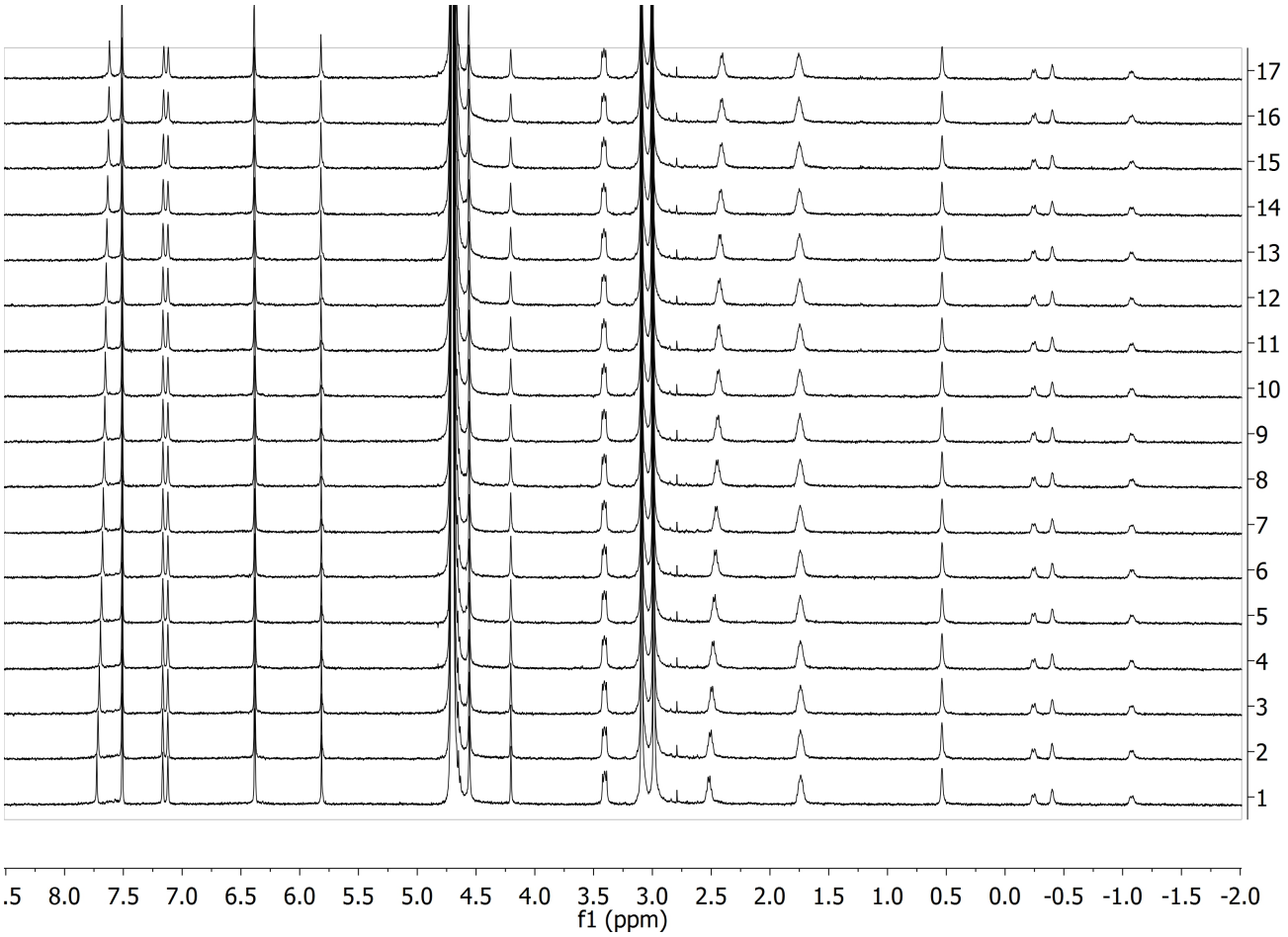

Figure S26: Representative NMR titration of the **2**.adamantane carboxylate complex with $NaReO_4$ (up to 6 equivalents).

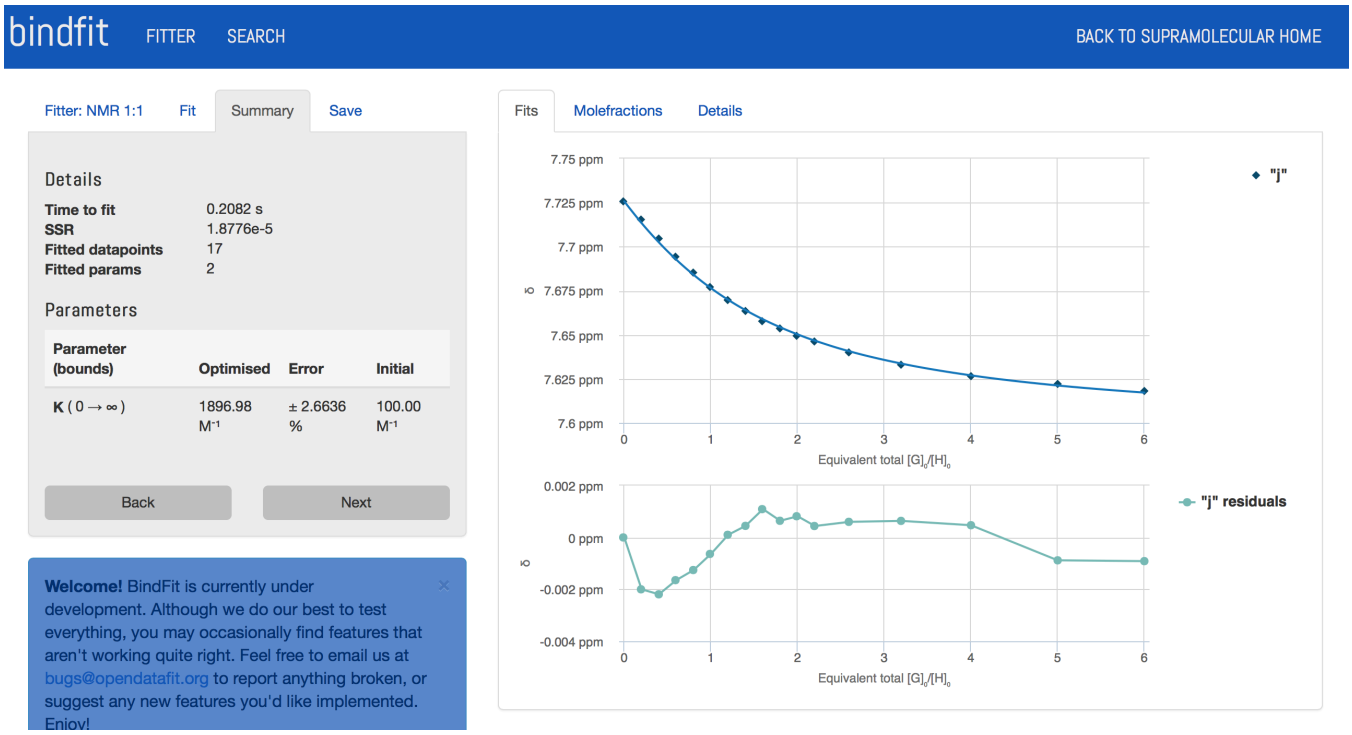

Figure S27: Fitting of H_j shift ($\Delta\delta$ ppm) from S26 using a 1:1 model.

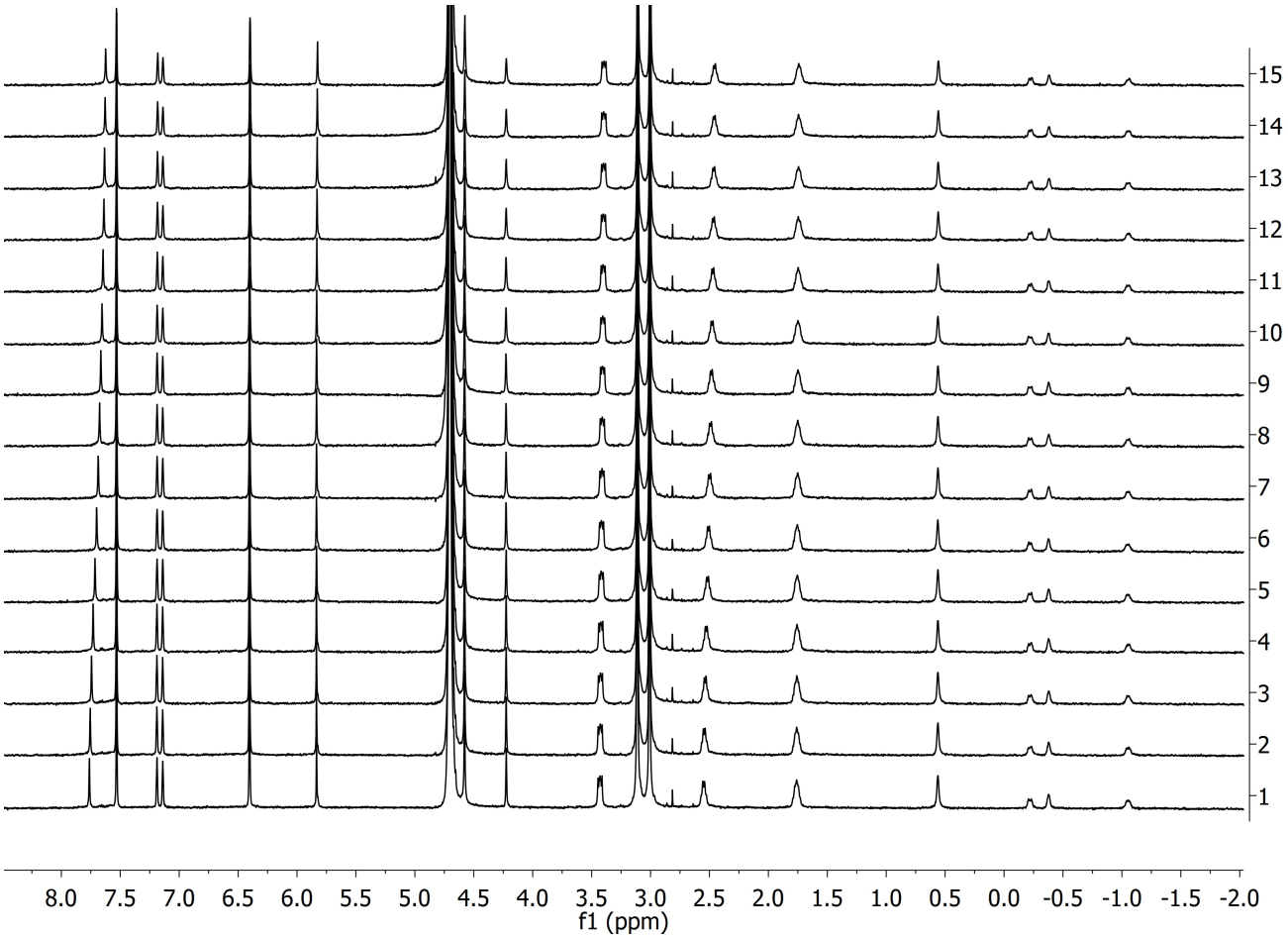

Figure S28: Representative NMR titration of the **2**.adamantane carboxylate complex with $NaCF_3SO_3$ (up to 15.5 equivalents).

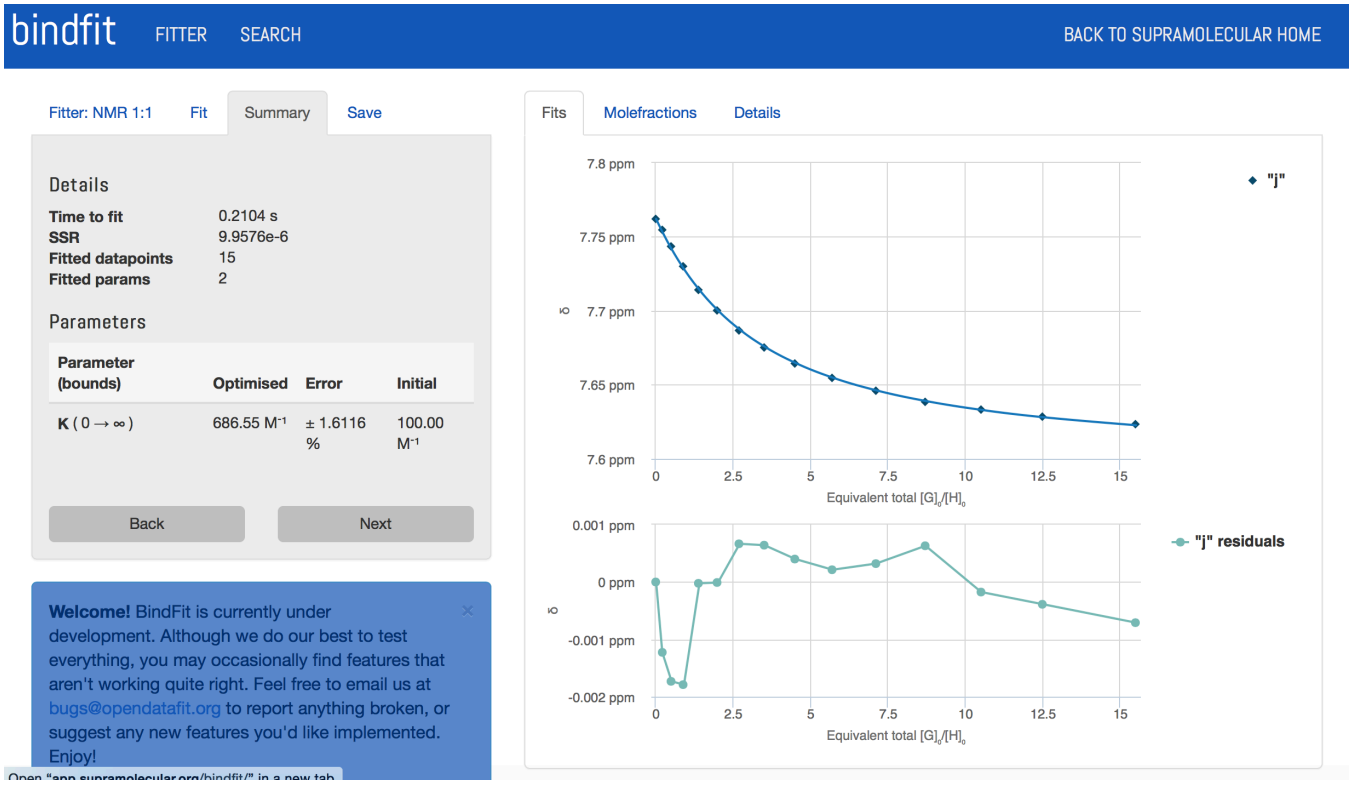

Figure S29: Fitting of H_j shift (Δδ ppm) from S28 using a 1:1 model.

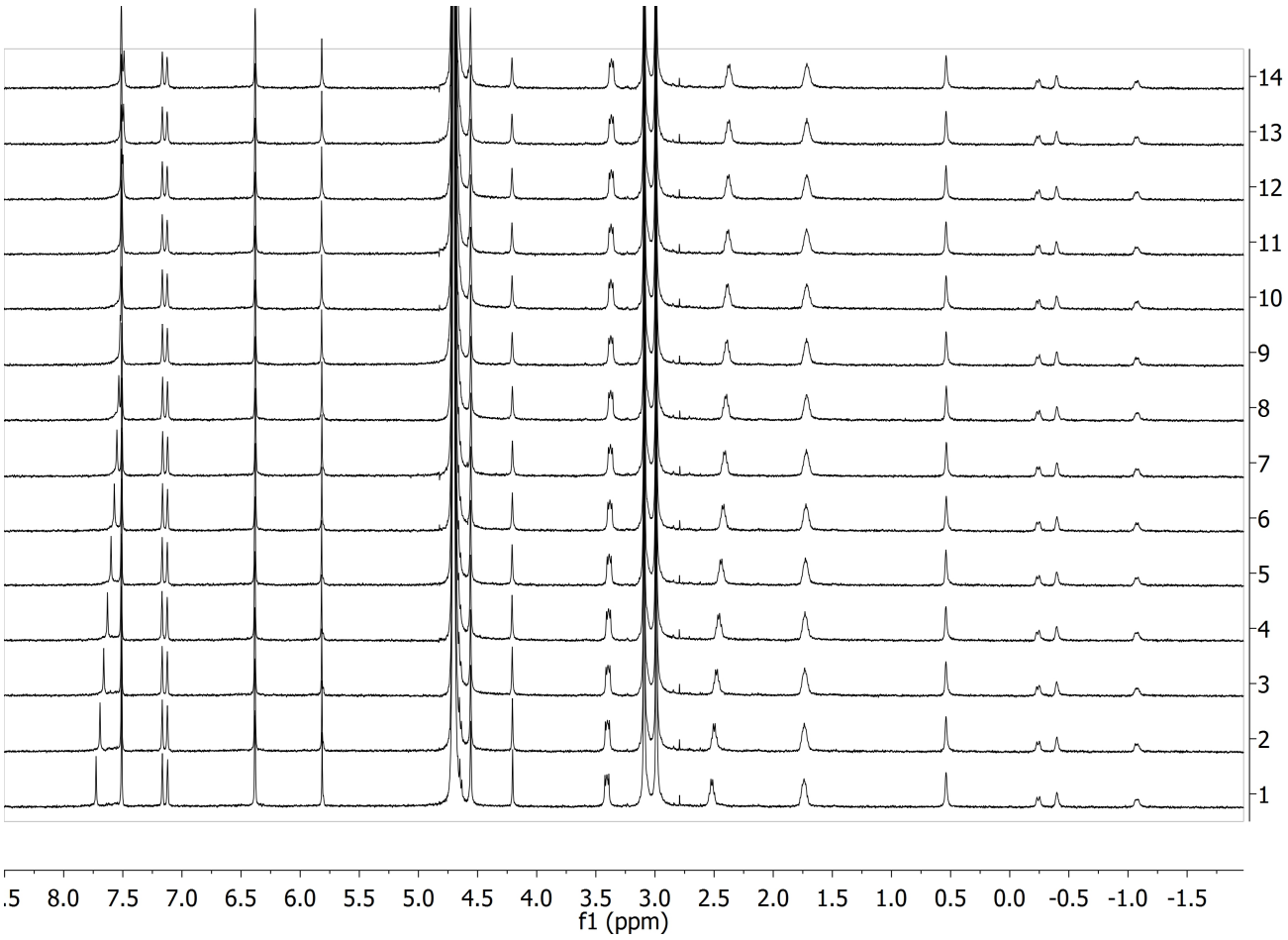

Figure S30: Representative NMR titration of the **2**.adamantane carboxylate complex with $NaPF_6$ (up to 2.6 equivalents).

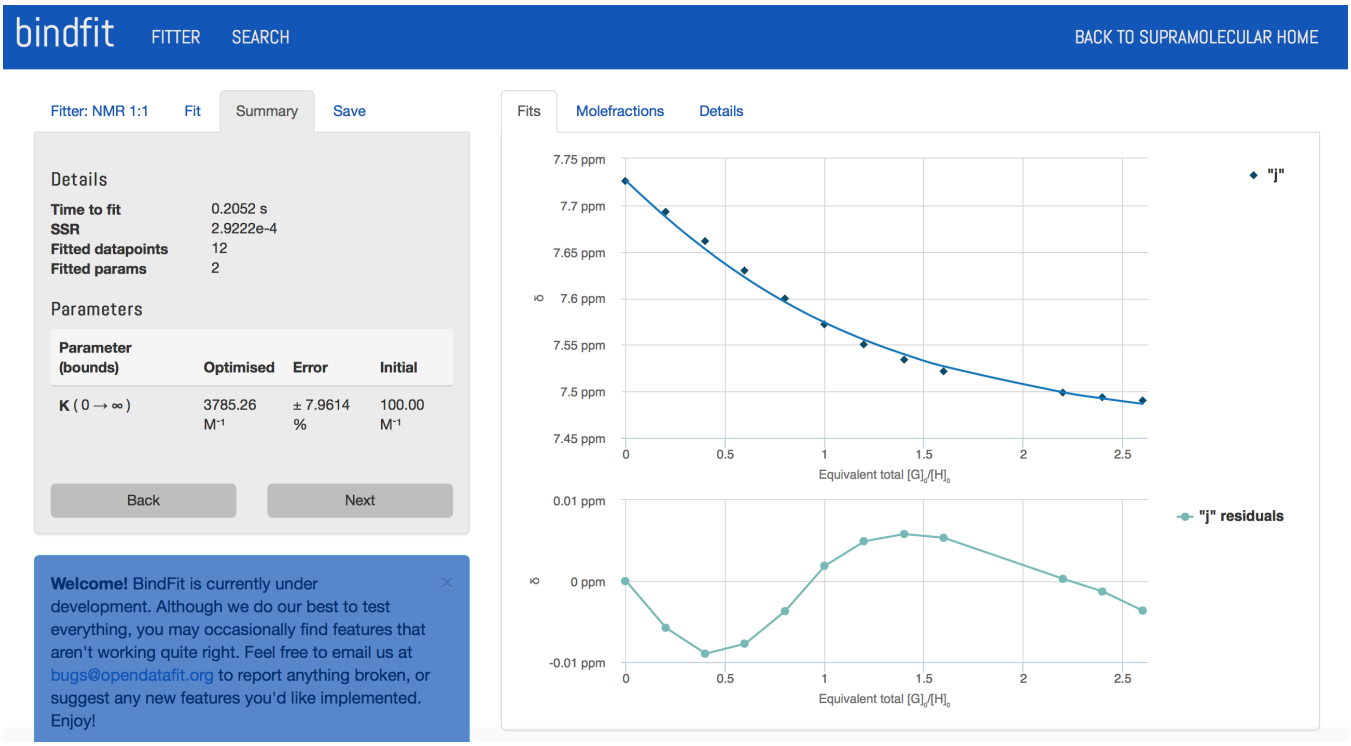

Figure S31: Fitting of H_j shift ($\Delta\delta$ ppm) from S30 using a 1:1 model.

Table S3 summarizes these results, giving the average K_a, coefficient of variation (%), % error of the fit using BINDFIT, and the average covariance in fit resulting from at least three titrations taken to ~80% complexation. As the fit of the resulting binding isotherms is not ideal (observed systematic error visual in the residual graph), the reported values for K_a are estimates of the true affinity. The residuals of fit indicate a systematic error typified by Figures S25 (ClO_4^-) and S31 (PF_6^-). This misfit, especially prevalent for anions inducing precipitation at low concentrations, is expected considering the stronger pseudo specific binding contributing to precipitation. The poorest fits were observed for ClO_4^-, ReO_4^-, and PF_6^- (Table S3).

It was noted that in contrast to the cases of well-behaved systems, the fitting results of these anions were dependent upon how near to saturation the titration was taken, particularly for the highest precipitating salts (Figure S32). In the case of the strongest precipitating anions we expect the pseudo specific interactions to be significant enough to invalidate the prior assumption (Eq. 3) such that:

$$G_t = [G] + [HG]_{crown} + n[HG_n]_{other} \neq [G] + [HG]_{crown} \qquad \text{Eq. (4)}$$

In these cases, $n[HG_n]_{other}$ is significant, and the concentration of these species becomes more prevalent and significantly affects the concentration of anion available for binding to the crown. Disappointingly, the model for binding at the crown and multiple external interactions is too complex to fit the obtained data, especially with probable cooperativity between different sites. However, the reported values for K_a in Table S3 are a very good estimation of the binding of the anions at the crown.

Salt	K^{a}_{crown} (M^{-1})	Coeffficient of Variation (%)	Average Error (%) in fit	Average Covariance in fit
$NaPF_6$	3600[a,c]	7	7	4.7×10^{-03}
CF_3SO_3Na	710[a]	6	1	4.5×10^{-04}
$NaReO_4$	1800[a,c]	9	3.1	2.3×10^{-03}
$NaClO_4$	2400[a,c]	11	4.7	1.6×10^{-03}
$NaBH_3CN$	1300[a]	9	2.3	7.0×10^{-04}
$NaBF_4$	1200[a]	14	2.1	4.7×10^{-04}
$NaSCN$	830[a]	8	2.0	5.2×10^{-04}
NaI	3200[b]	17	5.3	1.1×10^{-03}
$NaO_2C_2Cl_3$	—[d]		NA	NA
$NaCl_2CHCO_2$	—[e]		NA	NA
$NaBr$	740	8	3.2	6.3×10^{-04}
$NaNO_3$	180	9	2.0	5.2×10^{-04}
$NaCl$	120	5	1	7.5×10^{-05}
NaF	—[e]		NA	NA

[a] Apparent K_a with 1:1 model using H_j signal.
[b] Apparent K_a with 1:1 model fitting the H_l signal.
[c] Poor fit due to multiple binding sites.
[d] Competes with non-polar pocket, not possible to estimate 1:1 binding to crown.
[e] Too weak to measure accurately.

Table S3: Summary of 1:1 fitting of the titration of **2**.adamantane carboxylate complex with various salts.

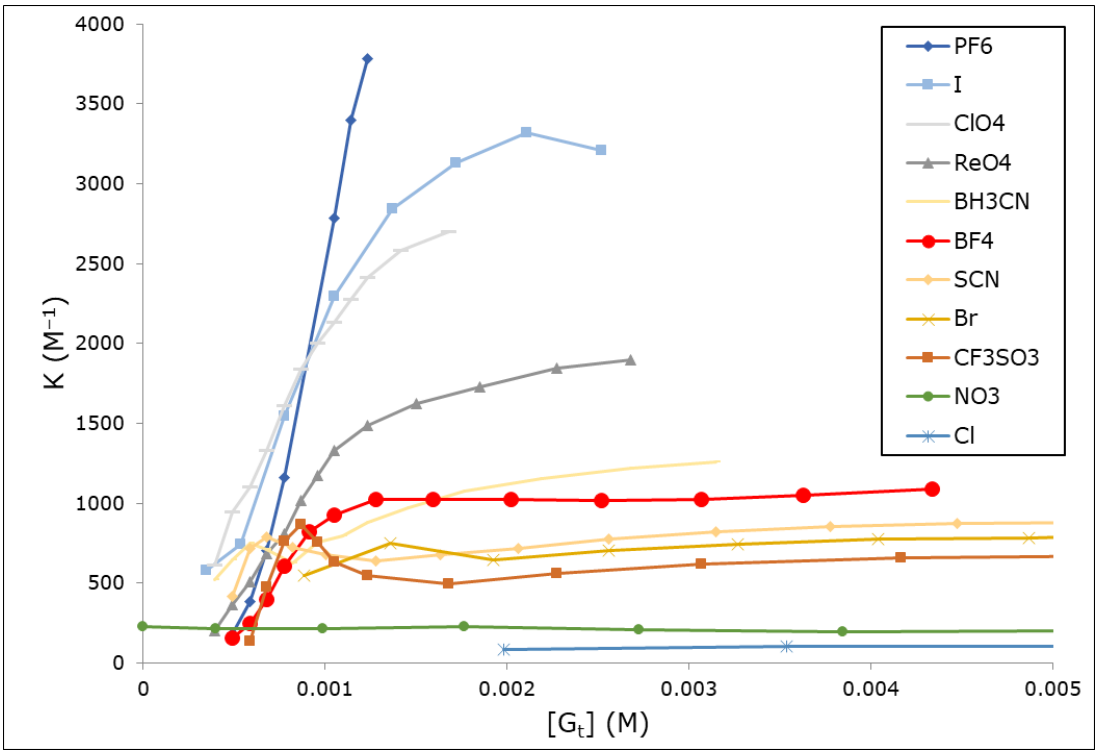

Figure S32: Variation in binding constant (K_a) as a function of limiting data for titration points between ~40 and 80% complexation.

d. ^{1}H NMR titrations of free positand **2** with salts

After characterization of the binding at the crown from the study of the blocked cavity, it is possible to study the binding of the free positand **2** and evaluate the binding in the cavity for the same sodium salts. For each anion, similarly to the studies with the blocked cavity, a ^{1}H NMR titration of the free host was carried out in an effort to determine the binding constant of the anion in the cavity (see example Figure S33). Figure S34 summarizes the data, showing an example of the shift in H_b proton for each anion. Monitoring changes in the H_b signal as a function of host-salt ratio revealed that chloride (Cl^-) and fluoride (F^-) did not bind to the cavity or bound too weakly to accurately yield a binding constant. H_b signal shifts were observed for the other anions. Eq. 5 defines the mass balance equation for these titrations:

$$G_t = [G] + [HG]_{cavity} + [HG]_{crown} + n[HG_n]_{other} \qquad \text{Eq. (5)}$$

where $[G_t]$ is the total guest concentration, $[HG]_{cavity}$ is the concentration of the host-guest complex for the anion binding to the cavity, $[HG]_{crown}$ is the concentration of the complex with the anion binding to the cationic crown at the feet of the cavitand, and $[HG_n]_{other}$ is the concentration of the complexes arising from pseudo specific complexations.

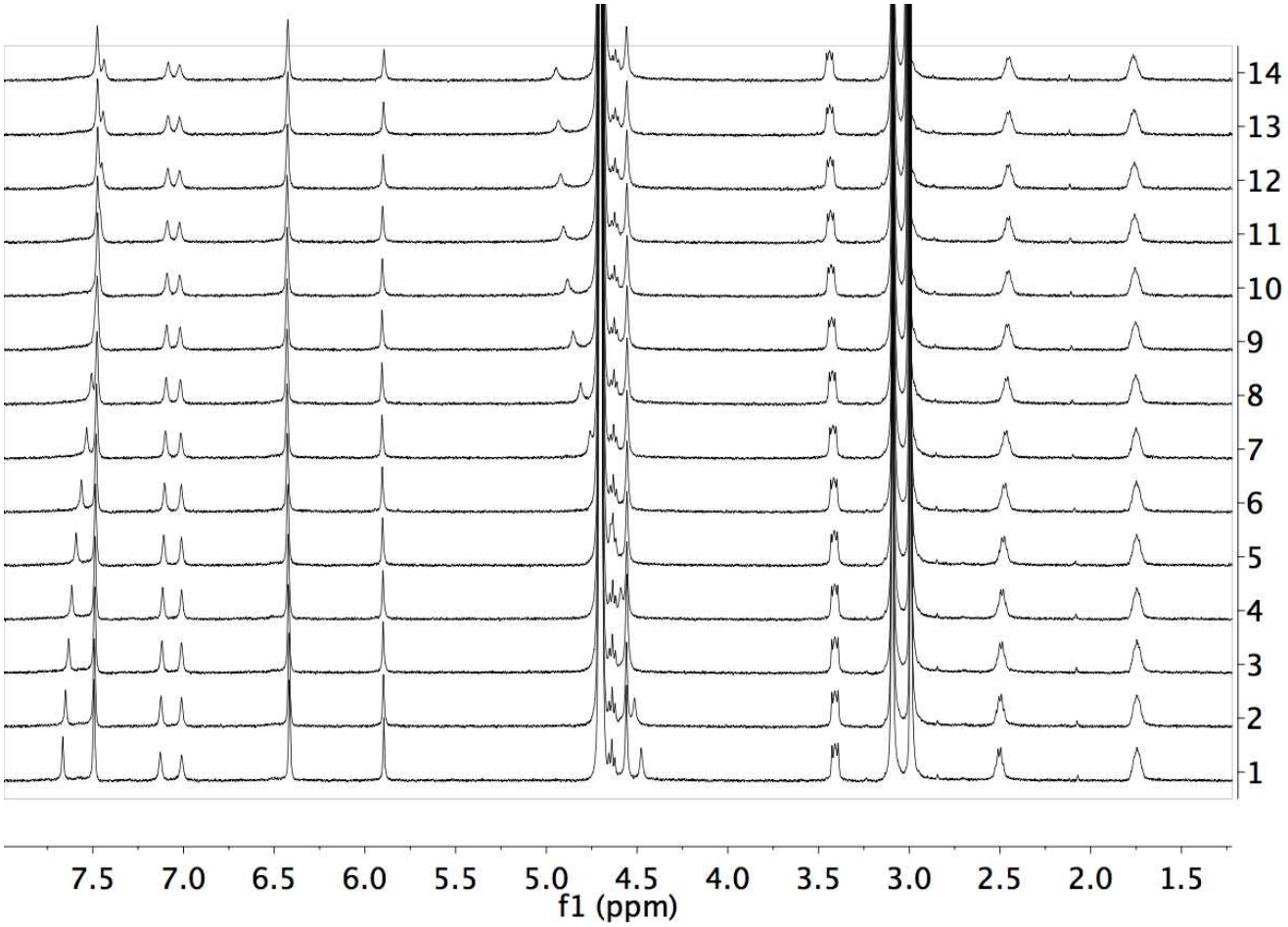

Figure S33: Representative NMR titration of free **2** with NaSCN (up to 8.5 equivalents).

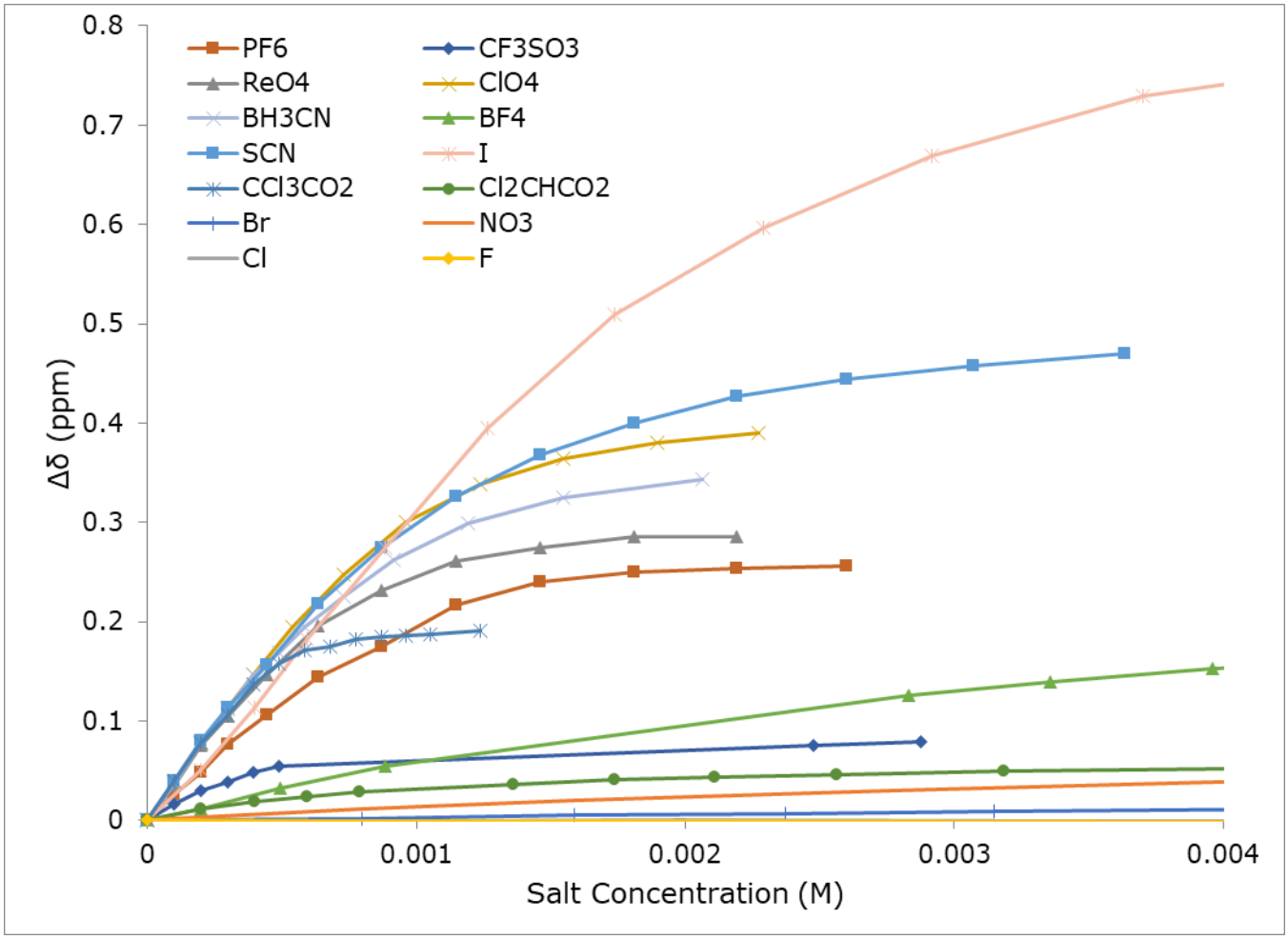

Figure S34: Plots of the shifts of the H_b proton vs. concentration of sodium salt added to the free positand **2** (0.5 mM), 10 mM phosphate pD 7.3.

In the same fashion as the analyses of the complex above, the titration conditions allowed Eq. (5) to be simplified to:

$$G_t \approx [G] + [HG]_{cavity} + [HG]_{crown} \qquad \text{Eq. (6)}$$

since we can assume again:

$$[G] + [HG]_{cavity} + [HG]_{crown} >> n[HG_n]_{other}$$

Using the 1:2 additive and non-cooperative model[4] and defining the microscopic constant as:

$$K_1 = K_{1cav} + K_{1crown}$$

$$K_2 = \frac{K_{2cav} + K_{2crown}}{K_{2cav} K_{2crown}}$$

Where k_{1cav} and k_{1crown} are the 1:1 microscopic binding constant respectively in the cavity or the crown of ammoniums and k_{2cav} and k_{2crown} are the microscopic constant of the binding of the anions to the 1:1 complex (HG_{crown} and HG_{cavity} respectively) resulting in HG_2.

Since we are assuming non-cooperativity:

$$K_{1cav} = K_{2cav} = K_{cav}$$

$$K_{1crown} = K_{2crown} = K_{crown}$$

Hence,

$$K_1 = K_{cav} + K_{crown}$$

$$K_2 = \frac{K_{cav} + K_{crown}}{K_{cav} K_{crown}} \qquad \text{Eq. (7)}$$

Following the derivations from Thodarson 1:2 binding[4] we can solve for the free guest concentration [G] using the macroscopic constant K_1 and K_2, then calculate the observed shift of H_b using Eq. (8) (derived from the same principle as the $\Delta\delta$ in Thodarson's review[4]):

$$\Delta\delta_{obs} = \frac{K_{cav}[G]\Delta\delta_{HG_{cav}} + K_{crown}[G]\Delta\delta_{HG_{crown}} + K_1K_2[G]^2\Delta\delta_{HG_2}}{1 + k_{cav}[G] + K_{crown}[G] + K_1K_2[G]^2} \qquad \text{Eq. (8)}$$

Where in our case for the proton H_b:

$\Delta\delta_{HG_{cav}}$ is the maximum shift of H_b with binding in the cavity, and

$\Delta\delta_{HG_{feet}}$ is zero as H_b does not shift upon binding at the crown.

Hence, for H_b

$$\Delta\delta_{HG_2} = \Delta\delta_{HG_{cav}} \qquad \text{Eq. (9)}$$

It follows that Eq. (8) can be simplified to

$$\Delta\delta_{obs} = \frac{K_{cav}[G]\Delta\delta_{HG_{cav}} + K_1K_2[G]^2\Delta\delta_{HG_{cav}}}{1 + K_{cav}[G] + K_{cronn}[G] + K_1K_2[G]^2} \qquad \text{Eq. (10)}$$

Note that attempts at fitting the shift of H_j or H_b globally using the 1:2 model did not yield stable or logical solutions, as the introduction of the shifts introduces extra unknowns since we do not have the same simplification as Eq. 9.

The experimental data obtained from the titration of the free host from Figure S34 could be fitted with SOLVER iteratively with Eq. (10) using the binding constant k_{crown} determined from the studies on the blocked positand **2** (Table S3), Eq (6) as well as the solution to [G] from a typical 1:2 binding model[4]. One is left with a simple fitting with two unknown: the microscopic constant K_a^{cav} and $\Delta\delta_{HG_{cav}}$ This effectively becomes a simple competitive binding model.

Figure S35 shows the results when fitting the data obtained from titration of SCN^- to the free host **2**. Table 4 summarized the results and gives the estimate of the bindings constant to the cavity and associated error for the various sodium anions from the average of fitting three separate titrations.

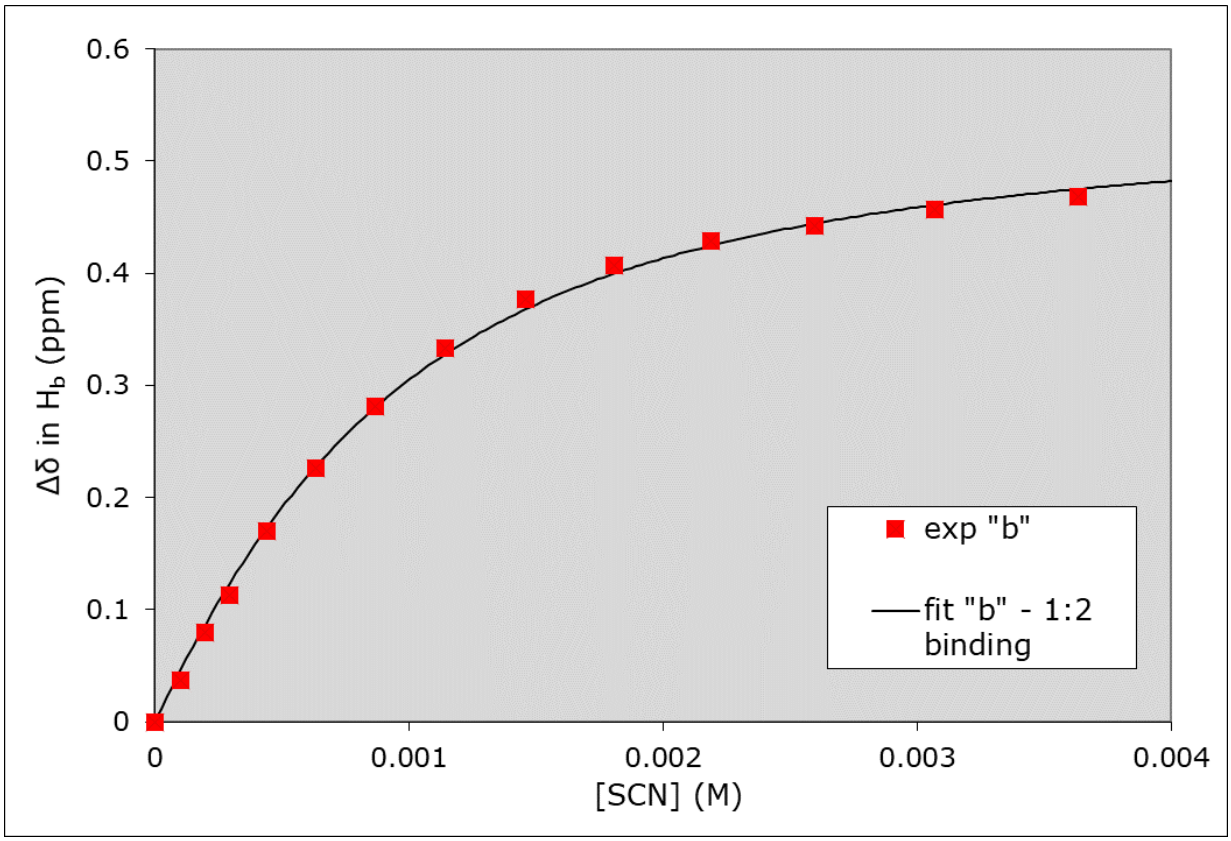

Figure S35 shows an example of the resulting fit using Eq.10 in the case of the titration of NaSCN to positand **2**.

Anion	$K_{cav}(M^{-1})$	*Coefficient of variation %*	*Average Covariance of Fit*
PF_6^-	>5000[a]	---	---
$CF_3SO_3^-$	>5000[b]	---	---
ReO_4^-	7200	5	1.05×10^{-3}
ClO_4^-	4300	5	1.57×10^{-3}
BH_3CN^-	3600	5	6.49×10^{-4}
BF_4^-	35	4	1.63×10^{-3}
SCN^-	2000	7	9.55×10^{-4}
I^-	930	6	2.79×10^{-3}
$CHCl_2CO_2^-$	1500[c]	6	2.02×10^{-3}
Br^-	17	37	1.83×10^{-3}
NO_3^-	95	5	1.80×10^{-3}
Cl^-	[d]	---	---
F^-	[d]	---	---
$CCl_3CO_2^-$	54500[e]	4	-----

[a] the H_b shift shows strong binding as saturation is observed at very low equivalence of anion. This strong binding and more prevalent non-specific binding did not allow determination of a stable or reproducible binding constant.
[b] strong binding observed in the shift of H_b, but unable to obtain enough data points around saturation as the H_b proton was hidden under the benzylic resonance at critical points during the titration.
[c] determined using a 1:1 binding model
[d] no binding or too weak to be measured
[e] Determined by ITC

Table S4: Selected sodium salts studied in depth. Binding constant (or estimate) of anions to the cavity determined from the titration of free positand **2** with sodium salts solution by NMR or ITC. Average of at least three titrations.

The guest trichloroacetate ($CCl_3CO_2^-$) was also observed to bind to the pocket of host **2** and only precipitated positand **2** at relatively high concentrations (> 100 mM). However, the binding of this anion to the cavity was too strong to be determined by NMR and was therefore measured directly by ITC to be 54,500 M^{-1} (± 4%) (see Section 3.B).

e. Titration of *p*–Toluic acid complex with ReO_4^-:

A solution of 0.5 mM positand **2**.*p*–toluic acid 1:1 complex was titrated with a solution of sodium perrhenate, see Figure S36. The bound *p*–toluic acid was displaced with the addition of sodium perrhenate. Only 3 eq of the anion was needed to displace 50% of the *p*–toluic acid (K = 3.05 × 10^4 M^{-1} see ITC section 3.B) and aggregation/precipitation was observed at higher concentration.

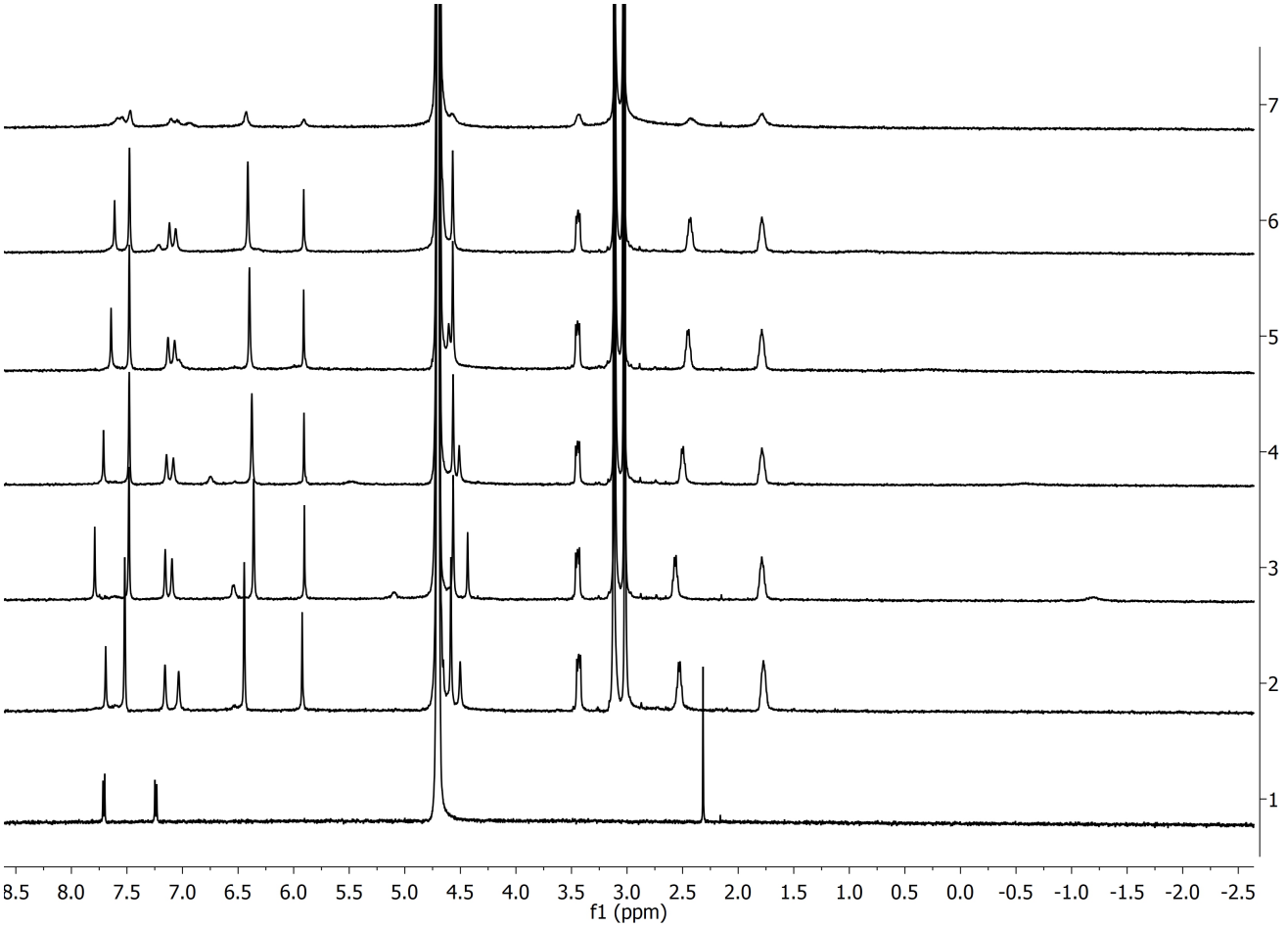

Figure S36: 1) 0.5 mM *p*–toluic acid, 2) 0.5 mM positand **2**, 3) 0.5 mM **2.**–-toluic acid complex (1:1), 4 – 7) titration of a solution of sodium perrhenate—1, 3, 6 and 60 eq. respectively.

B. Isothermal Titration Calorimetry Data

Micro-calorimetric experiments were performed using a VP-ITC isothermal titration calorimeter from MicroCal, USA. Each run consisted of 28 consecutive injections of the solutions of guest (the first injection was of 2 µl and the 27 next injections were of 9 µl) into the ITC reaction cell charged with a solution of positand **2**. Experiments were run at 25 ˚C with a stirring speed of 450 rpm. Integration of the heat released and curve fitting of the resulting binding isotherm to a 1:1 binding model (stoichiometry confirmed by NMR) were performed using ORIGIN 7.0 software included in the VP-ITC. A typical ITC run is shown in Figure S37. Each run was repeated three times, and the *K*, *ΔH*, *–TΔS* values are reported as the averages with their coefficient of variation (%) in Table S5 for adamantane carboxylate, $Cl_3C_2O_2^-$ and *para*-toluic acid.

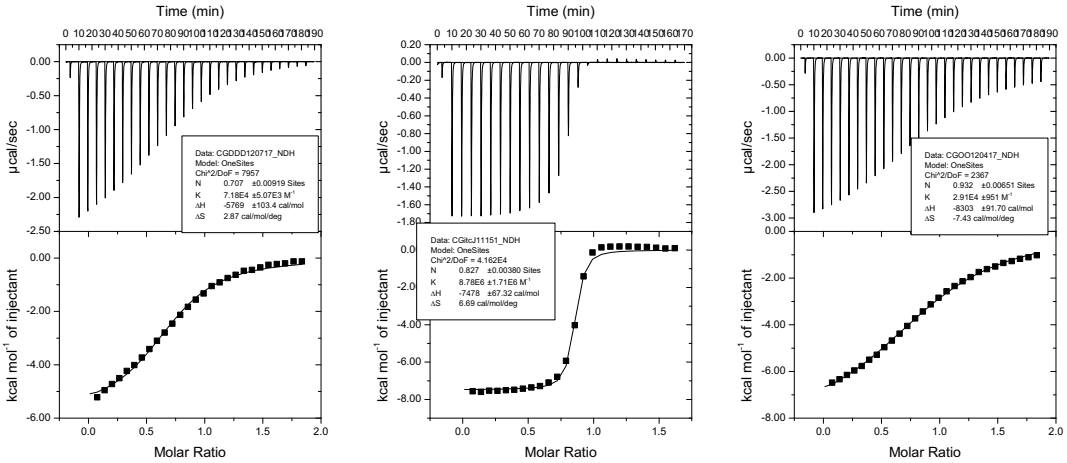

Figure S37: Example of ITC titration of left) 1.50 mM $Cl_3C_2O_2^-$ into 0.150 mM positand **2**, middle) 1.50 mM adamantane carboxylic acid to 0.150 mM positand **2,** and right) 1.50 mM *para*-toluic acid into 0.150 mM positand **2** in 10 mM phosphate buffer (pH = 11.3)

Guest	K_a (M^{-1})	ΔH	$-T\Delta S$
$Cl_3C_2O_2^-$	7.03×10^4 (± 5)	–-5780 (± 1)	-830 (± 4)
Ada–CO_2^-	7.21×10^6 (± 8)	–7510 (± 1)	–1850 (± 8)
para-Toluic acid	$3.05x\ 10^4$ (± 9)	-8308 (± 3)	1980 (± 10)

Table S5: Summary of 1:1 fitting of the titration of positand **2** with adamantane carboxylate**,** $Cl_3C_2O_2^-$ and *p*-toluic acid. Average of at least three titrations with %CV between parentheses.

C. Precipitation assay data

Solutions were prepared as described in sample preparation (Section 2.D). The total mixing time (of host and salt) for each plate was < 5.0 min. Plates were allowed to rest for 15 min and then read using an Enspire multimode plate reader at 500 nm equipped with a temperature controller set to 23 °C. The wavelength selected was chosen to minimize interference from the intrinsic absorbance of the anions (Figure S38) and to give sufficient signal for data analysis.

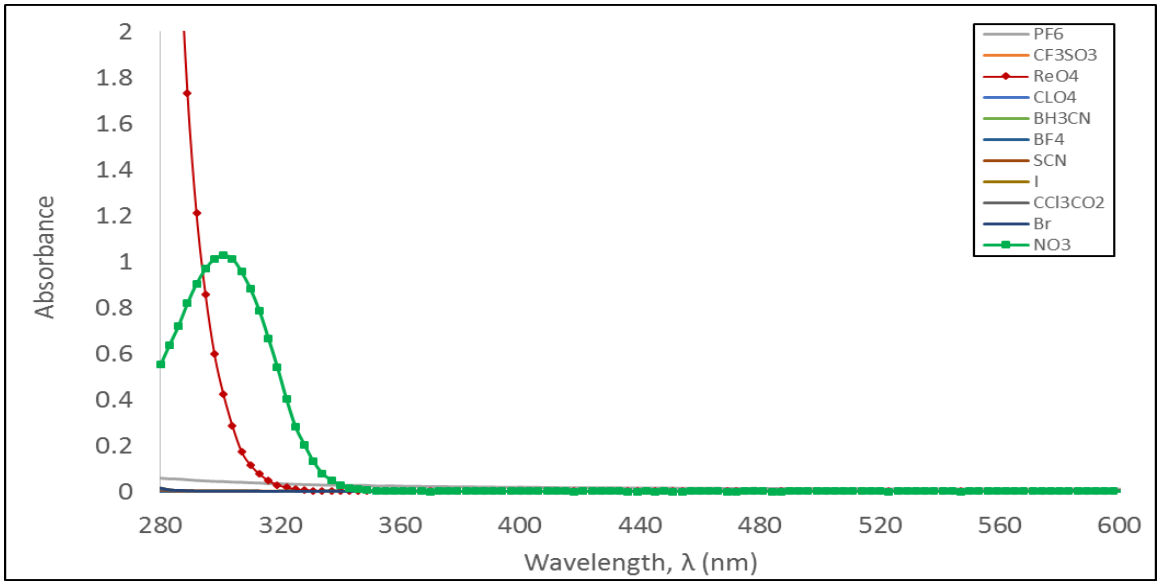

Figure S38: Graph of the UV-Vis Absorbance spectrum of precipitating salts from 280 – 600 nm. ReO_4^- marked with red diamonds (♦) and NO_3^- marked with green squares (■). All other anions had negligible absorbance at 500 nm.

a. Precipitation assay screening and CPC determinations

For initial screening (Figure S39), the spectrum scan (300 – 600 nm) for each well was obtained following the initial absorbance reading (Figure S40). Plate background absorption for all wells was measured at 0.038 ± 0.002. Solution turbidity was assessed as an increase in absorbance relative to baseline values at 500 nm, reference-subtracted and normalized values were then plotted using OriginPro software. Ranges for determination of the individual CPC fall between the screening assay concentrations in 0.5, 1, 2, 3 or 4 mM increments of salt depending on the expected precipitation concentration based on the initial screening assay.

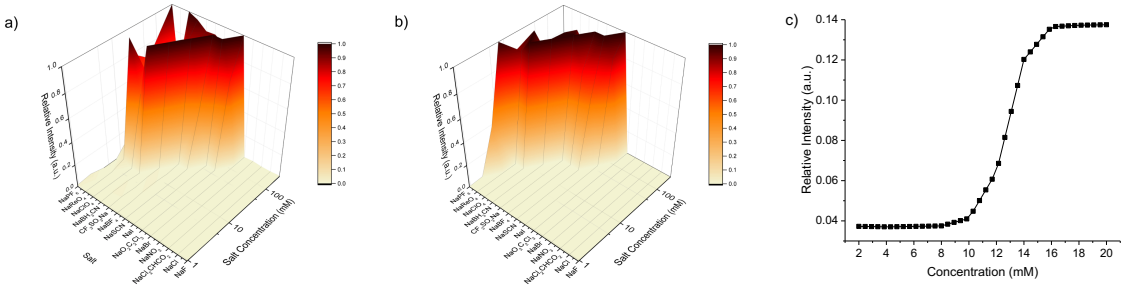

Figure 39. a) Surface plot of the normalized absorption intensity for **2** as measured by UV-spectroscopy; b) Surface plot of the normalized absorption intensity for the complex between **2** and Ada-CO_2^- as measured by UV-spectroscopy c) as an example, the averaged light scattering intensity curve obtained from triplicate measurements during CPC determination for ClO_4^- and the complex, derived from (b).

For determination of the CPC values, measurements were performed in at least triplicate from separate stock solutions of hosts and salts (Table S6). For each determination, 25 µL of host or host-guest complex (2.0 mM) were added to wells containing 25 µL buffer, 0–50 µL of salts of variable concentration, and 0–50 µL assay buffer for a final volume of 100 µL. At minimum three measurements were recorded from separate stock solutions of host and salt with the host added to the buffer-salt mixture once, the salt added to the buffer-host mixture, and then by increasing the initial concentration of salt and adding to the buffer-host mixture to ensure the order or state of mixing had minimal effect on results. Samples were read at 500 nm and the resulting absorbance plotted as a function of salt concentration. Changes in reference subtracted absorbance levels associated with signal to noise (S/N) ratios of > 5.0 (+ 0.010) were considered significant. The coefficient of variation as a percentage was ≤ 10 % for all results.

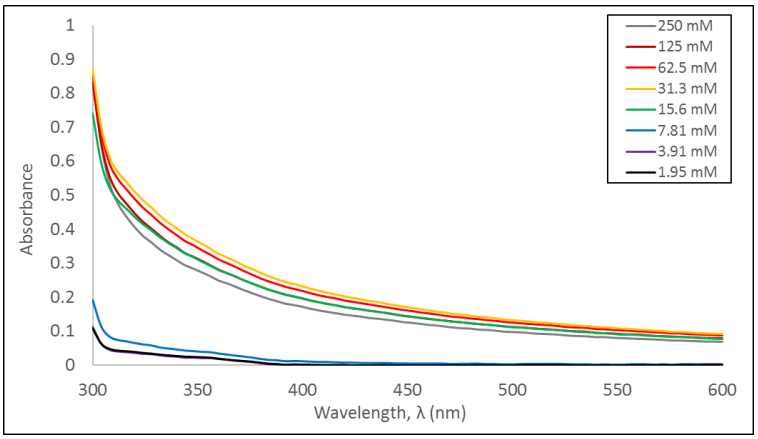

Figure S40: Representative example (ReO_4^-) graph of the UV-vis absorbance spectrum (300 – 600 nm) of positand **2** (0.5 mM) at various concentrations of salt for precipitation screening. Sharp increase in absorbance (turbidity) after precipitation is the result of scattering of excitation wavelength due to small particle aggregates in the wells.

	Free Positand 2			Positand 2 : $AdaCO_2H$ complex		
Salt	**CPC (mM)**	***S.D.***	**%CV**	**CPC (mM)**	***S.D.***	**%CV**
$NaPF_6$	4	0.0	0 %	3	0.0	0 %
CF_3SO_3Na	9.2	0.8	9 %	22.7	1.1	5 %
$NaReO_4$	9.4	0.9	10 %	9.6	0.9	9 %
$NaClO_4$	12	0.0	0 %	11.5	1.0	9 %
$NaBH_3CN$	19	1.7	9 %	18.8	1.5	8 %
$NaBF_4$	35	1.7	5 %	34	1.7	5 %
$NaSCN$	63	2.4	4 %	65	3.0	5 %
NaI	103	10	10 %	115	4.6	4 %
$NaO_2C_2Cl_3$	110	3.5	3 %	—[b]	—[b]	—[b]
$NaBr$	—[a]	—[a]	—[a]	—[a]	—[a]	—[a]
$NaNO_3$	—[a]	—[a]	—[a]	—[a]	—[a]	—[a]
$NaCl_2CHCO_2$	—[a]	—[a]	—[a]	—[a]	—[a]	—[a]
$NaCl$	—[a]	—[a]	—[a]	—[a]	—[a]	—[a]
NaF	—[a]	—[a]	—[a]	—[a]	—[a]	—[a]

Table S6: Summary of the precipitation data for free positand **2** and the **2**.$AdaCO_2^-$ complex with various salts. CPC values (mM) reported as mean of three or more observations.

[a] No precipitation observed under screening conditions.

[b] Precipitation only observed at higher host concentrations (≥ 2.0 mM). All errors ≤ 10 %.

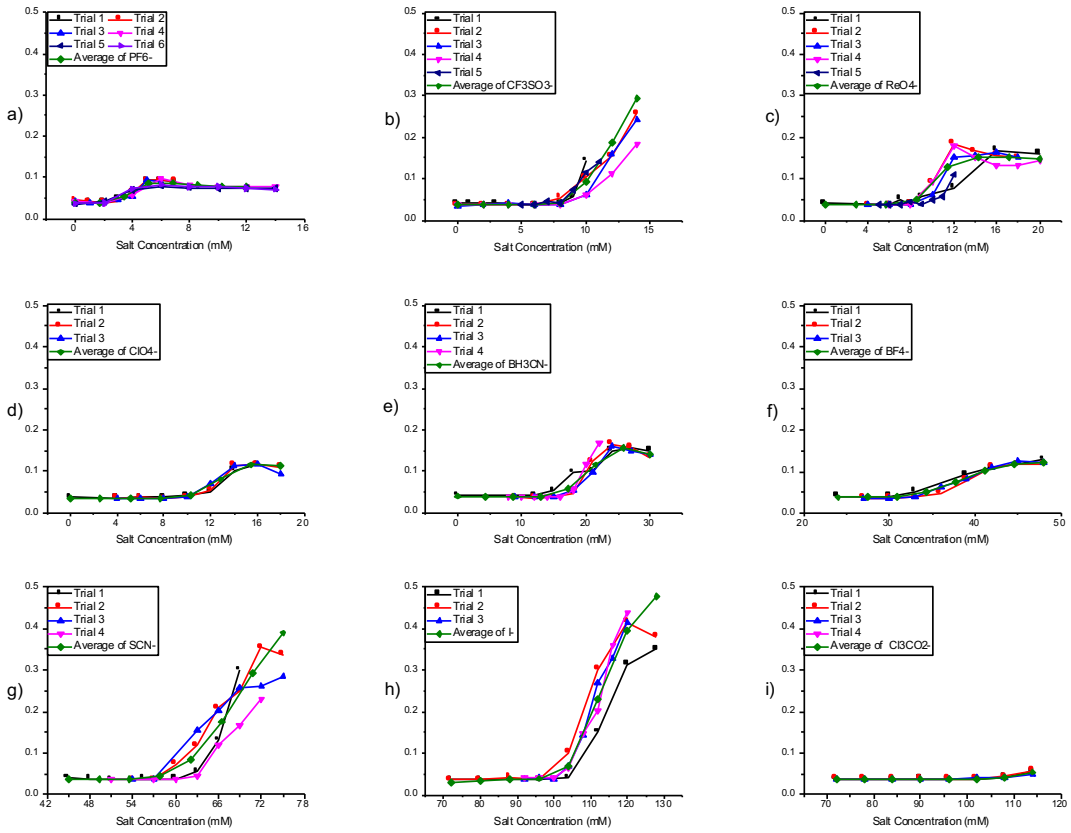

Figure S41: Plots of the absorbance intensity (y-axis) as a function of salt concentration (x-axis) in a solution of **2** (0.5 mM) a) PF_6^-, b) $CF_3SO_3^-$, c) ReO_4^-, d) ClO_4^-, e) BH_3CN^-, f) BF_4^-, g) SCN^-, h) I^-, i) $CCl_3CO_2^-$.

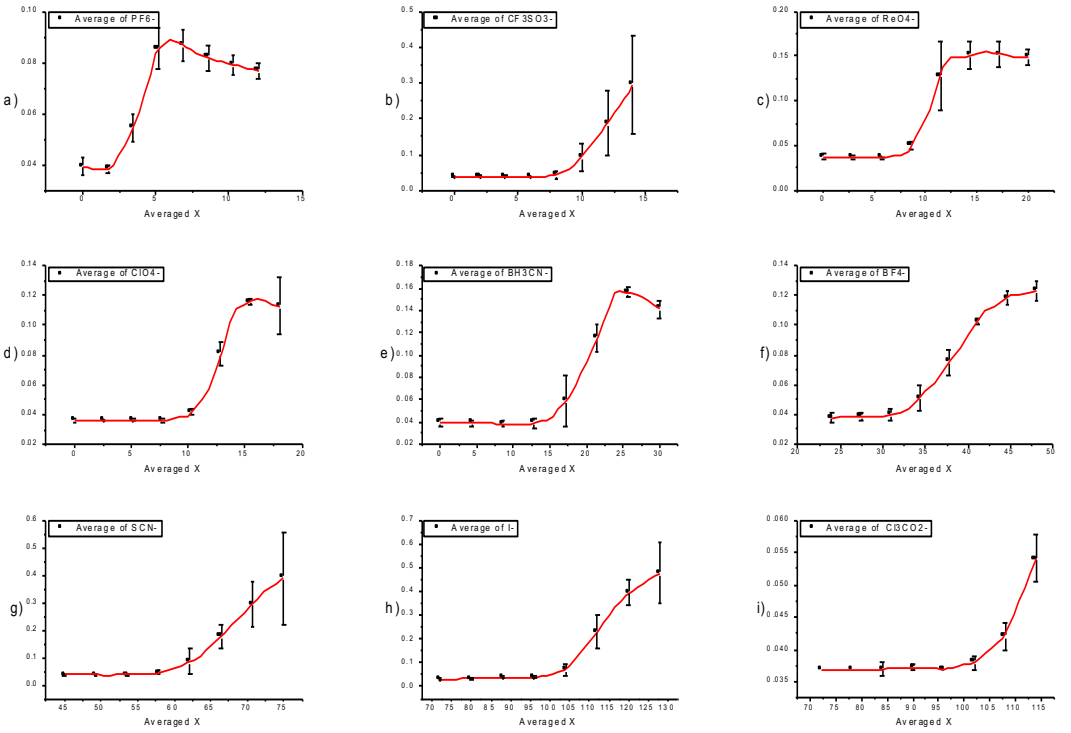

Figure S42: Average of the individual turbidity curves of Figure S41. a) PF_6^-, b) $CF_3SO_3^-$, c) ReO_4^-, d) ClO_4^-, e) BH_3CN^-, f) BF_4^-, g) SCN^-, h) I^-, i) $CCl_3CO_2^-$.

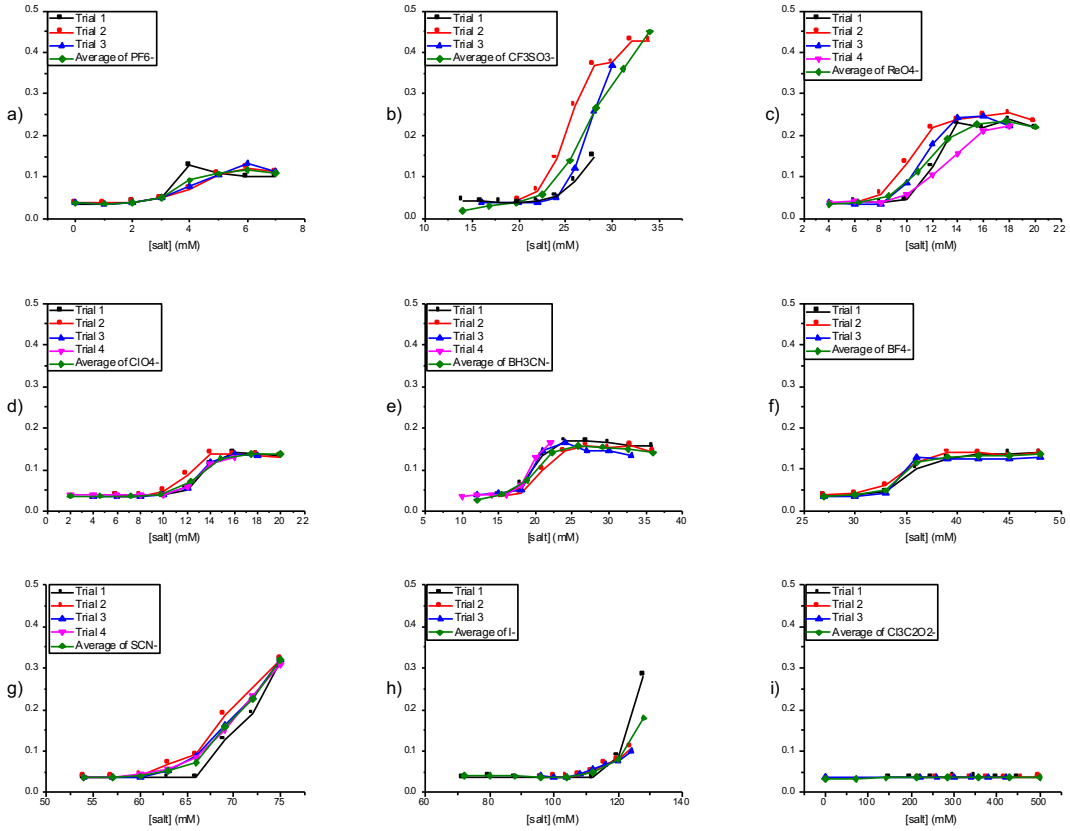

Figure S43: Plots of the absorbance intensity (y-axis) as a function of salt concentration (x-axis) in a solution of **2**.AdaCO_2^- complex (0.5 mM) a) PF_6^-, b) $CF_3SO_3^-$, c) ReO_4^-, d) ClO_4^-, e) BH_3CN^-, f) BF_4^-, g) SCN^-, h) I^-, i) $CCl_3CO_2^-$.

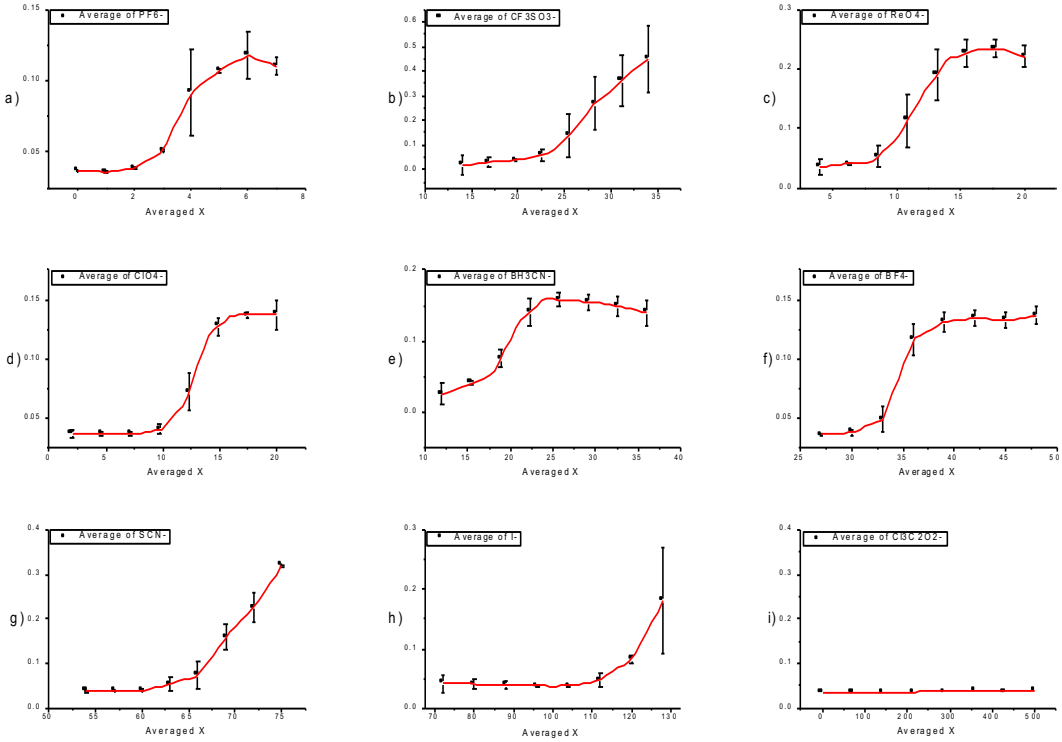

Figure S44: Average of the individual turbidity curves of Figure S43. a) PF_6^-, b) $CF_3SO_3^-$, c) ReO_4^-, d) ClO_4^-, e) BH_3CN^-, f) BF_4^-, g) SCN^-, h) I^-, i) $CCl_3CO_2^-$.

CPCs were determined both by a departure of the average curve from the baseline (Figure S41 & S43), and by averaging the concentration at which significant solution turbidity was measured with respect to the background (Figure S42 & S44). There was agreement (within error) between these methods (Table S7).

Salt	Free Positand 1		Positand 1 : $AdaCO_2H$ complex	
	Averaged Concentration (mM)	Averaged from Intensity (mM)	Averaged Concentration (mM)	Averaged from Intensity (mM)
$NaPF_6$	4	3.2	3	2.9
CF_3SO_3Na	9.2	8.6	22.7	22.3
$NaReO_4$	9.4	9.0	9.6	8.5
$NaClO_4$	12	11.2	11.5	10.8
$NaBH_3CN$	19	16.2	18.8	17.5
$NaBF_4$	35	34.0	34	32.9
$NaSCN$	63	59.1	65	62.0
NaI	103	100.7	115	112.2
$NaO_2C_2Cl_3$	110	111.8	—[a]	—[a]

Table S7. Experimental average and calculated CPC from turbidity curve for the 9 precipitating salts of **2** and the **2**.$AdaCO_2^-$ complex. Calculated CPC determined from the average turbidity curve from all measurements from each salt where the calculated intensity ≥ 0.050.

[a] No precipitation observed at the concentration of the **2**.$AdaCO_2^-$ complex tested.

A plot (Figure S45) of the inverse critical precipitation concentration (CPC^{-1}) is useful to gauge the relative strength of precipitators and to compare data from multiple techniques. In this regard the CPC^{-1} data is ordered by the precipitating power of salts on free host **1**. The same plot is obtained from the DLS data (Figure S75) with the same trend although slightly different values attributed to both the higher ionic strength of the solutions and the higher concentration of host or **2**.$AdaCO_2^-$ complex.

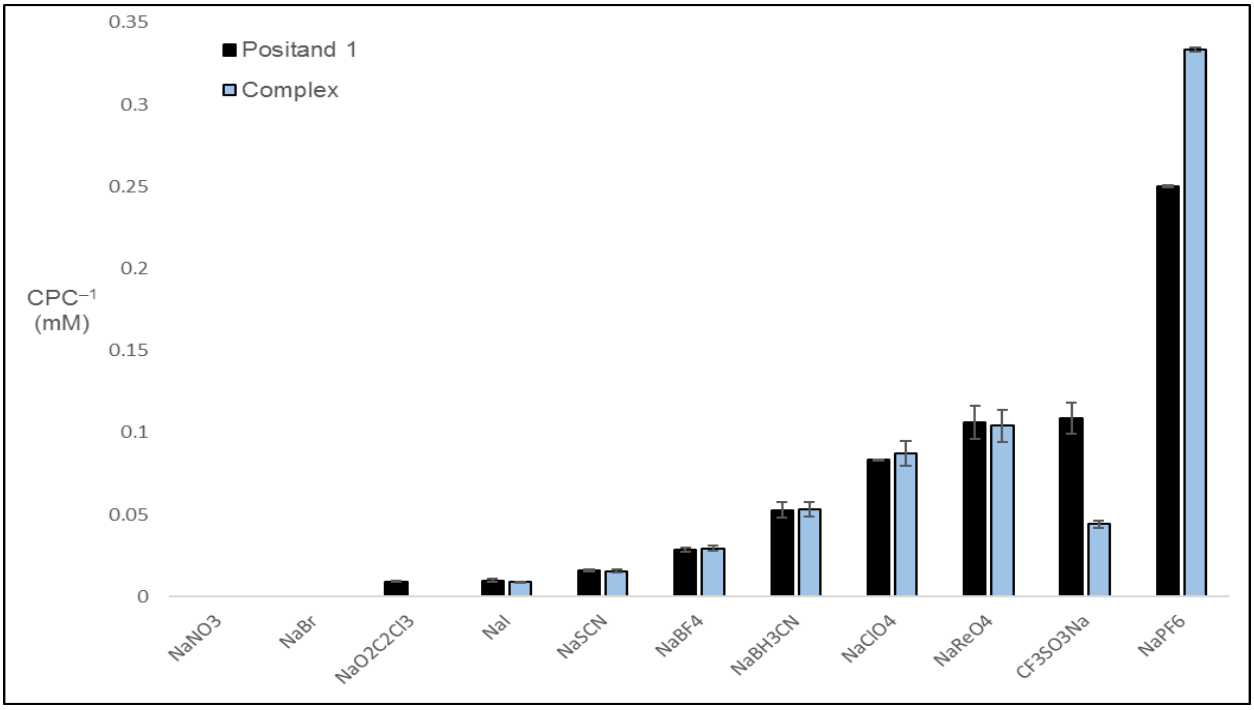

Figure S45: Graph of the UV-vis obtained inverse Critical Precipitation Concentration (CPC^{-1}) plotted for each salt against the free host positand **2** (0.5 mM) and the **2.3** complex.

b. Kinetic determination of induction delayed precipitation

Plots of the kinetics of precipitation were conducted from 50–95 % of the CPC values (Table S6), over 168 hours (7 days). It should be noted that for most salts, maximal precipitation was only observed within this time period within 10 % of the CPC. While the stronger precipitators required a lower overall concentration of salt to induce immediate, rapid precipitation, they were generally poorer precipitators in a kinetic sense. The most powerful precipitator was $CF_3SO_3^-$, which effectively precipitated the host at nearly all concentrations tested and reached maximum precipitation with as little as 65 % of the CPC (~6 mM) in only 16 hours (Figure S46–S47). Anions Cl^-, Br^-, and NO_3^- did not induce precipitation over the 168-hour time period.

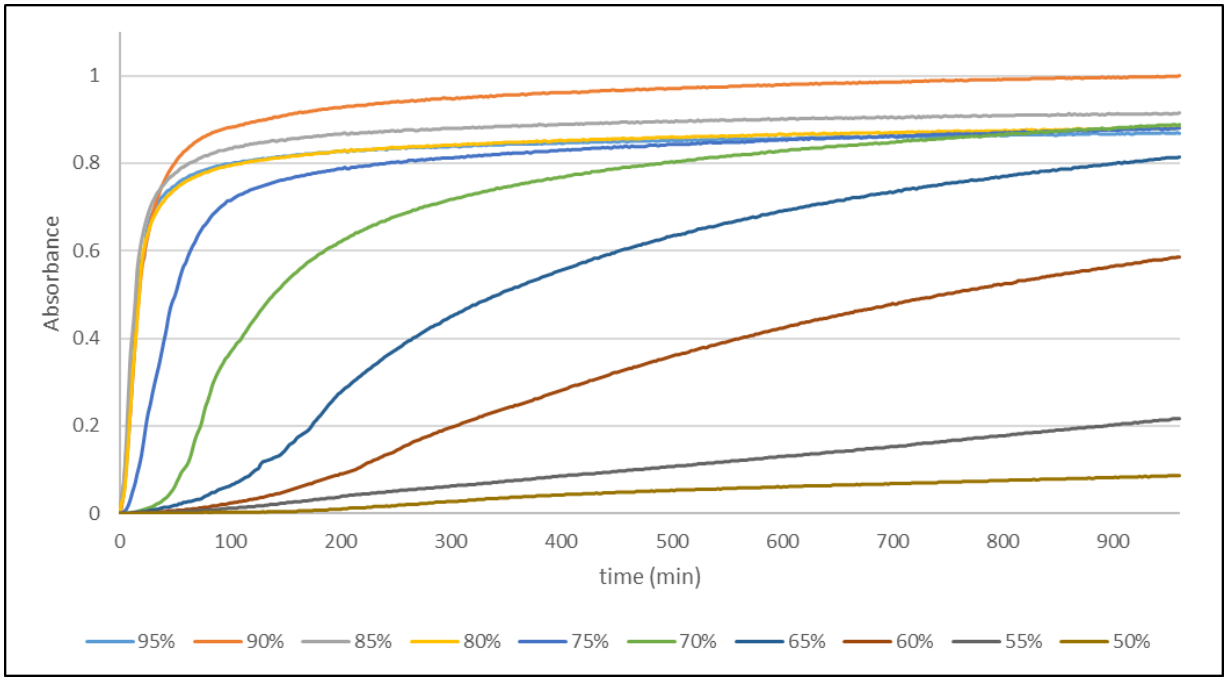

Figure S46: Normalized precipitation kinetics of positand **2** in the presence of various concentrations of $CF_3SO_3^-$.

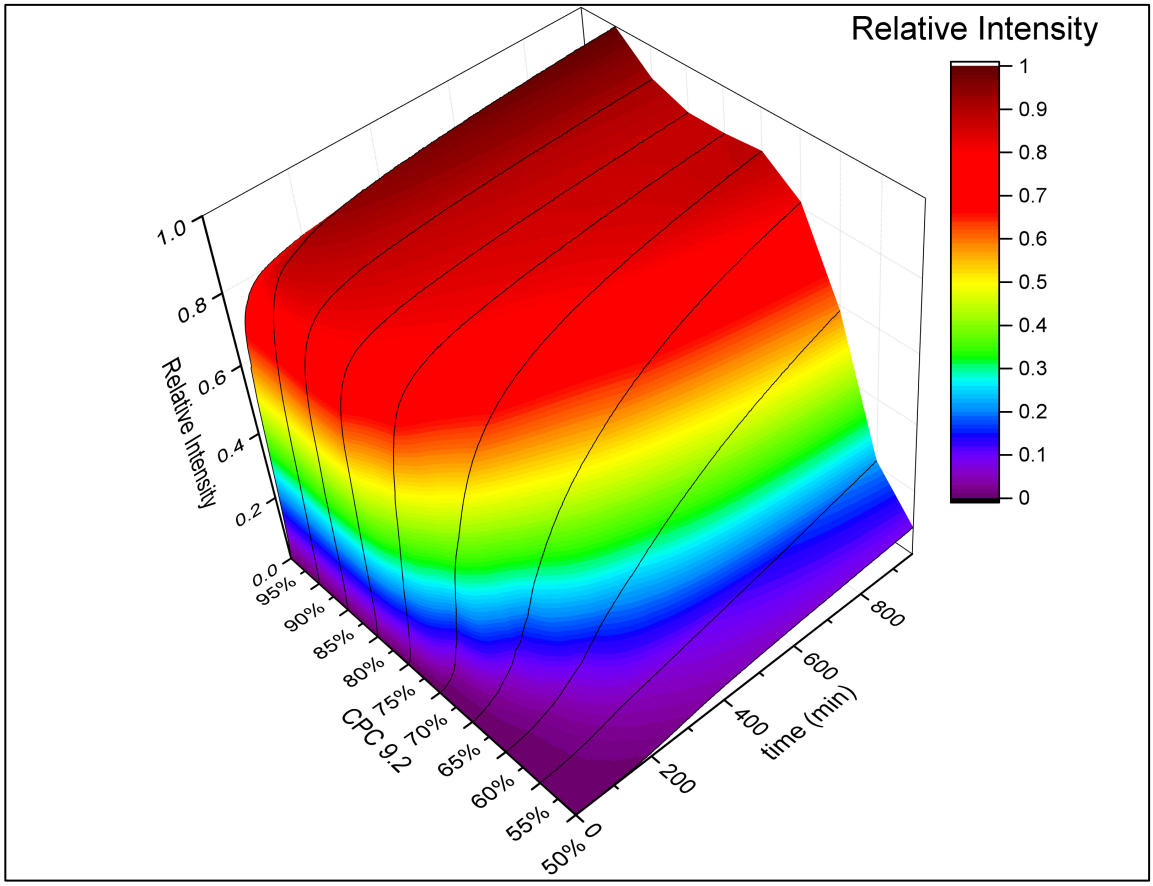

Figure S47: Surface plot of the data shown in Figure S46.

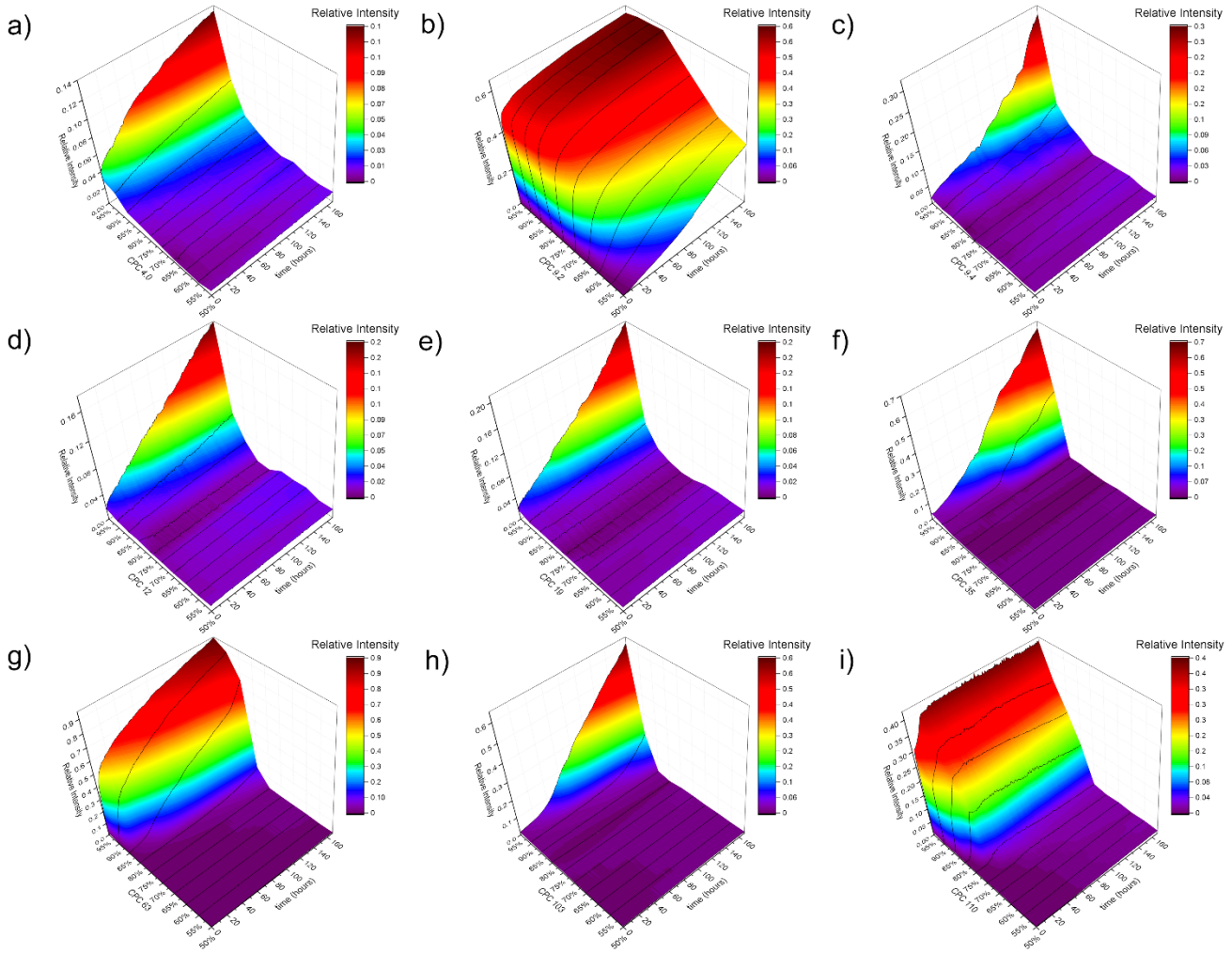

Figure S48: Surface plots of the precipitation kinetics of positand **2** in the presence of salts at 50 – 95 % of the experimental CPC value. X-axis is the time hours, y-axis is the salt concentration expressed as the percentage of the CPC value for each salt, and z-axis the relative intensity of absorption with the intensity scale expressed normalized to the maximal value for each plot. a) PF_6^-, b) $CF_3SO_3^-$, c) ReO_4^-, d) ClO_4^-, e) BH_3CN^-, f) BF_4^-, g) SCN^-, h) I^-, i) $CCl_3CO_2^-$.

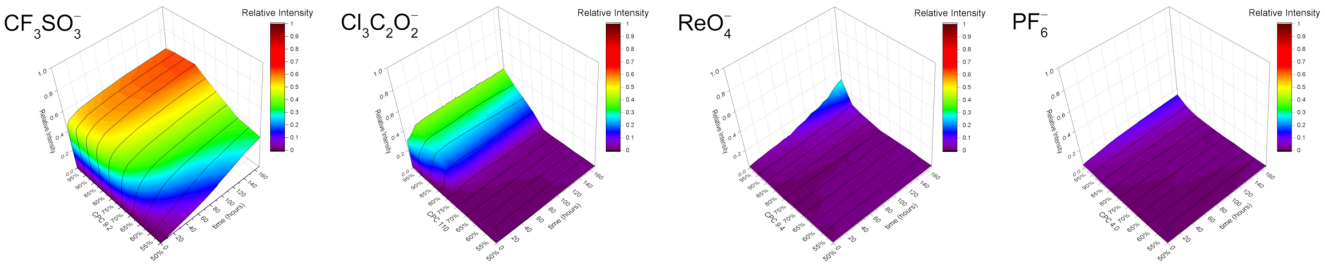

Figure S49: Intensity plots showing the non-normalized surface plots of data shown in figure S48 for the respective anions shown above. Maximal absorbance is set to 1.0 with the same relative intensity scale expressed on each plot.

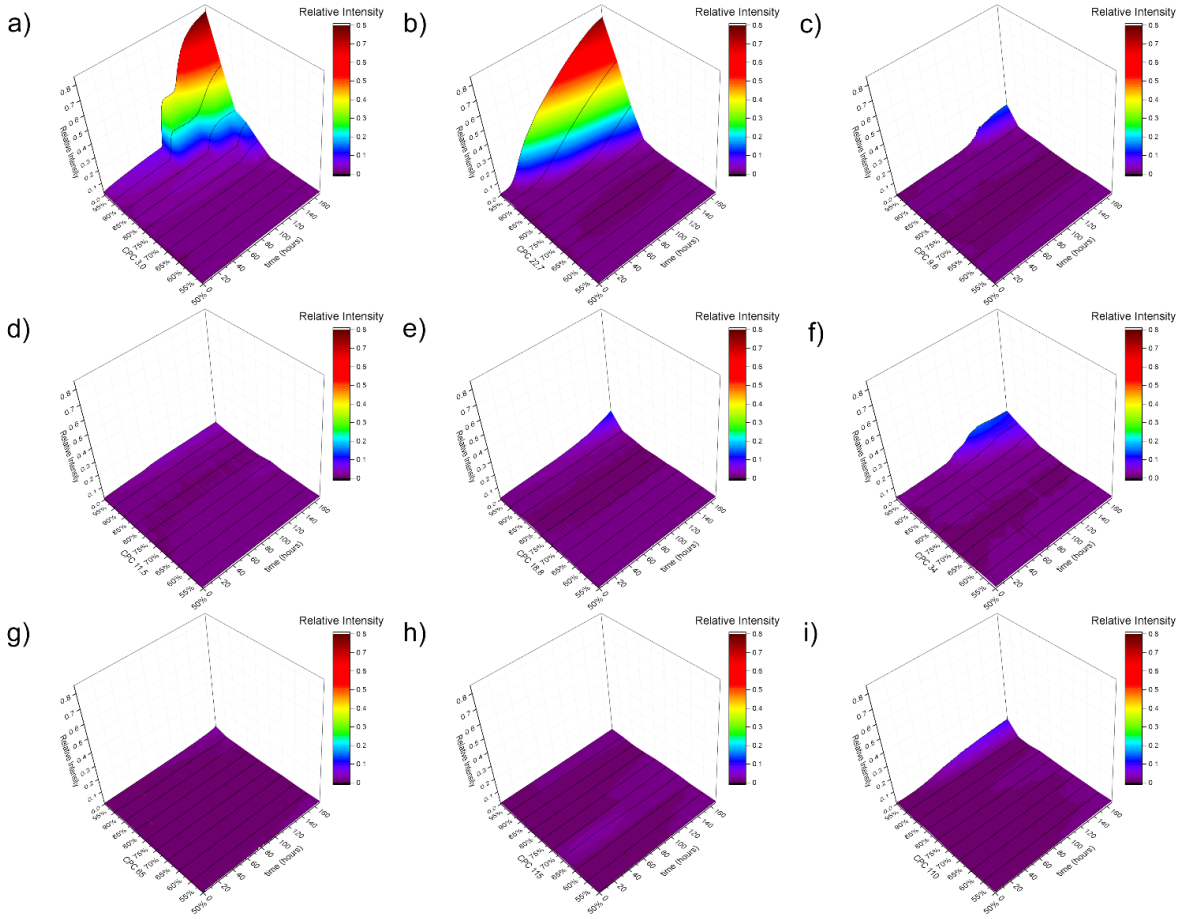

Figure S50: Surface plots of the precipitation kinetics of the **2**.AdaCO_2^- complex in the presence of salts at 50 – 95 % of the experimental CPC value. X-axis is the time in hours, y-axis is the salt concentration expressed as the percentage of the CPC value for each salt, and z-axis the relative intensity of absorption with all plots normalized to the same intensity scale. a) PF_6^-, b) $CF_3SO_3^-$, c) ReO_4^-, d) ClO_4^-, e) BH_3CN^-, f) BF_4^-, g) SCN^-, h) I^-, i) $CCl_3CO_2^-$.

Figure S48 shows the induction delayed precipitation plots for the free host with the intensity scale for each plot separately normalized to the maximal intensity. Figure S49 shows the data for selected anions from S48 with the plots normalized to the same intensity scale. Figure S50 shows the data for the complex with the same treatment as per Figure S49 with the maximal intensity set to 0.8. Wells which resulted in the formation of solid particles are tabulated in Table S8 for the free host and Table S9 for the complex. In some cases, competing precipitation/crystallization occurred (See Section 2.C.c) with the complex, resulting in the formation of microcrystals that were unsuitable for x-ray analysis. In most cases with positand **2**, precipitation occurred above 85% of the recorded CPC while induction delays were typically not observed for the complex. In the case of $CF_3SO_3^-$ while the free host **2** resulted in precipitation with as little as 4.6 mM salt (50 % of the CPC) in under sixteen hours (Figure S47), for the **2**.AdaCO_2^- complex (Figure S50.b), only above 80 % of the CPC (> 18 mM) was precipitate observed, with a much longer induction delay and delayed onset of precipitation (2 – 6 days). In general, the formation of the complex reduced the propensity to form a precipitate over extended time both in the concentration required and in the resultant time to precipitation when below the CPC. For the remaining induction delayed precipitation curves, the data is presented in the order of increasing CPC for the free host (reproduced in Tables S8–S9); for wells which resulted in precipitation, the individual precipitation curves are shown (S51 – S68) for each anion.

Salt	K^{crown}	K^{cav}	CPC	.95	.90	.85	.80	.75	.70	.65	.60	.55	.50
PF_6^-	3600	>5000	4.0	P	P	P	—	—	—	—	—	—	—
ReO_4^-	1800	7200	9.4	P	P	P	—	—	—	—	—	—	—
$CF_3SO_3^-$	710	>5000	9.2	P	P	P	P	P	P	P	P	P	P
ClO_4^-	2400	4300	12	P	P	P	—	—	—	—	—	—	—
BH_3CN^-	1300	3600	19	P	P	P	—	—	—	—	—	—	—
BF_4^-	1200	35	35	P	P	—	—	—	—	—	—	—	—
SCN^-	830	2000	63	P	P	P	P	P	—	—	—	—	—
I^-	3200	930	103	P	P	P	—	—	—	—	—	—	—
$Cl_3C_2O_2^-$	—	54500	110	P	P	P	P	P	P	—	—	—	—

Table S8. Summary of the binding constant to the crown of ammoniums, the non-polar pocket, the CPC, and the results of the end-point precipitation from the induction delay curves from 0.5 × CPC to 0.95 × CPC listed in Table S6 for positand **2**, where (P) indicates precipitate formation was observed after 7 d.

Salt	K^{crown}	K^{cav}	CPC	.95	.90	.85	.80	.75	.70	.65	.60	.55	.50
PF_6^-	3600	>5000	4.0	P	P	P	P	P	—	—	—	—	—
ReO_4^-	1800	7200	9.6	P	P	—	—	—	—	—	—	—	—
$CF_3SO_3^-$	710	>5000	22.7	P	P	P	P	—	—	—	—	—	—
ClO_4^-	2400	4300	12	P	P	—	—	—	—	—	—	—	—
BH_3CN^-	1300	3600	19	P	P	—	—	—	—	—	—	—	—
BF_4^-	1200	35	35	P	P	P	—	—	—	—	—	—	—
SCN^-	830	2000	63	P	—	—	—	—	—	—	—	—	—
I^-	3200	930	103	P	—	—	—	—	—	—	—	—	—
$Cl_3C_2O_2^-$	—	54500	n/a*	P	—	—	—	—	—	—	—	—	—

Table S9: Summary of the binding constant to the crown of ammoniums, the non-polar pocket, the CPC, and the results of the end-point precipitation from the induction delay curves from 0.5 × CPC to 0.95 × CPC listed in Table S6 for the **2**.$AdaCO_2^-$ complex, where (P) indicates precipitate formation was observed after 7 d,. *The CPC (110 mM) of the free host was used, since no precipitation was observed during the precipitation assays.

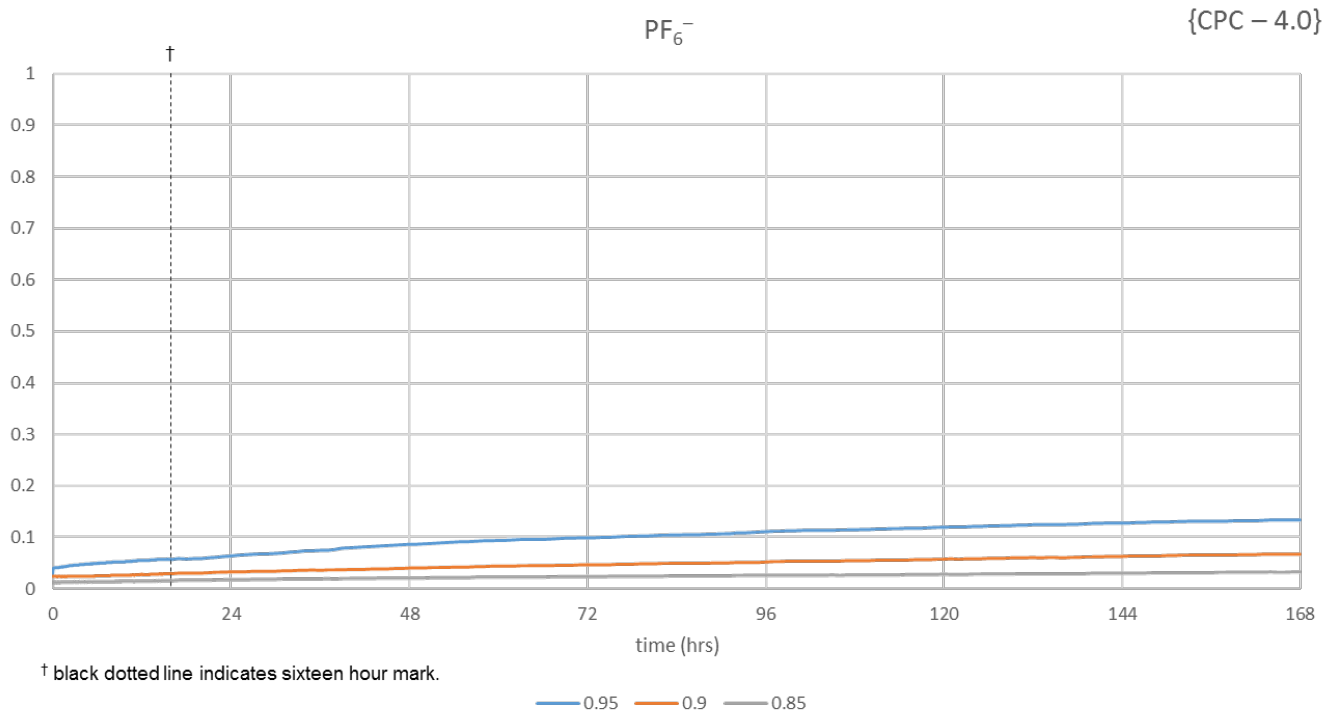

Figure S51: Precipitation kinetics of positand **2** in the presence of PF_6^- at 85 – 95 % of the CPC (3.4 – 3.8 mM).

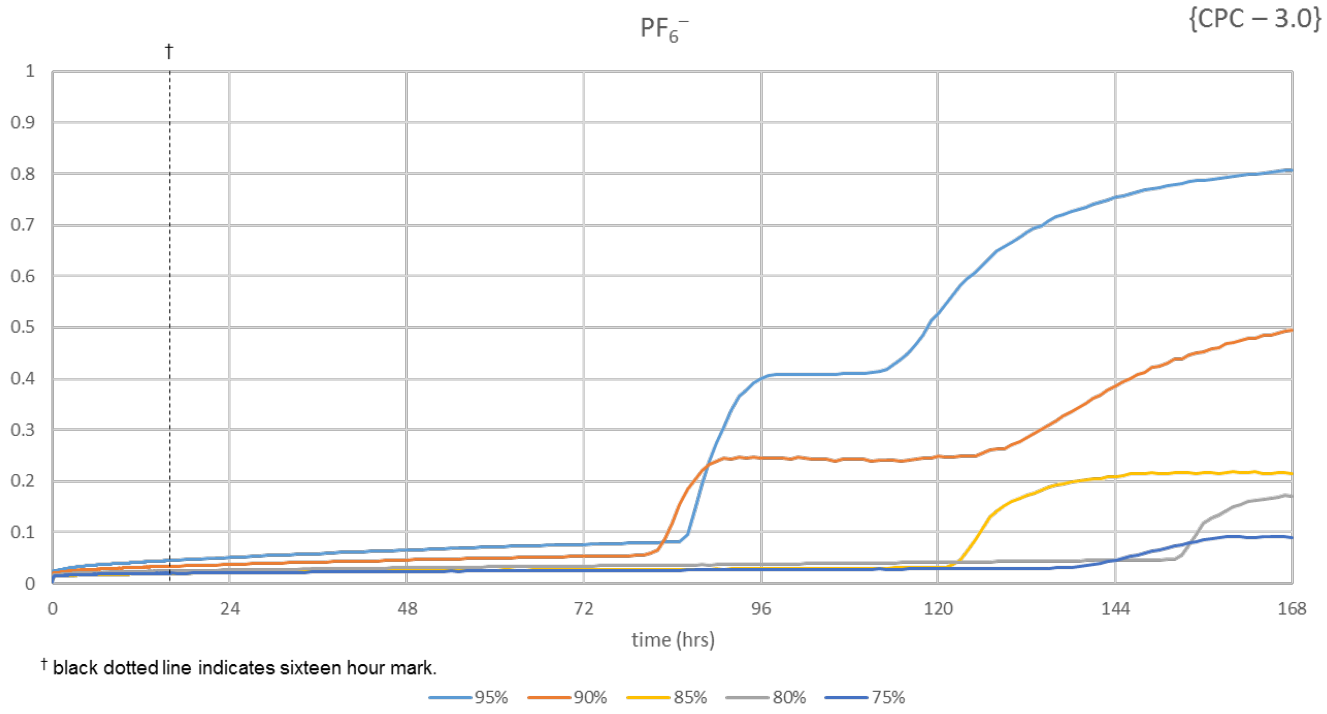

Figure S52: Precipitation kinetics of the **2**.AdaCO_2^- complex in the presence of PF_6^- at 75 – 95 % of the CPC (2.25 – 2.85 mM).

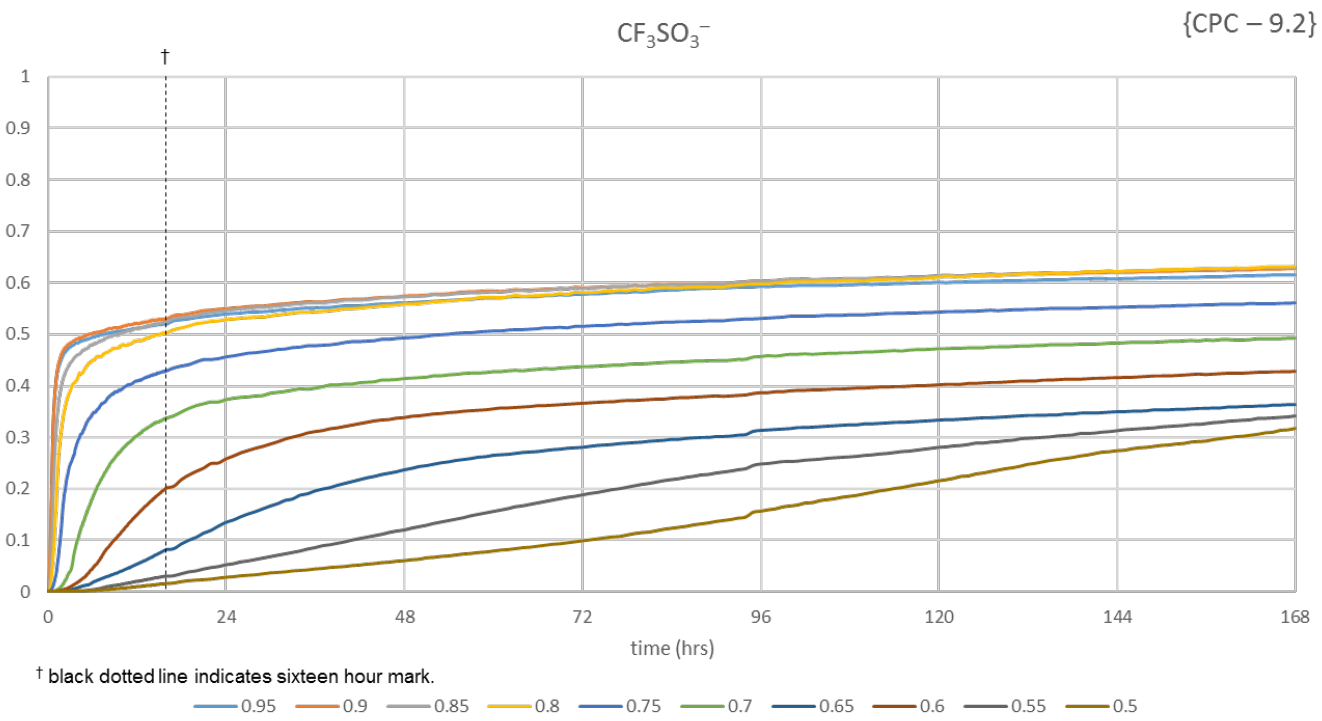

Figure S53: Precipitation kinetics of positand **2** in the presence of $CF_3SO_3^-$ at 50 – 95 % of the CPC (4.6 – 8.74 mM).

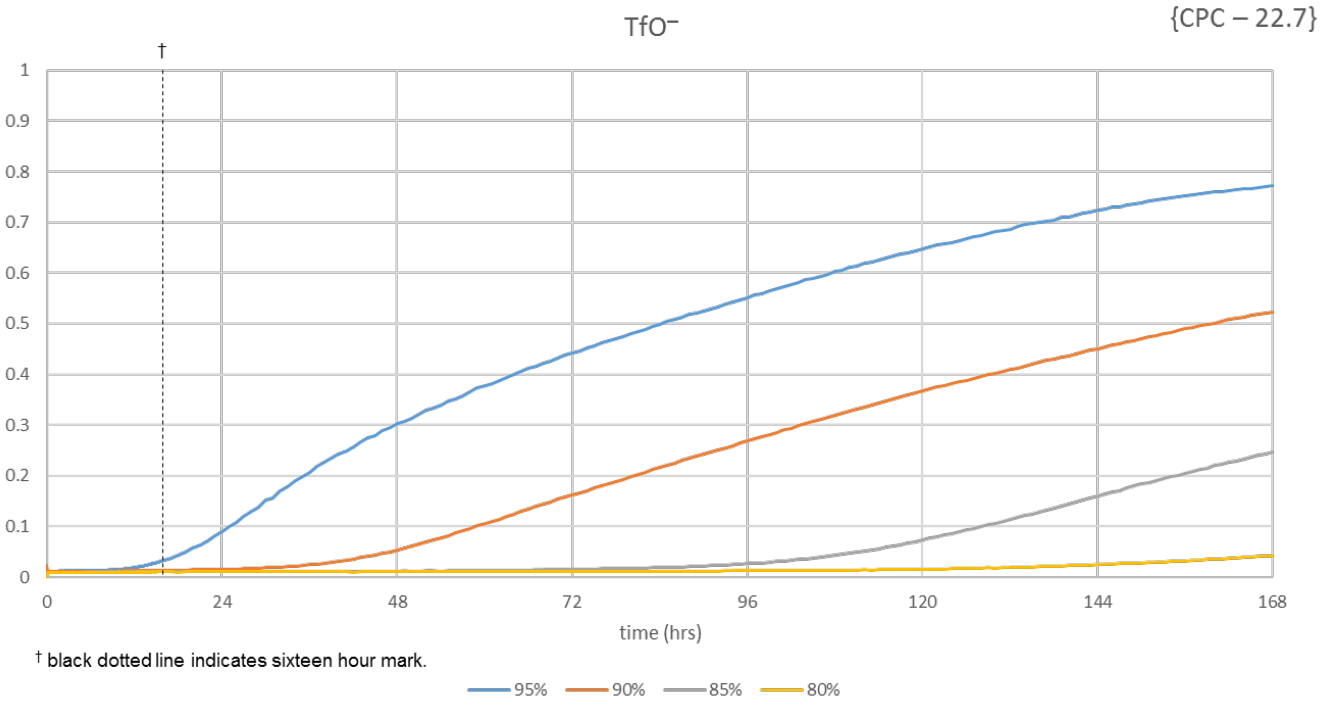

Figure S54: Precipitation kinetics of the **2**.AdaCO_2^- complex in the presence of $CF_3SO_3^-$ at 80 – 95 % of the CPC (18.16 – 21.57 mM).

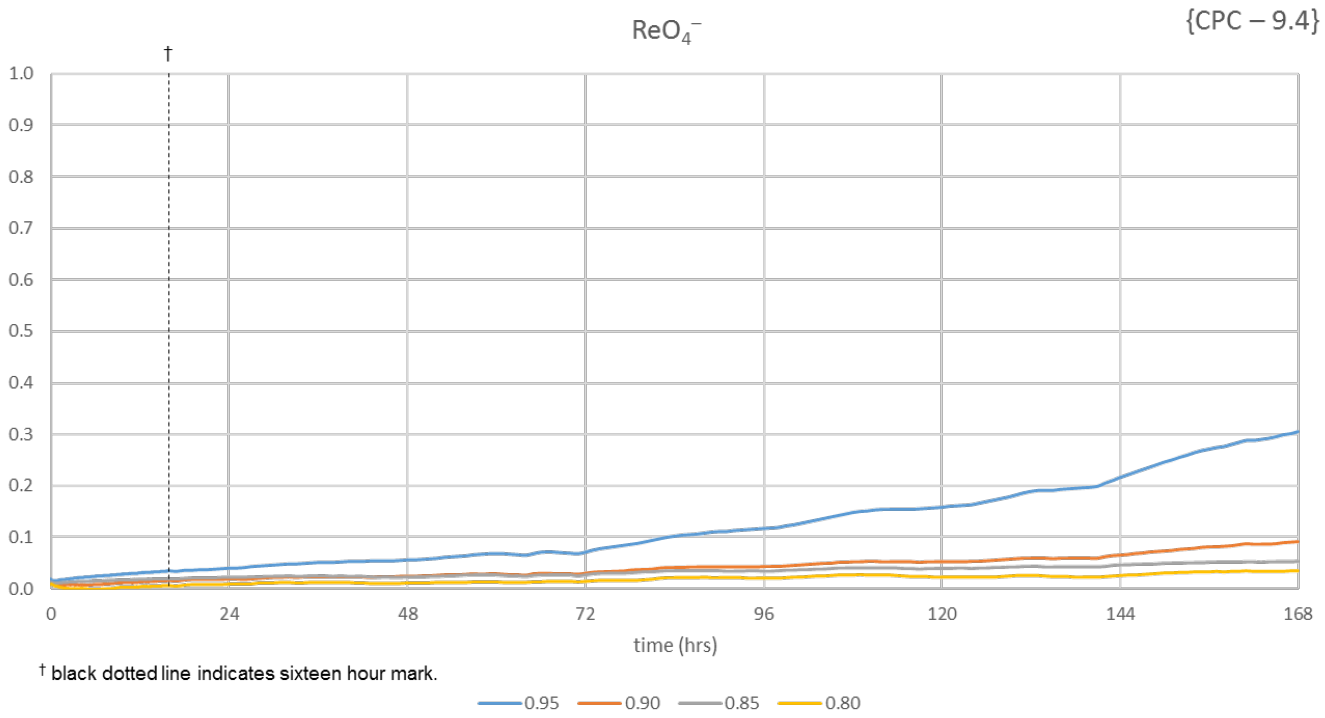

Figure S55: Precipitation kinetics of positand **2** in the presence of ReO_4^- at 80 – 95 % of the CPC (7.52 – 8.93 mM).

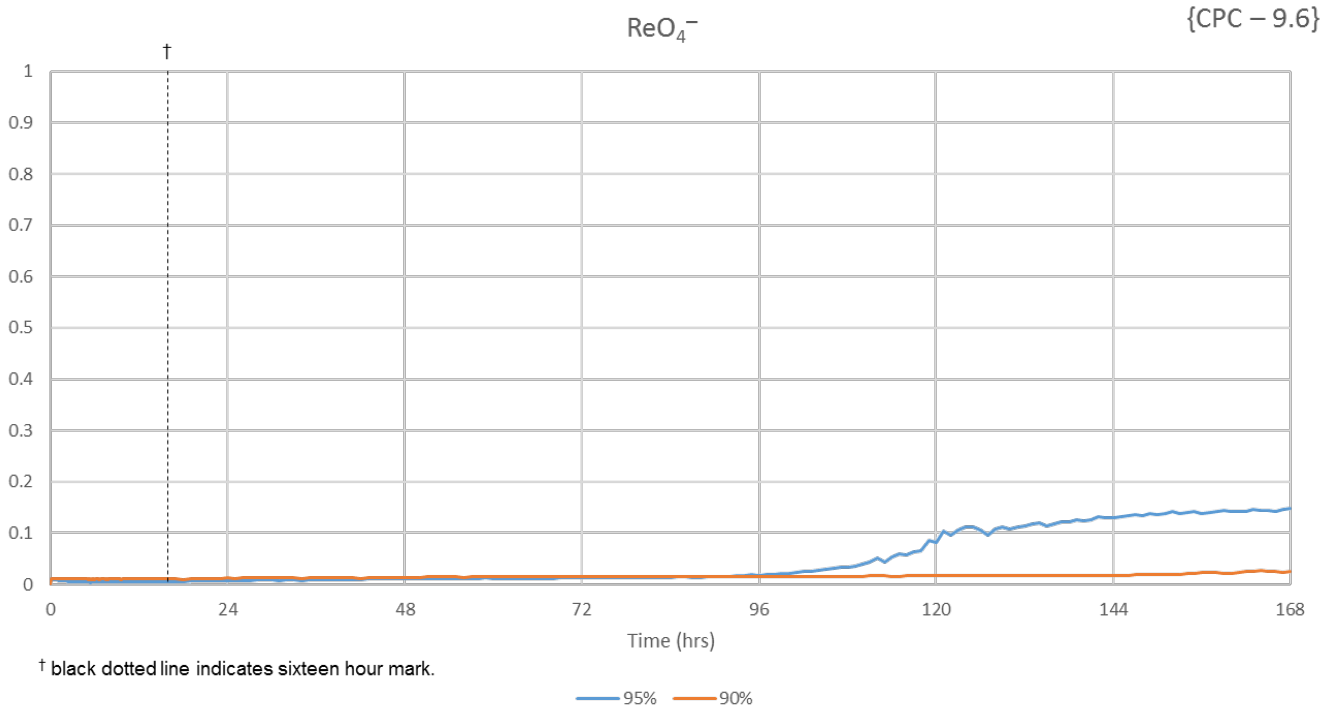

Figure S56: Precipitation kinetics of the **2**.AdaCO_2^- complex in the presence of ReO_4^- at 90 – 95 % of the CPC (8.64 – 9.12 mM).

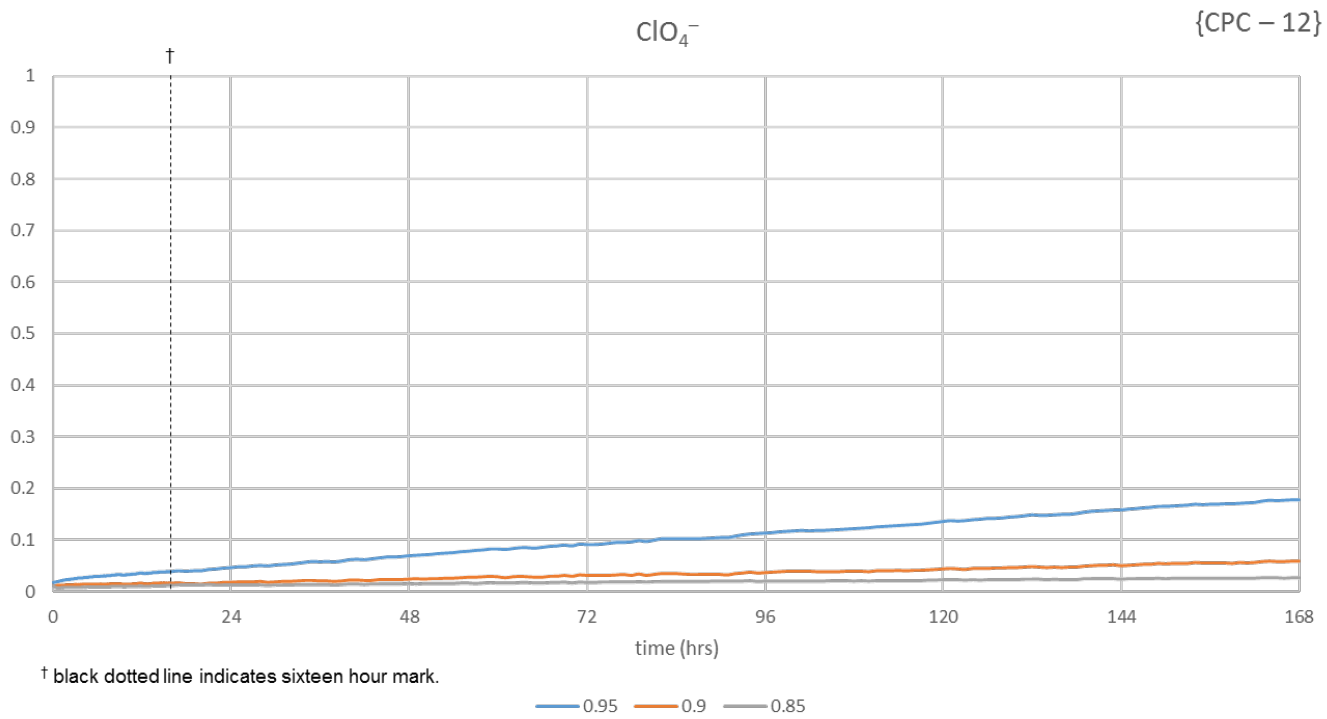

Figure S57: Precipitation kinetics of positand **2** in the presence of ClO_4^- at 85 – 95 % of the CPC (10.2 – 11.4 mM).

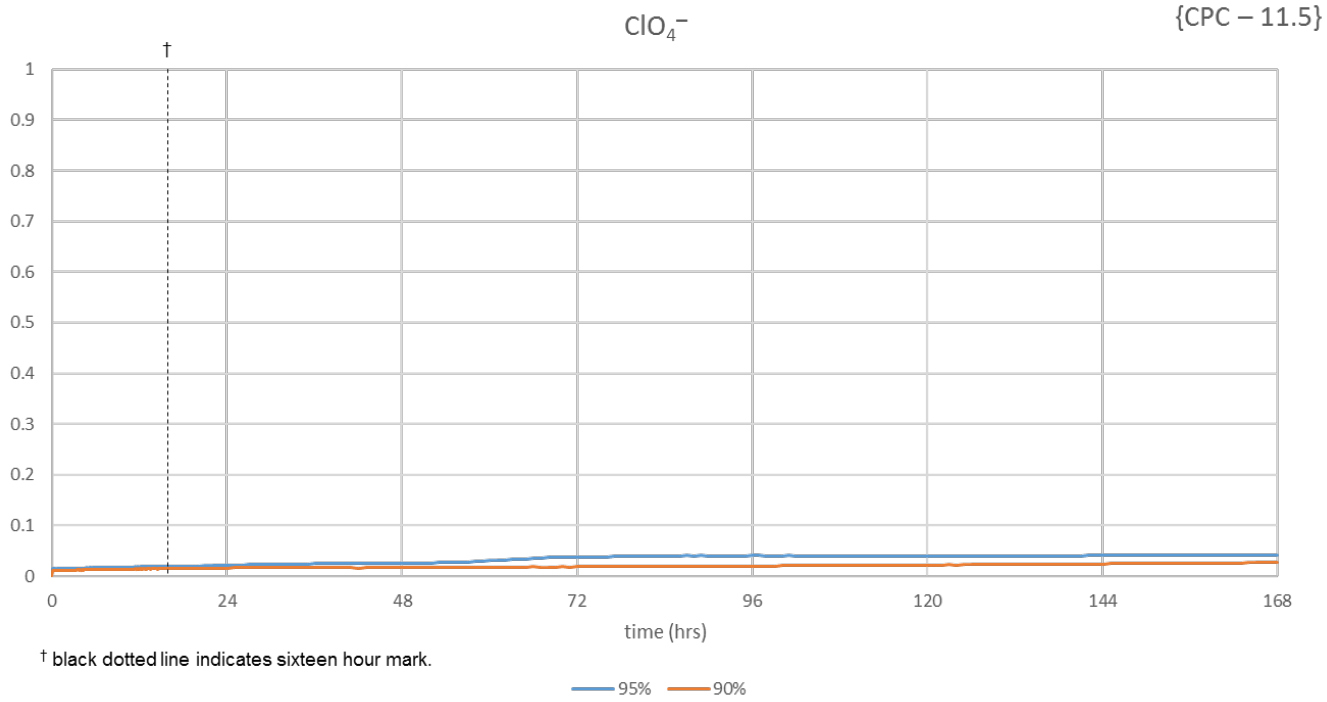

Figure S58: Precipitation kinetics of the **2**.AdaCO_2^- complex in the presence of ClO_4^- at 90 – 95 % of the CPC (10.35 – 10.93 mM).

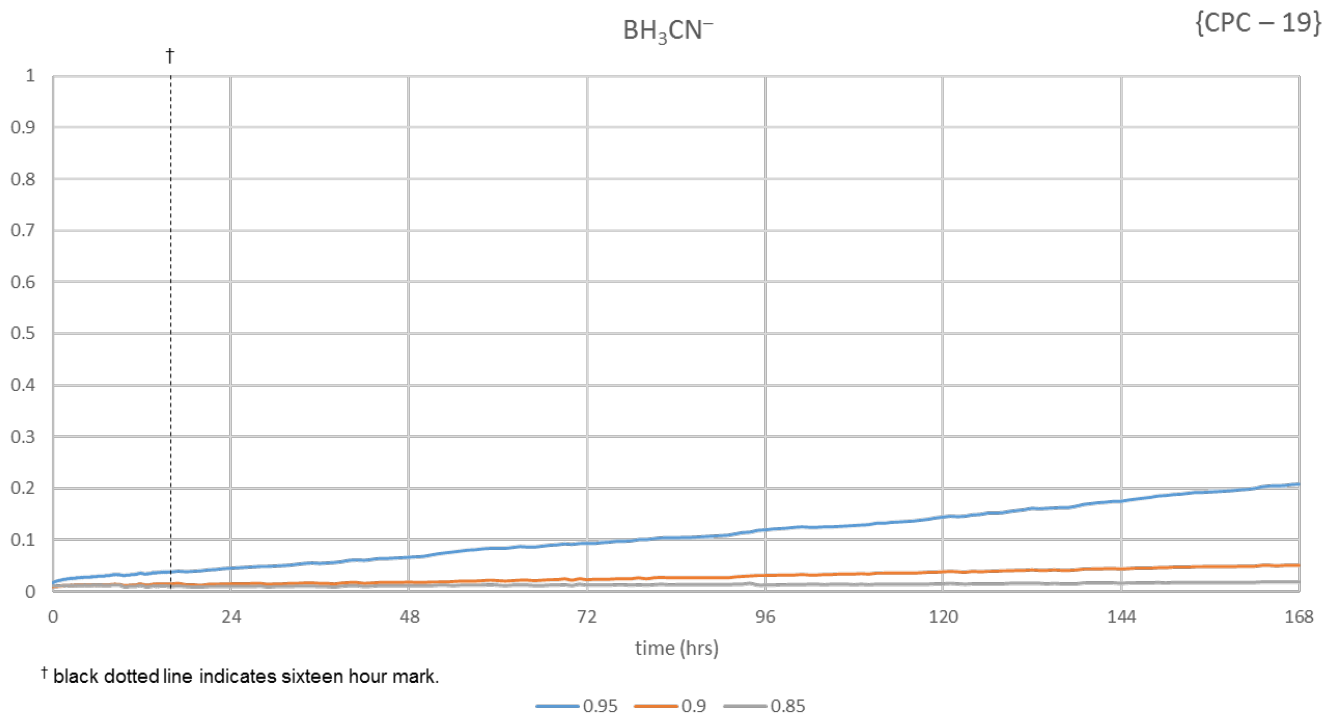

Figure S59: Precipitation kinetics of positand **2** in the presence of BH_3CN^- at 85 – 95 % of the CPC (16.15 – 18.05 mM).

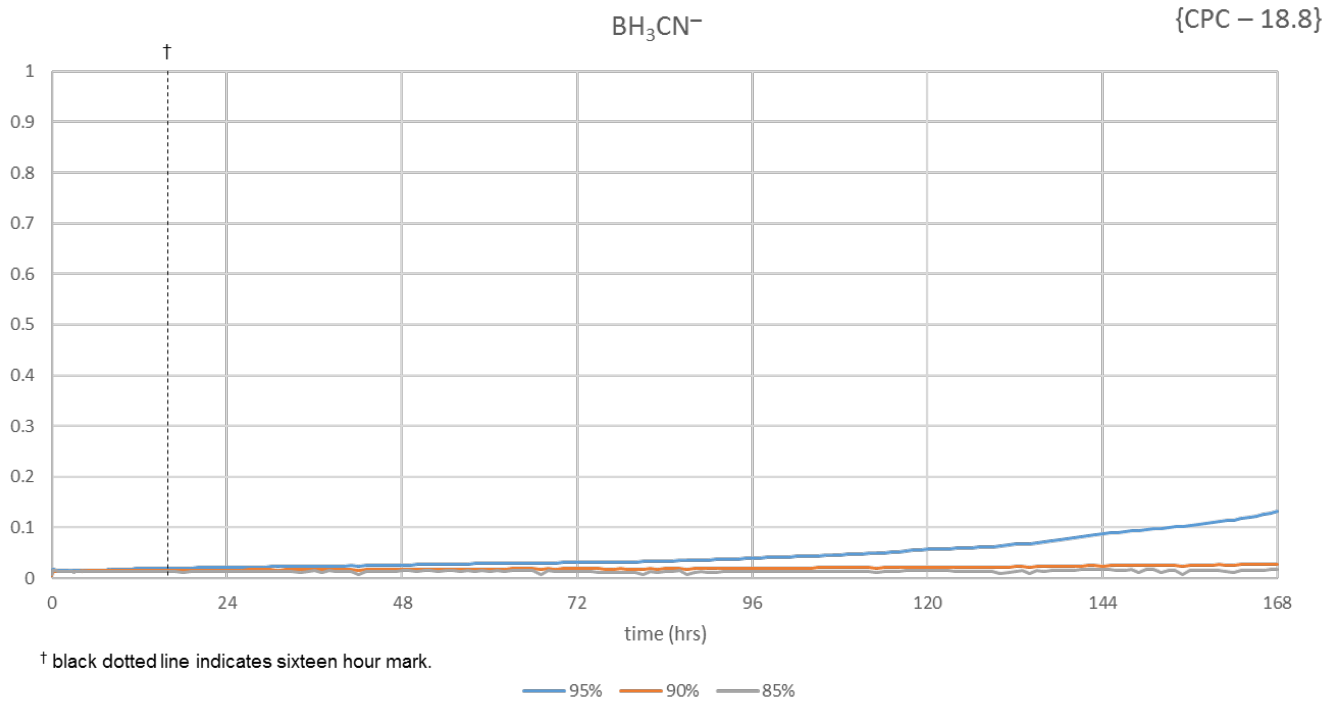

Figure S60: Precipitation kinetics of the **2**.AdaCO_2^- complex in the presence of BH_3CN^- at 85 – 95 % of the CPC (15.98 – 17.86 mM).

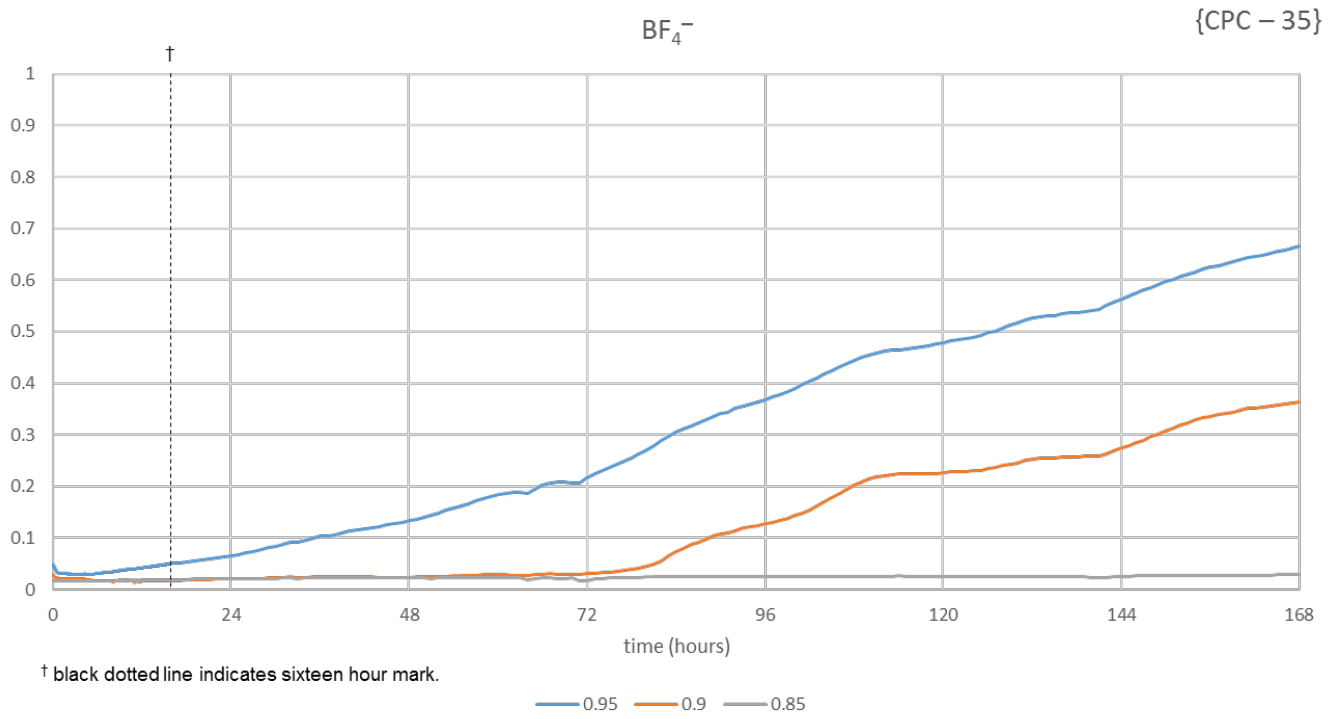

Figure S61: Precipitation kinetics of positand **2** in the presence of BF_4^- at 85 – 95 % of the CPC (29.75 – 33.25 mM).

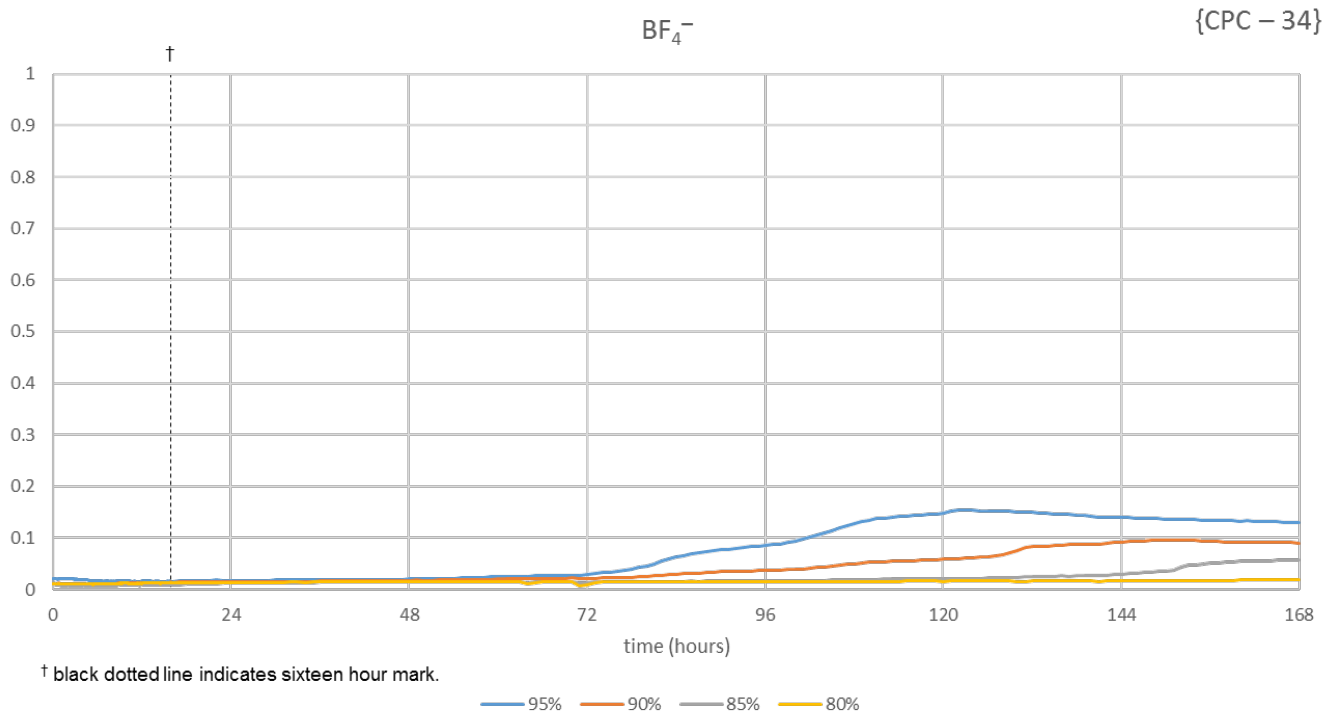

Figure S62: Precipitation kinetics of the **2**.AdaCO_2^- complex in the presence of BF_4^- at 80 – 95 % of the CPC (27.2 – 32.3 mM).

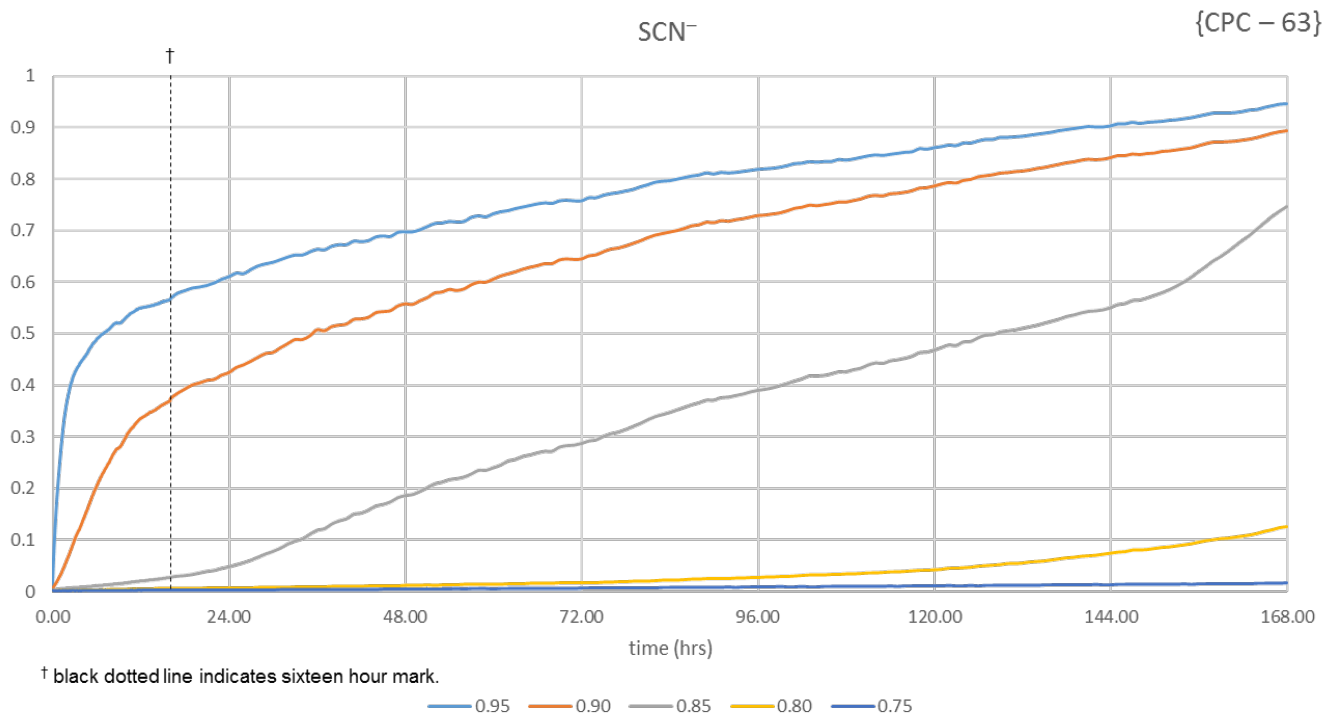

Figure S63: Precipitation kinetics of positand **2** in the presence of SCN^- at 75 – 95 % of the CPC (47.25 – 59.85 mM).

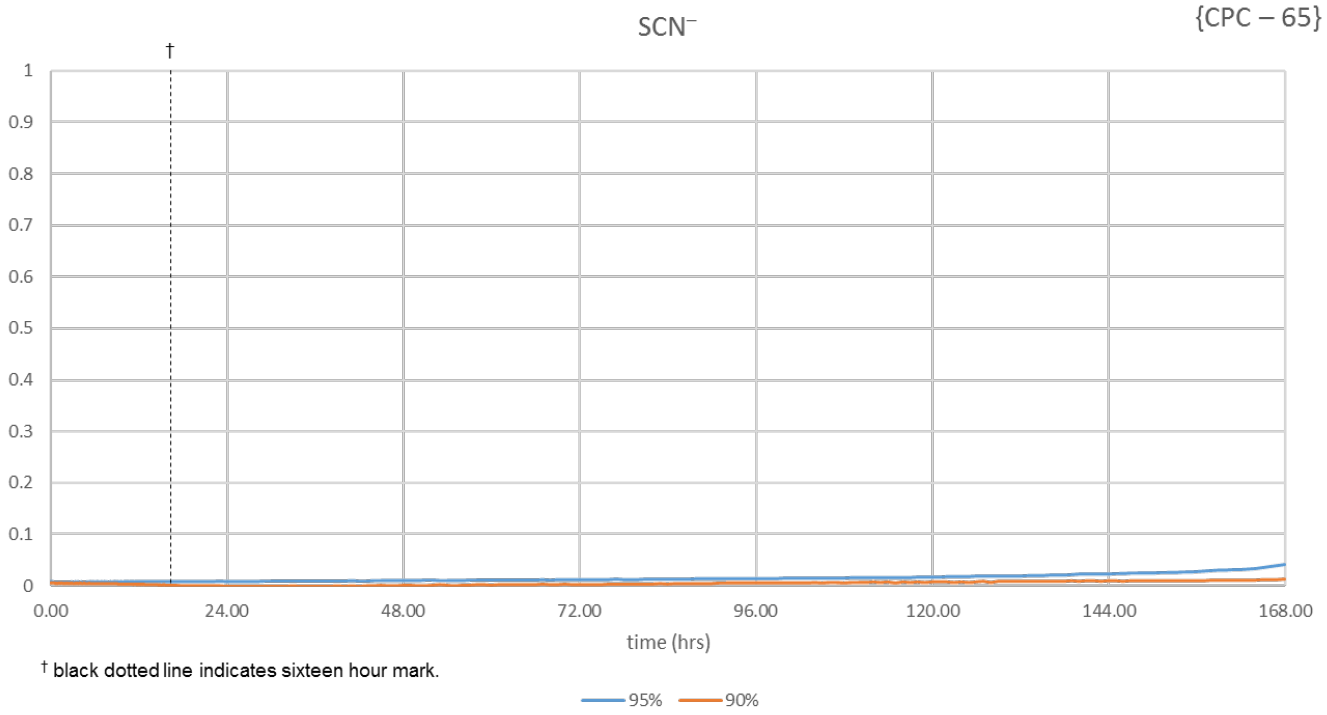

Figure S64: Precipitation kinetics of the **2**.AdaCO_2^- complex in the presence of SCN^- at 90 – 95 % of the CPC (58.5 – 61.75 mM).

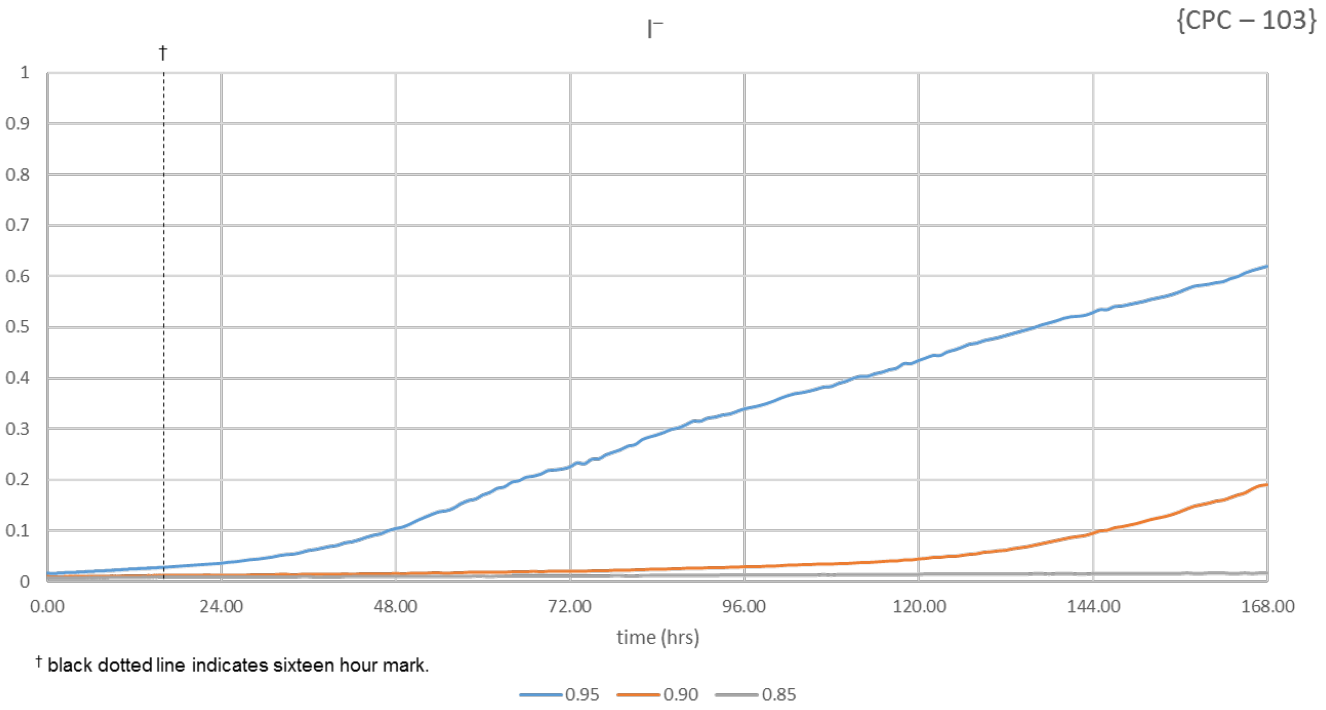

Figure S65: Precipitation kinetics of positand **2** in the presence of I^- at 85 – 95 % of the CPC (87.55 – 97.85 mM).

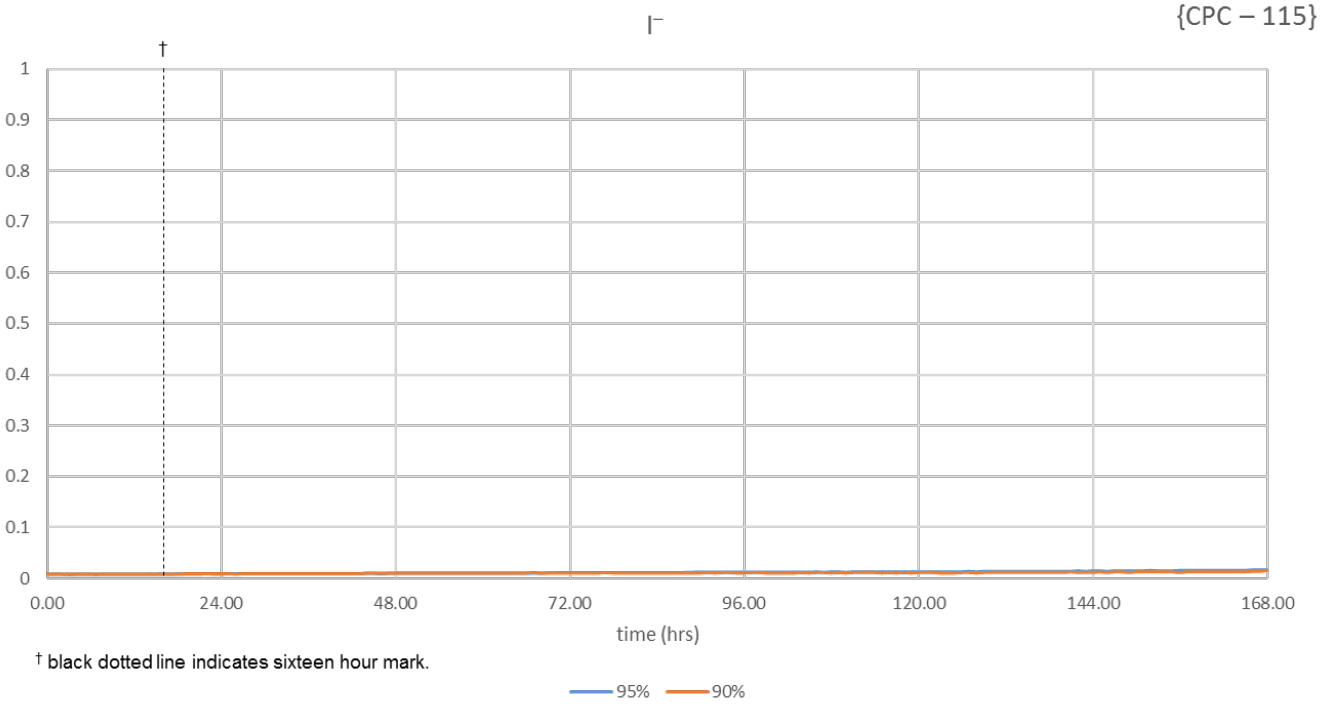

Figure S66: Precipitation kinetics of the **2**.AdaCO_2^- complex in the presence of I^- at 90 – 95 % of the CPC (103.5 – 109.25 mM).

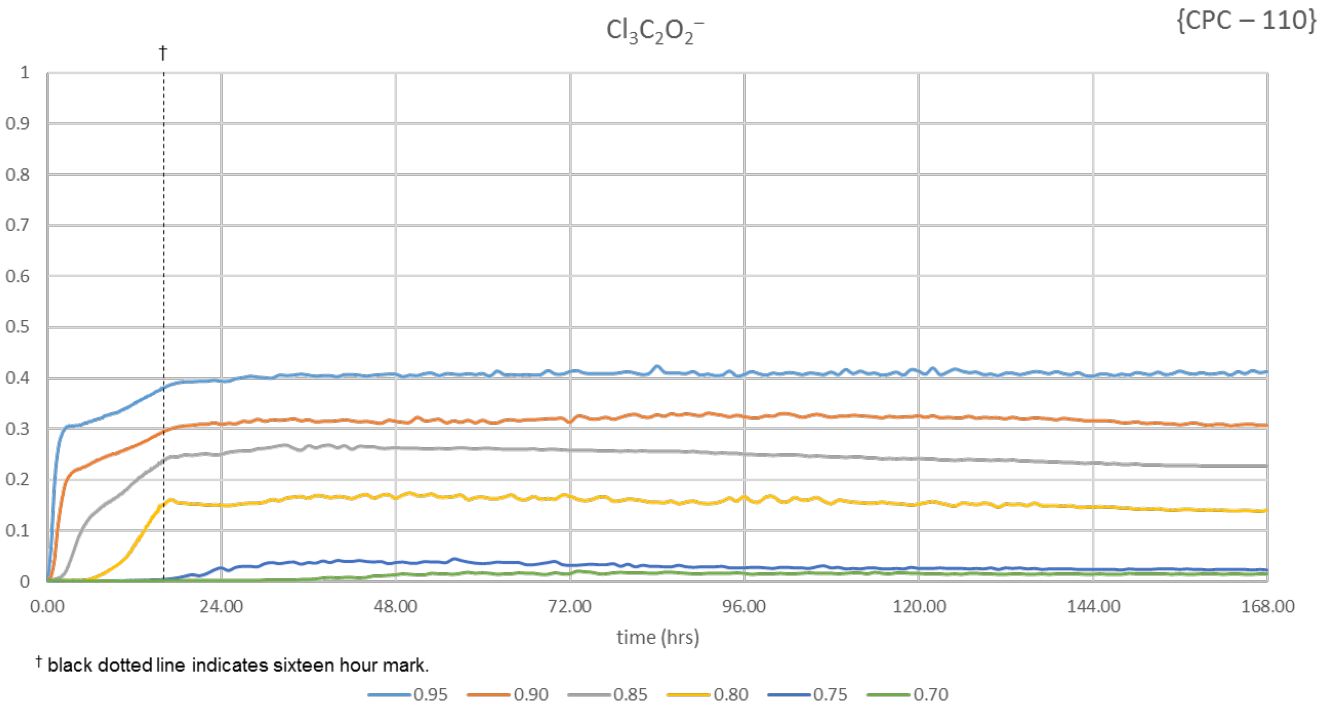

Figure S67: Precipitation kinetics of positand **2** in the presence of $Cl_3C_2O_2^-$ at 70 – 95 % of the CPC (77.0 – 104.5 mM).

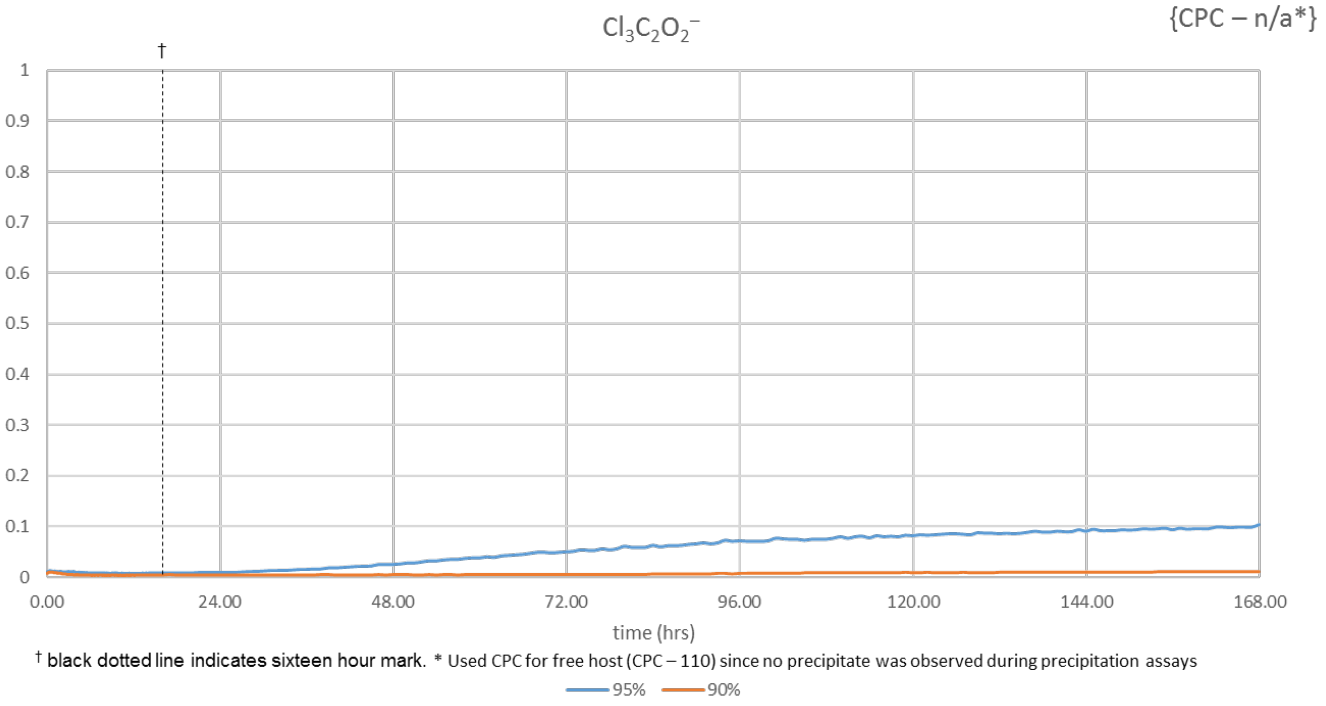

Figure S68: Precipitation kinetics of the **2**.AdaCO_2^- complex in the presence of $Cl_3C_2O_2^-$ at 90 – 95 % of the CPC for free positand **2** (99.0 – 104.5 mM).

D. Correlations

The CPC data and binding constants in hand, attempts were made to draw several correlations between the different data sets. While a modest correlation was observed for the reciprocal CPC (M^{-1}) and the association constants for the same anions to the cavity (Figure S69), the same could not be said of the CPC for the complex and K_a^{crown}. There was however a similarly modest correlation shown between results of the CPC determination and the volume of the hydrated anion ($R^2 > 0.72$) and the CPC (Figure S70) while the anions radius ($R^2 > 0.80$) (Figure S71) is a much stronger correlation. The best correlation ($R^2 > 0.96$) was between the aqueous entropy of the anions under study and the CPC (Figure S72) albeit relatively few points could be compared due to the lack of literature data available.[5] The K_a was fairly well correlated ($R^2 > 0.82$) with the hydration number of the solvated ions (Figure S73) to the crown, but not so with the cavity with the more-weakly solvated ions bearing the stronger affinity. Only a modest correlation was observed between for K_a^{cav} ($R^2 \approx 0.66$) and for K_a^{crown} ($R^2 \approx 0.53$) and the ions radius (Figure S74).

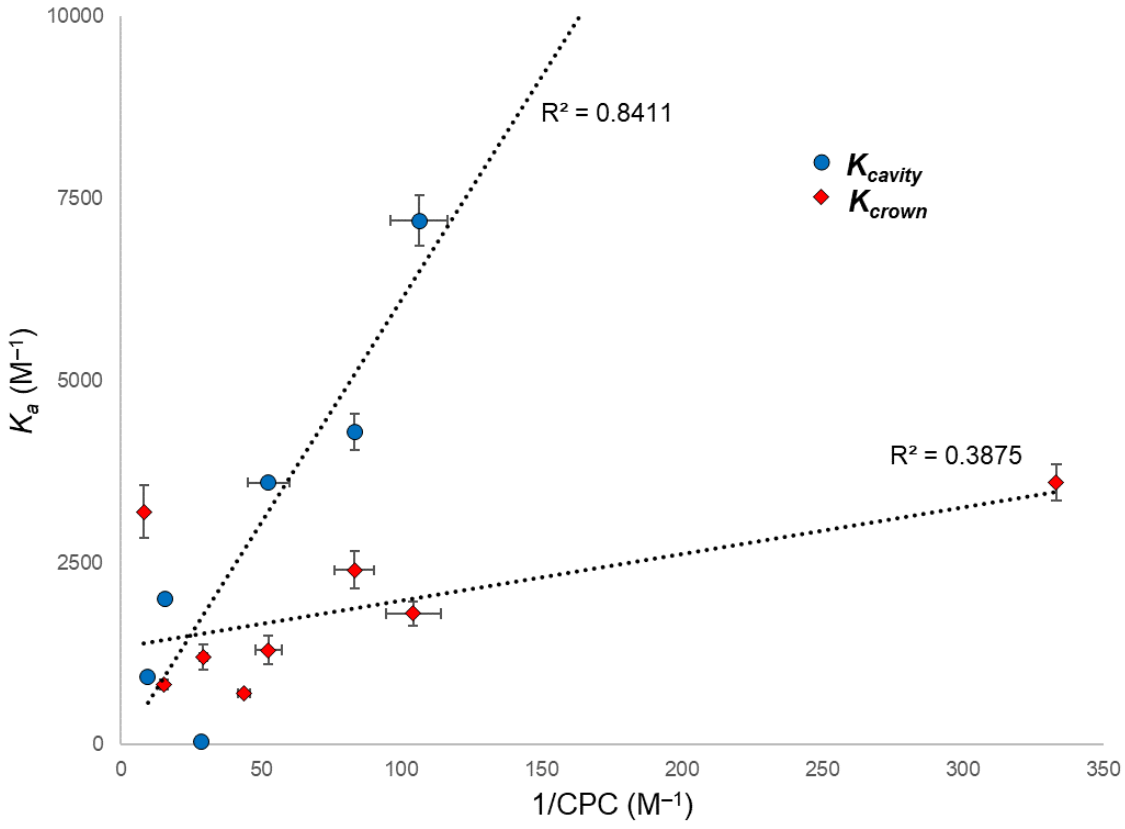

Figure 69: Plot of CPC for each of the precipitating salts (I^-, SCN^-, BF_4^-, BH_3CN^-, ClO_4^-, and ReO_4^- and PF_6^-) against the $K_a^{cav}$and K_a^{crown} for host **2.** PF_6^- and $CF_3SO_3^-$ not shown as reliable fitting data could not be obtained for K_a^{cav}. $Cl_3C_2O_2^-$ not shown as reliable fitting data could not be obtained for K_a^{crown} respectively.

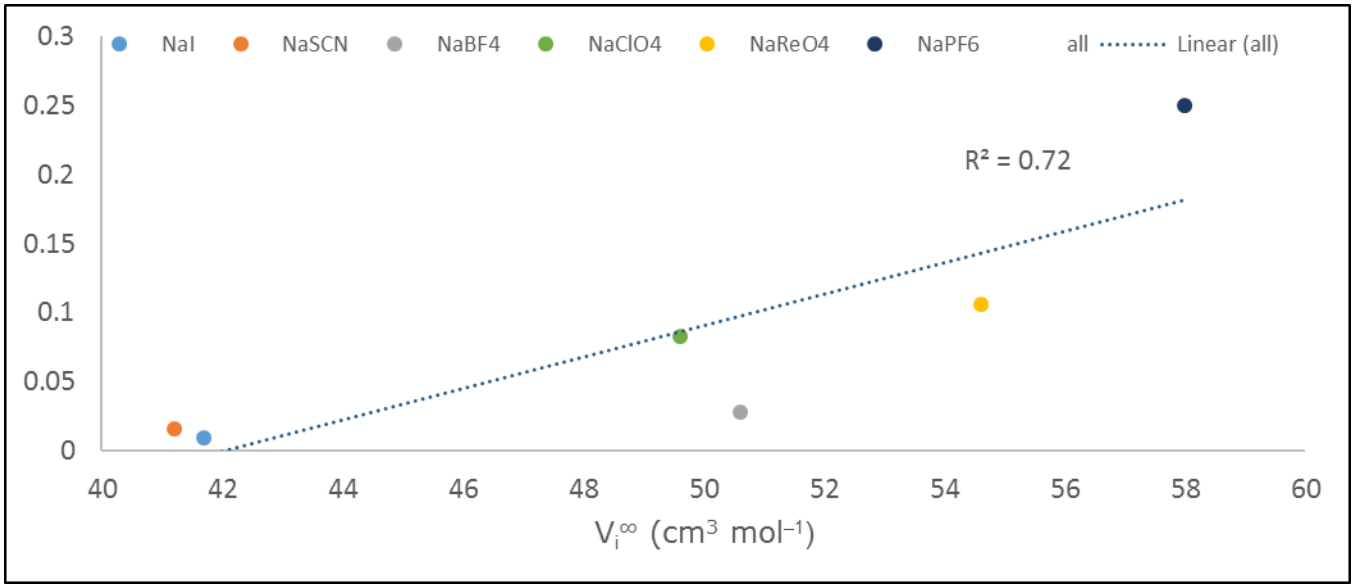

Figure S70: Correlation between partial molar volume at infinite dilution (x-axis) and CPC^{-1} (mM, y-axis) for precipitating anions where the volume is known.[5] Literature values for BH_3CN^-, $CF_3SO_3^-$ and $Cl_3C_2O_2^-$ not readily available.

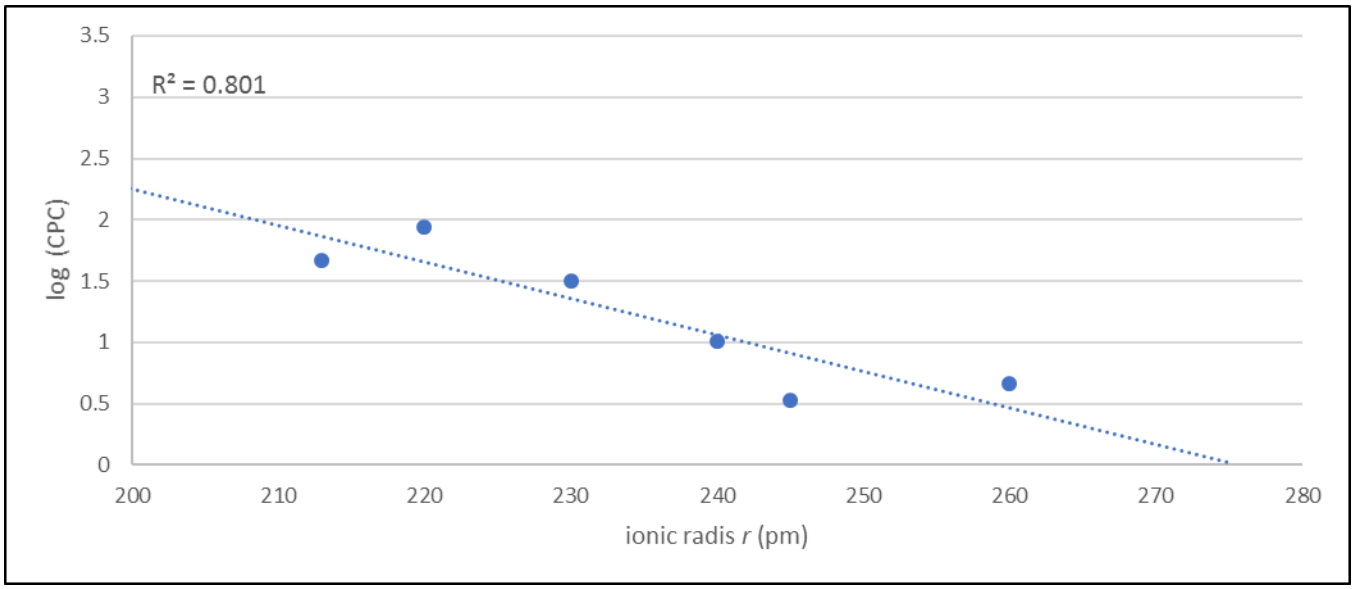

Figure S71: Correlation between the adjusted CPC (y-axis) and the ionic radius (x-axis) for precipitating anions (SCN^-, I^-, BF_4, ClO_4^-, PF_6^-, ReO_4^-) where the radii is established.[5]

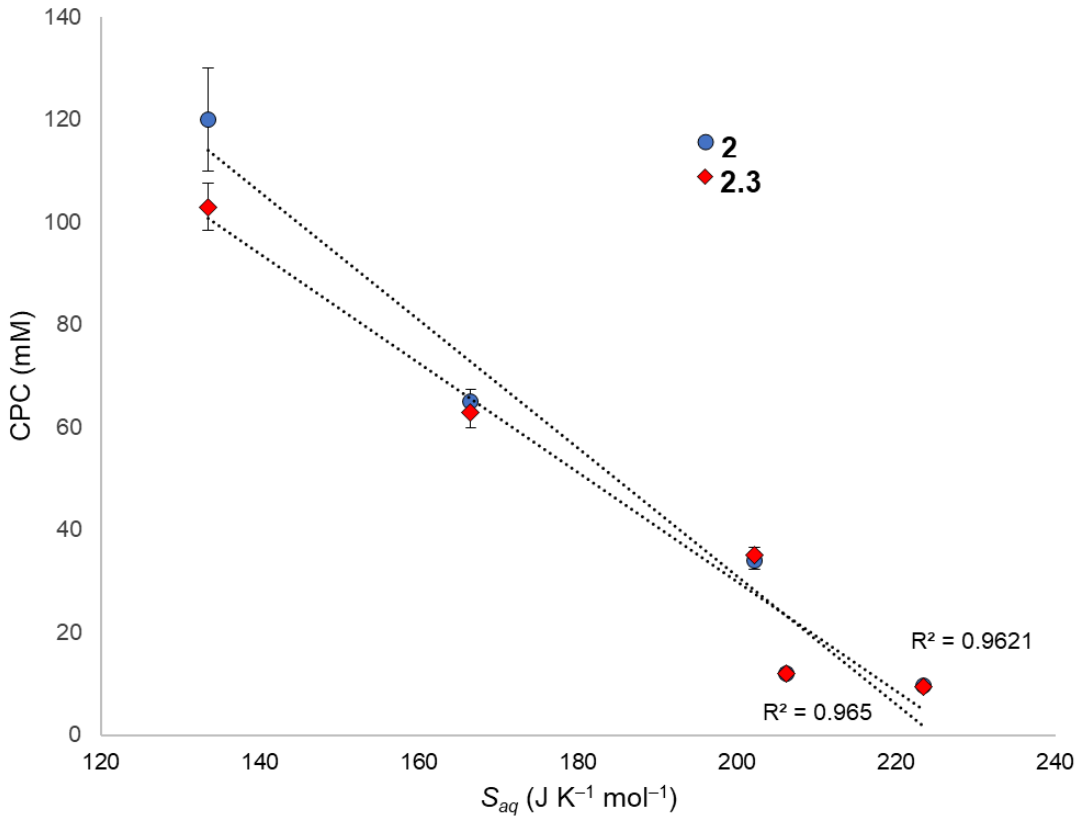

Figure S72: Correlation between partial molar entropy for the aqueous ions (y-axis) and the CPC (x-axis) for precipitating ions (where data is readily available).[5]

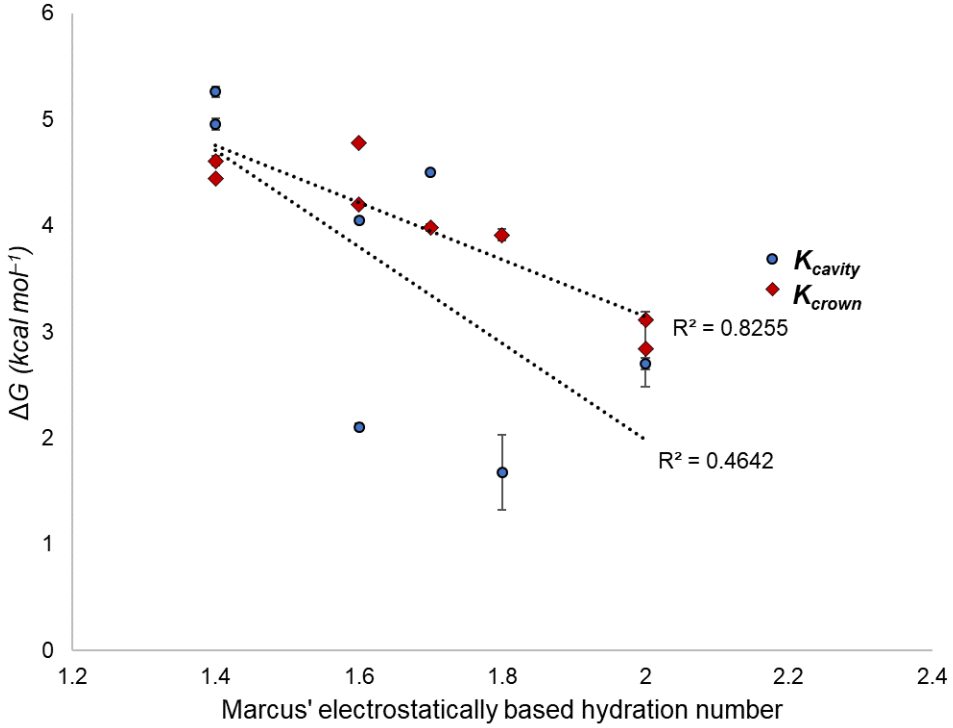

Figure S73: Correlation between hydration number (x-axis) and the free energy of complexation to cavity and crown (y-axis) for investigated anions where data was readily available.[5]

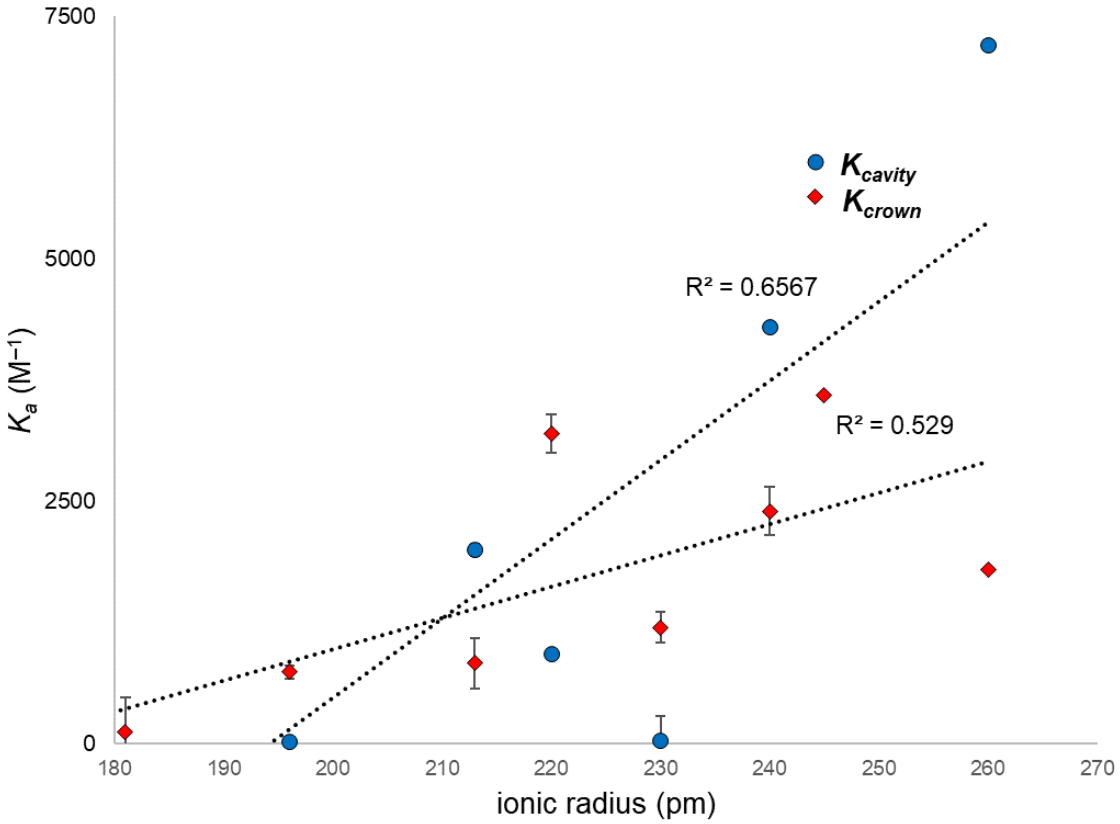

Figure S74: Correlation between ionic radii (x-axis) and K_a^{cav} and K_a^{crown} (y-axis) for investigated anions. *Literature values for BH_3CN^-, and $CF_3SO_3^-$ not readily available.

D. Dynamic Light Scattering (DLS) data

Solutions were prepared as described in the sample preparation procedure (Section 2.C). Solutions of **2** or the complex between **2** and adamantane carboxylate were titrated with a concentrated salt solution and then the volume-weighted size distributions were recorded. Surface plots of the raw data were exported and plotted using OriginPro software. The CPC was determined based on when particle sizes in solution exceeded 20 nm in diameter, unless the maximum size did not exceed 20 nm in which case the maximum size was used (Table S10). While the particle size (Figure S75) was essentially constant for the non-precipitators NO_3^-, Cl^-, Br^-, $Cl_2CHCO_2^-$, and F^- for **2** (and for NO_3^-, Cl^- for the complex between **2** and adamantane carboxylate (Br^-, $Cl_2CHCO_2^-$, and F^- were not examined for the complex)), for the remaining anions large increases in particle size were observed for both free **2** (Figure S76) and the complex (Figure S77). The results are summarized in Table S10 and graphed as the CPC^{-1} in Figure S78.

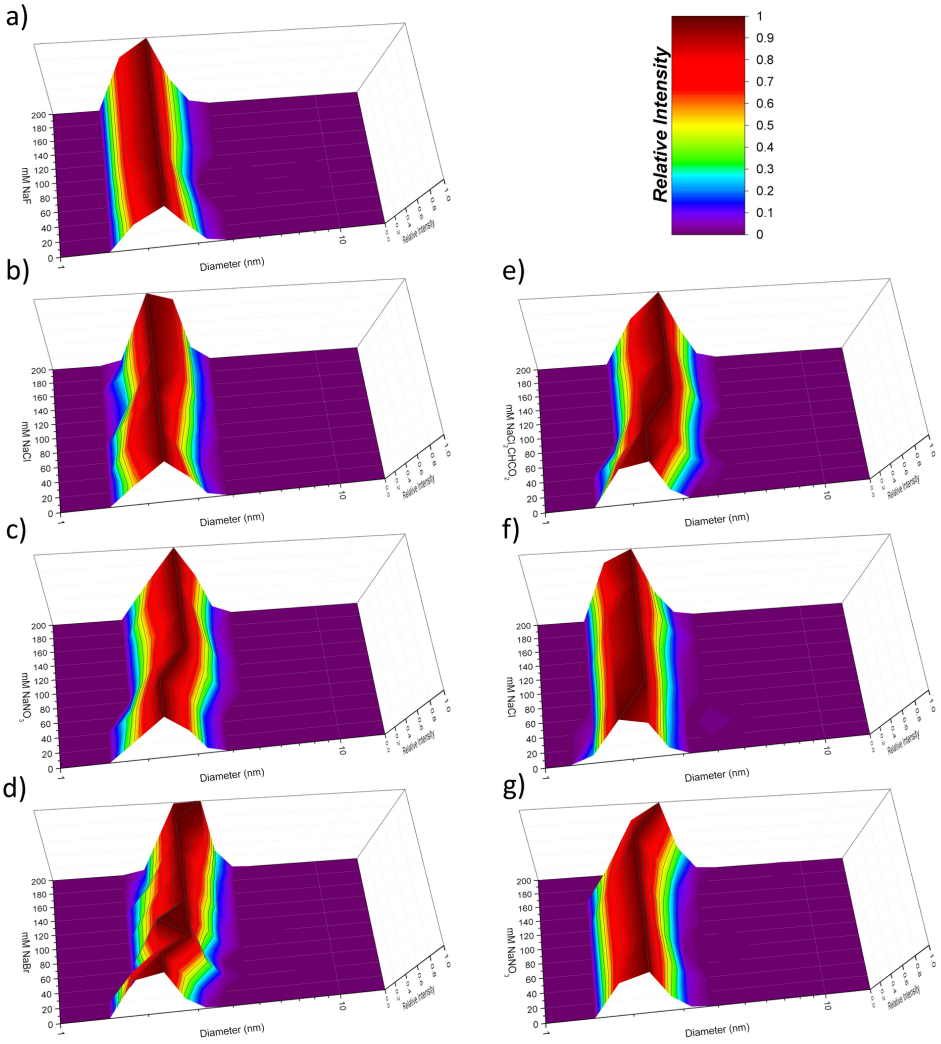

Figure S75: Dynamic Light Scattering surface plots of the volume weighted size distribution of the non-precipitating sodium salts titrated into 2.0 mM **2**. a) F^-, b) Cl^-, c), Br^- d) NO_3^-, e) $Cl_2CHCO_2^-$, and titrated into 2.1/2.0 mM **2.3** f) Cl^-, g) NO_3^-. Scale shown in upper right corner. X-axis represents particle size distribution, y-axis the concentration of the respective salt (mM), and z-axis the relative intensity.

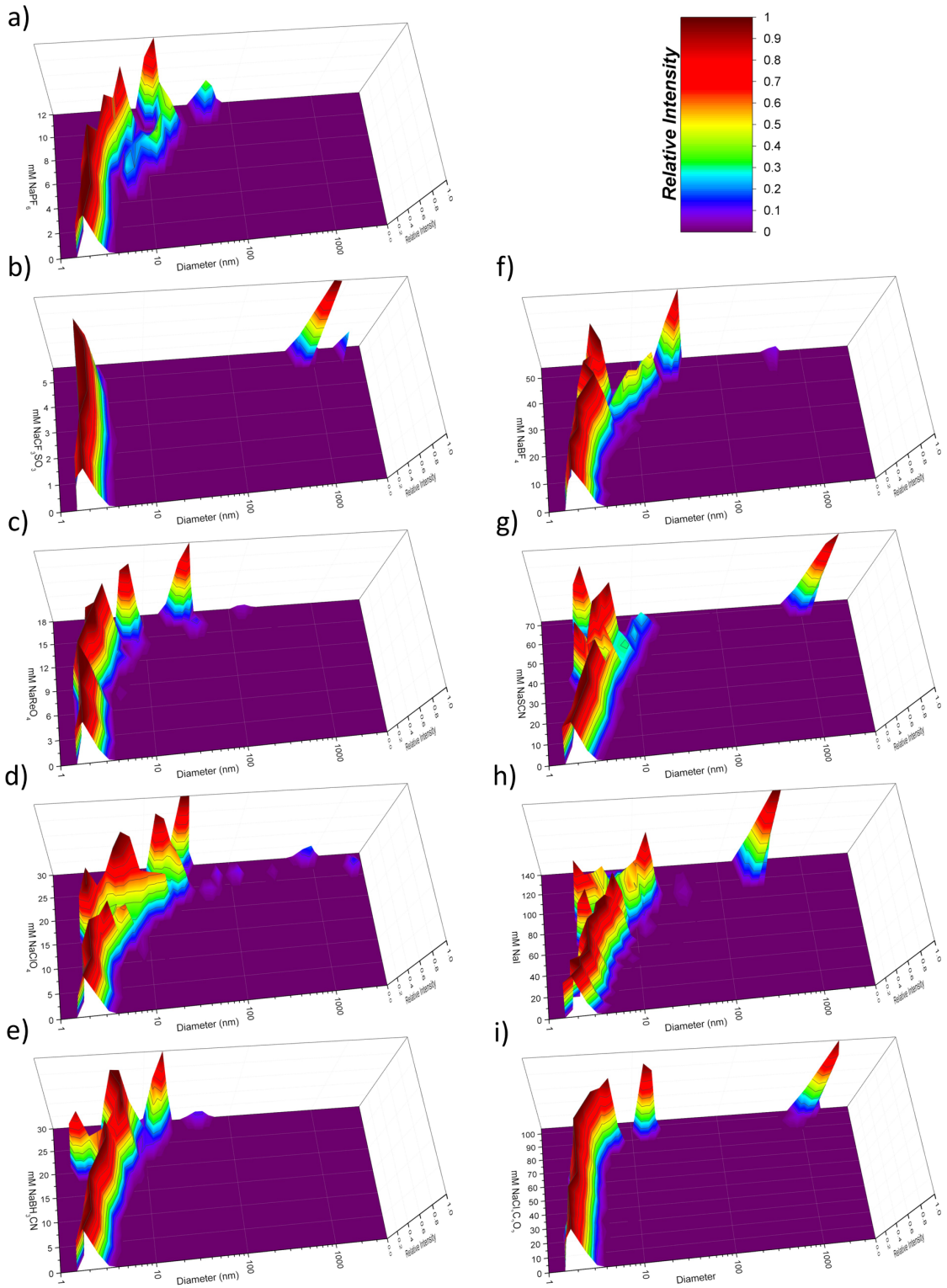

Figure S76: Dynamic Light Scattering surface plots of the volume weighted size distribution of the precipitating sodium salts titrated into 2.0 mM **2**. a) PF_6^-, b) $CF_3SO_3^-$, c) ReO_4^-, d) ClO_4^-, e) BH_3CN^-, f) BF_4^-, g) SCN^-, h) I^-, i) $CCl_3CO_2^-$. Scales shown in upper-right corner. X-axis represents particle size distribution, y-axis the concentration of the respective salt (mM), and z-axis the relative intensity.

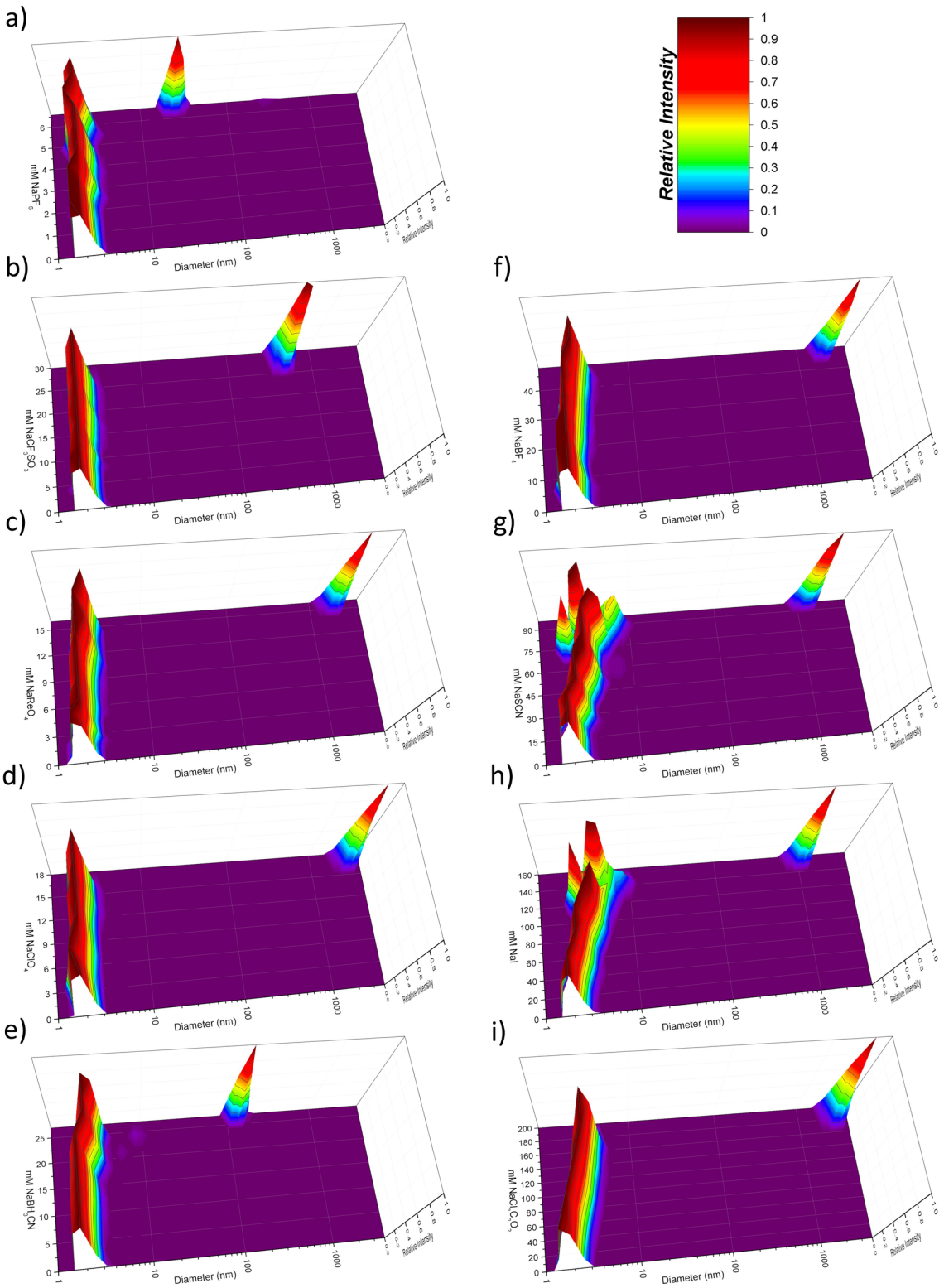

Figure S77: Dynamic Light Scattering surface plots of the volume weighted size distribution of the precipitating sodium salts titrated into 2.0/2.1 mM of the **2**.AdaCO_2^- complex: a) PF_6^-, b) $CF_3SO_3^-$, c) ReO_4^-, d) ClO_4^-, e) BH_3CN^-, f) BF_4^-, g) SCN^-, h) I^-, i) $CCl_3CO_2^-$. Scales shown in upper-right corner. X-axis represents particle size distribution, y-axis the concentration of the respective salt (mM), and z-axis the relative intensity.

	Free Positand 1		Positand 1 : $AdaCO_2H$ complex	
	[Salt] / (mM) sizes > 20 nm	Maximum Size (nm)	[Salt] / (mM) sizes > 20 nm	Maximum Size (nm)
$NaPF_6$	12[a]	12.0 ± 1.4	6.6	23.3 ± 4.1
CF_3SO_3Na	5.6	764.9 ± 101.9	30	437.7 ± 64.0
$NaReO_4$	18	25.5 ± 3.5	16	1818.1 ± 239.7
$NaClO_4$	30	25.1 ± 2.9	18	2692.9 ± 348.5
$NaBH_3CN$	30[a]	14.6 ± 1.8	27	124.3 ± 27.7
$NaBF_4$	54	26.6 ± 5.6	48	1925.5 ± 324.4
$NaSCN$	72	972.9 ± 140.4	96	1193.3 ± 168.5
NaI	140	248.2 ± 39.1	160	1016.5 ± 134.6
$NaO_2C_2Cl_3$	104	1118.8 ± 177.7	200	2649.3 ± 356.6
$NaBr$	—[b]	3.0 ± 0.4	n/a	n/a
$NaNO_3$	—[b]	2.7 ± 0.5	—[b]	2.6 ± 0.3
$NaCl_2CHCO_2$	—[b]	2.7 ± 0.6	n/a	n/a
$NaCl$	—[b]	2.4 ± 0.3	—[b]	2.2 ± 0.5
NaF	—[b]	2.1 ± 0.3	n/a	n/a

Table S10. Summarized DLS data for positand **2** and **2**.$AdaCO_2^-$ complex. Sizes are volume weighted distributions. a) For PF_6^- and BH_3CN^- with the free host, maximum size was used. b) Size increase (precipitation) not observed even at 200 mM (ca. 100 equivalents).

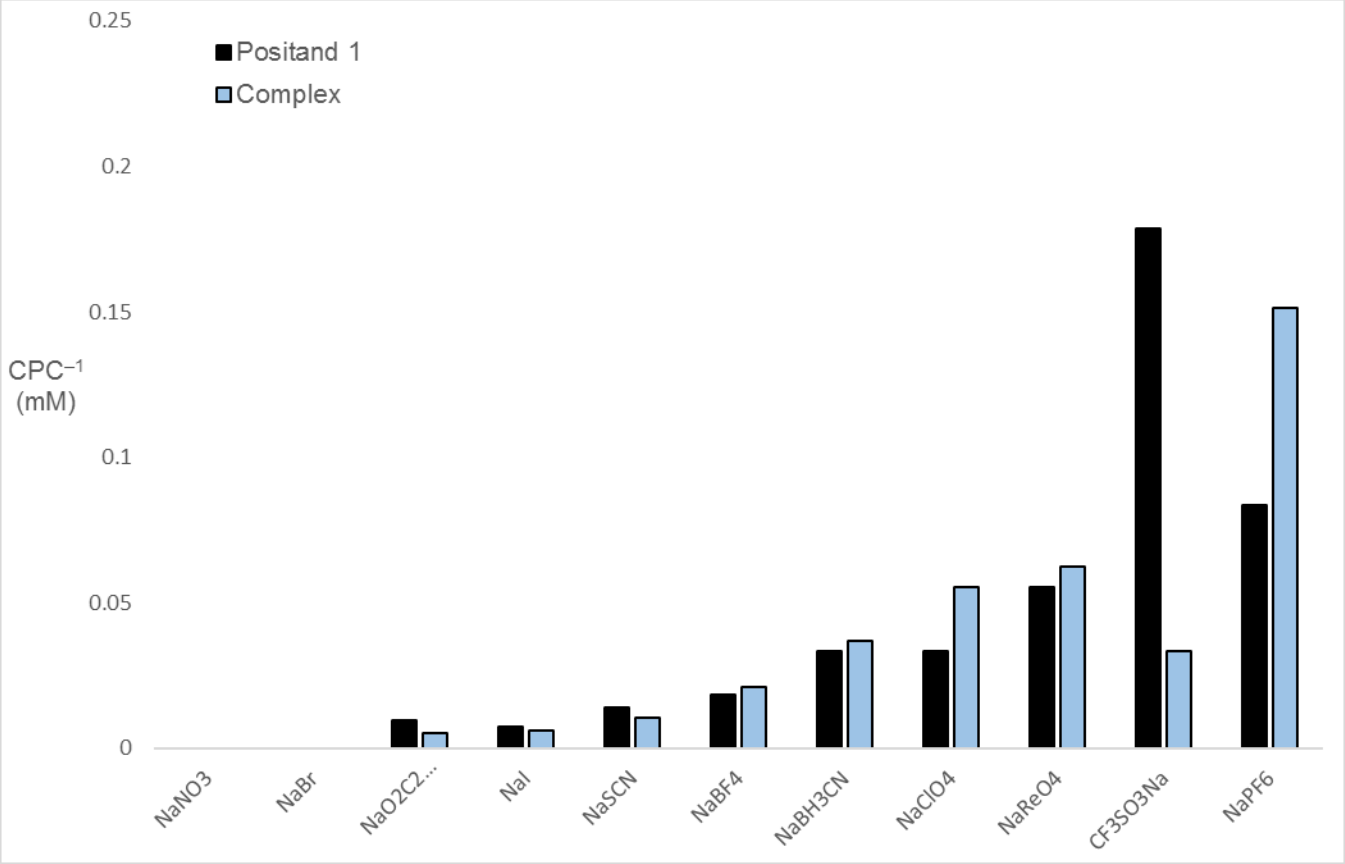

Figure S78: Graph of the inverse DLS obtained Critical Precipitation Concentration (CPC^{-1}) plotted for each salt against the free host positand **2** (2.0 mM), and the **2**.$AdaCO_2^-$ complex.

6. References

1. Hillyer, M. B.; Gibb, C. L.; Sokkalingam, P.; Jordan, J. H.; Ioup, S. E.; Gibb, B. C., *Org Lett* **2016,** *18* (16), 4048-51.
2. Liu, S.; Whisenhunt-Ioup, S. E.; Gibb, C. L.; Gibb, B. C., *Supramol Chem* **2011,** *23* (6), 480-485.
3. http://supramolecular.org/ (accessed 01/06/2017).
4. Thordarson, P., *Chem. Soc. Rev.* **2011,** *40* (3), 1305-1323.
5. Marcus, Y., *Ion Properties*. Dekker: New York, 1997.